

University of Alberta

An Experimental Study of Spontaneous Imbibition in Horn River Shales

by

Kaiyrzhan Khalilullaevich Makhanov

A thesis submitted to the Faculty of Graduate Studies and Research
in partial fulfillment of the requirements for the degree of

Master of Science
in
Petroleum Engineering

Department of Civil and Environmental Engineering

©Kaiyrzhan Khalilullaevich Makhanov

Fall 2013
Edmonton, Alberta

Permission is hereby granted to the University of Alberta Libraries to reproduce single copies of this thesis and to lend or sell such copies for private, scholarly or scientific research purposes only. Where the thesis is converted to, or otherwise made available in digital form, the University of Alberta will advise potential users of the thesis of these terms.

The author reserves all other publication and other rights in association with the copyright in the thesis and, except as herein before provided, neither the thesis nor any substantial portion thereof may be printed or otherwise reproduced in any material form whatsoever without the author's prior written permission.

Abstract

Massive hydraulic fracturing operations conducted in shale reservoirs create extensive fracture networks to enhance recovery of hydrocarbons from low permeability shale reservoirs. Fluid invasion into the shale matrix is identified as one of the possible mechanisms leading to low fracturing fluid recovery after the fracturing operations. Studying the mechanisms of liquid imbibition into shale matrix is essential for understanding the fate of non-recovered fracturing fluid that can eventually lead to better utilization of water resources by reducing cost and environmental impact.

This study aims to investigate effects of base fluid type (aqueous vs. oleic phase), polymer enhanced viscosity, salinity and surfactants in aqueous solutions on the imbibition rate in actual shale samples. The shale samples were collected from Fort Simpson, Muskwa and Otter Park formations, all belong to greater the Horn River Basin. The samples were characterised by measuring porosity, wettability (through contact angle measurements), mineralogy (through XRD analysis), TOC, and interpreting wire line log data.

We find that imbibition rate of aqueous phase is higher than that of oleic phase. Moreover, we find that imbibition rates of KCl brine, surfactants and viscous polymer solutions are lower than that of fresh water. We find that dimensionless time used to model spontaneous imbibition in conventional rocks requires specific adjustments for application in shales. Based on applied upscaling method, it was found that spontaneous imbibition can cause significant water loss at the field scale during shut-in period after hydraulic fracturing.

ACKNOWLEDGEMENTS

It is with tremendous gratitude that I acknowledge the support and help of my supervisors Dr. Ergun Kuru and Dr. Hassan Dehghanpour for their valuable guidance, support and engagement through the learning process of this master thesis. I wish to express my appreciation for their positive outlook and confidence in my research that inspired me and gave me motivation. Their kindness and encouragement will be always remembered.

Furthermore, I would like to express my deepest gratitude to my family, who has supported me throughout the entire process of studying. I will be grateful forever for their love, understanding and encouragement.

I am grateful to the people who helped me make my stay enjoyable through the duration of my studies in Canada. Special thanks to all my graduate friends and housemates. Not forgetting to my best friends who always been there. Their friendship has made my life so much interesting and memorable.

I would like to thank the Bolashak International Scholarship Program for providing the constant support and financial assistance. I thank BC Ministry of Energy and Mines, the Oil and Gas Commission for providing core samples of the Horn River basin. I acknowledge Nexen, FMC Technologies and Natural Sciences and Engineering Research Council of Canada (NSERC) for measurement and provision of the field data. I also acknowledge Dr. Dipo Omotoso for analyzing the XRD data and Engineering Technologist Mr. Todd Kinnee for his help and assistance in conducting laboratory experiments. Without them all this study would not have been successful.

TABLE OF CONTENTS

1. INTRODUCTION.....	1
1.1 Overview and Background.....	1
1.2 Statement of the Problem.....	4
1.3 Objectives of the Research.....	5
1.4 Methodology of the Research.....	5
1.5 Structure of the Thesis.....	6
2. LITERATURE REVIEW.....	8
2.1 Overview of Unconventional Resources.....	8
2.2.1 Hydraulic Fracturing Technique.....	9
2.2.2 Problems Associated with Hydraulic Fracturing of Shale Formations.....	10
2.2 Overview of the Horn River Basin Shale.....	12
2.2.1 Origins and Geology.....	12
2.2.2 Marketable Reserves.....	14
2.3 Specific Shale Properties.....	15
2.4 Fracturing Fluid Compositions.....	16
2.4.1 Water Based Fluids.....	17
2.4.2 Additives to Water-Based Fluids.....	19
2.4.3 Oil Based Fluids.....	20
2.5 Scaling of Spontaneous Imbibition.....	21
2.5.1 Handy Models.....	22
2.5.2 Li and Horne Model.....	22
2.5.3 Schmid and Geiger Model.....	23

2.6 Estimation of Water Loss at the Field Scale	25
3. PETROPHYSICAL CHARACTERIZATION OF SHALE CORES.....	26
3.1 Wire Line Log Interpretations.....	26
3.2 Total Organic Carbon (TOC).....	29
3.3 XRD Analysis	30
3.4 Porosity Determination.....	31
3.5 Contact Angle Measurements	32
4. SPONTANEOUS IMBIBITION EXPERIMENTS.....	34
4.1 Materials Used	34
4.1.1 Imbibing Fluids	34
4.1.2 Epoxy Seal.....	36
4.2 Shale Samples	36
4.3 Experimental Setup.....	40
4.4 Experimental Procedure	40
4.4.1 Sample Preparation Procedure	40
4.4.2 Core Imbibition Procedure	41
5. IMBIBITION EXPERIMENTS: RESULTS AND DISCUSSION.....	42
5.1 Imbibition of Aqueous Solutions.....	42
5.1.1 Fresh Water Imbibition Tests	42
5.1.2 Effects of Brine Solution Imbibition.....	44
5.1.3 Effects of Surfactant Solutions Imbibition	47
5.1.4 Effects of Xanthan Gum Polymer Solution Imbibition	51
5.2 Imbibition of Oleic Phase.....	54
5.3 Anisotropy in Shale Samples	57
6. IMBIBITION SCALING RESULTS.....	61

6.1 Dimensionless Scaling of Spontaneous Imbibition	61
6.1.1 Dimensionless Time Formulation	61
6.1.2 Analyses of Lab Data by Using Dimensionless Time	62
6.1.3 Results of Spontaneous Imbibition Scaling.....	66
6.1.4 Discussions of Dimensionless Scaling Results	80
6.2 Fluid Loss at the Field Scale	89
6.2.1 Introduction.....	89
6.2.2 Estimation of Water Imbibition at the Field Scale	91
6.2.3 Determination of A-parameter from the Experimental Data	92
6.2.4 Determination of the Fracture Matrix Interface at the Field Scale....	94
6.2.5 Brine Imbibition Results at the Field Scale	96
6.2.6 Limitations of the Proposed Methodology for Fluid Loss Predictions	100
7. CONCLUSIONS AND RECOMMENDATIONS.....	102
7.1 Conclusions	102
7.2 Recommendations.....	104
8. REFERENCES.....	106

LIST OF FIGURES

Fig. 2.1 -North American Shale plays.....	9
Fig. 2.2- Schematics of hydraulic fracturing	10
Fig. 2.3- Location of the Horn River basin.....	12
Fig. 2.4- Depositional cross-section of the Horn River basin	14
Fig. 2.5- Average Hydraulic Fracturing Fluid Composition	17
Fig. 2.6- Schematics of Counter-current and Co-current imbibition	21
Fig. 3.1-Well Logs Recorded in the Fort Simpson and Horn River Formations and the locations of samples selected for imbibition experiment	28
Fig. 3.2-Contact angle by Image J software	33
Fig. 4.1-Photopictures of Shale Samples covered by epoxy	36
Fig. 4.2-Comparative pictures of large and small samples covered by epoxy	37
Fig. 4.3- Orientation of rock/fluid contact surface area with respect to bedding plane and how it might relate to actual fractures in hydraulically fractured horizontal well	38
Fig. 4.4-Images of rock samples indicating directional anisotropy	39
Fig. 4.5-Schematic of set-up used for counter-current imbibition experiments	40
Fig 5.1-Spontaneous imbibition curves of different rock types	44
Fig. 5.2- Effect of Salinity on imbibition of various shale samples.....	46
Fig. 5.3- Imbibition of surfactants solutions in various shale samples.....	50
Fig. 5.4- Effects of viscosity on imbibition of various shale samples	53
Fig. 5.5-Imbibition of aqueous and oleic fluids in shale samples	56

Fig. 5.6-The effect of anisotropy on spontaneous imbibition rate	59
Fig. 5.7- The directional anisotropy index in shale samples	60
Fig. 6.1-Permeability vs. Porosity cross plot for various shales	65
Fig. 6.2-Dimensionless scaling of aqueous and oil phase imbibition data in large samples.....	69
Fig. 6.3- Dimensionless scaling of DI water, brine, and surfactant solutions.....	72
Fig 6.4- Dimensionless scaling of DI water, brine, and XG solutions	74
Fig. 6.5- Dimensionless scaling of directional brine imbibition in large samples.	77
Fig. 6.6- Dimensionless scaling of imbibition in large and small samples	79
Fig. 6.7- Pictures of Fort Simpson samples before and after 1 day of fluid exposure	83
Fig. 6.8- Pictures of Middle Muskwa samples before and after 1 day of fluid exposure.....	84
Fig. 6.9- Typical load recovery values during the flowback operations from multi-fractured wells completed in Muskwa and Otter Park formations.....	90
Fig. 6.10- Plots of cumulative imbibed volume per unit area versus square root of time.....	93
Fig. 6.11- Schematic of a multi-fractured horizontal well.....	95
Fig. 6.12- Imbibed volume of brine into the Muskwa shale versus the soaking time.....	98

Fig. 6.13- Percentage of injected water that is imbibed into the Muskwa shale versus the fracture aperture.....	99
Fig. 6.14- Ratio of the imbibed volume to the injected volume for different periods of soaking time.....	100

LIST OF TABLES

Table 2.1- Fracturing Fluid Additives.....	18
Table 3.1-Selected Sample for Petrophysical Analysis	29
Table 3.2-Results of XRD Mineralogy Analyses	30
Table 3.3-Matrix Density and Absolute Porosity Values.....	32
Table 3.4-Static Contact Angle Measurements.....	33
Table 4.1-Physical Properties of Fluids Systems.....	35
Table 4.2-Physical Properties of Shale Samples.....	37
Table 6.1-Parameters Used for Dimensionless Scaling.....	63
Table 6.2- <i>A</i> -Parameter Values Obtained from the Experimental Data.....	94
Table 6.3- Parameters Used for a Sensitivity Analysis of the Fracture-matrix Interface in Muskwa Shale	97

CHAPTER 1

INTRODUCTION

1.1 Overview and Background

Increasing energy demand shifted the focus of petroleum industry towards vast unconventional resources worldwide. In North America, shale gas production has gained tremendous importance. Commonly, shale reservoirs require special stimulation ‘jobs’ in order to produce hydrocarbons in a commercial scale. Improvement of current production technologies requires putting more efforts in economic, safety and environmental compromises.

Stimulation of natural gas production from tight reservoirs is based on the ability to create fracture networks that greatly enlarge a contact with the shale matrix. Advanced technologies have been developed to meet these challenges and explore resources in shale reservoirs. As we are witnessing today, recovery of hydrocarbons has been enhanced using horizontal wells coupled with the multistage hydraulic fracturing.

Hydraulic fracturing is a key technology for unlocking oil and gas resources from the unconventional shale reservoirs, which would have been otherwise stranded. First applications of hydraulic fracturing for stimulation of oil and gas wells date back to 19-th century although its wide practical application started only in 1950s. For successful operations in tight reservoirs, it is often combined with horizontal drilling technique. Advent of horizontal drilling in 1980s has promoted

technologies for producing shale gas from unconventional reservoirs (King, 2010).

Successful operations in Barnett shale in North-Central Texas in 1980s and 1990s have started commercial scale production of natural gas from shale formations. By 2005 Barnett shale alone was producing half trillion cubic feet per year of natural gas (EIA, 2012). Industry quickly noticed emerging energy sector with abundant resources. With estimated technically recoverable shale gas resources at 862 trillion cubic feet (AEO, 2011), development of shale gas plays has become a “game changer” for the US natural gas market. The growing confidence of the US in ability to profitably produce natural gas from shale rock spread to other countries.

Solid interest in shale gas production along with financial investments and shale gas technologies has crossed into Canadian shales. With decline in conventional natural gas sources in Canada, industry has shifted their focus to unconventional resources, including shale gas. While large-scale commercial production of shale gas in Canada has not yet gained full strength, many companies are now exploring for and developing shale gas resources in Alberta, British Columbia of Western Canada and Quebec, New Brunswick of Eastern Canada.

Development of gas bearing shale formations around the world still faces engineering challenges. There are significant environmental concerns over the hydraulic fracturing or “fracking” process. Hydraulic stimulation involves high pressure pumping of fracturing fluids into the well to create fractures or fissures in the rock formation. Fracturing fluids include water, proppant and chemicals.

Fractures remain open with “proppant” or sands, creating pathway to released gas flowing out of the formation and into the well bore. Created fracture surface contacts with fracturing fluids, which leads to the alteration of petrophysical properties of rock. This rock-fluid interplay causes fracturing fluid invasion into rock matrix through a mechanism, which is commonly referred as imbibition. Imbibing wetting fluid such as water may spontaneously displace a non-wetting fluid like gas from porous space. When water flows against the direction of a gas flow, it is called spontaneous counter-current imbibition. It has been reported that imbibition is, partly, responsible for huge volumes of water loss to the formation and may significantly impact natural gas production (Oduşina *et al.*, 2011 Dutta *et al.*, 2012).

Number of research work has been performed for last decades to understand imbibition process in low permeable rocks (Schembre *et al.*, 1998; Takahashi *et al.*, 2010; Wang *et al.*, 2011). Extensive literature is available and mainly aimed to understand shale formations in term of drilling engineering (Mody and Hale, 1993; Tan *et al.*, 1998). Several authors conducted laboratory experiments of spontaneous imbibition to duplicate processes in fractured shale reservoirs (Roychaudhury *et al.*, 2011; Akin *et al.*, 2000; Dutta *et al.*, 2012). However, the understanding of complex shale properties and their effects on spontaneous imbibition process needs further investigations to get best of fractured shale reservoirs.

1.2 Statement of the Problem

The key objective of multistage hydraulic fracturing in shale reservoirs is to generate extensive fracture-matrix interface for enhancing the hydrocarbon production rate (Novlesky *et al.*, 2005). Fracturing fluids enriched with assorted chemicals are pumped into the formation to fracture shale reservoirs. Recent studies show that stimulated shale reservoirs retain significant amount of injected frac fluids (Soeder, 2011), which can be, at least partly, caused by fluid imbibition into shale matrix (Oduşina *et al.*, 2011).

Imbibition of fracturing fluids into the shale pores is important mechanism for fluid loss and the reservoir damage (Dutta *et al.*, 2011; Agrawal *et al.*, 2013). Spontaneous imbibition in porous media controlled by capillary, viscous and gravity forces (Akin *et al.*, 2000; Li and Home, 2006). However, what is the importance of clay swelling effect, wettability, electrostatic charge and organic content in the process of spontaneous imbibition in shale media? This question has significant bearings on fracturing fluid management issues and has been scarcely studied in the context of reservoir engineering. Experimental studies of fluid imbibition in relevant formations are necessary to select appropriate model that best describes imbibition in shales. Questions such as how much of fracturing fluid goes in to the shale matrix and how much stays in the fracture are critical for designing fractures and treatment fluids. Interpretation of lab results together with field data would improve understanding of water loss during and after hydraulic fracturing operations.

1.3 Objectives of the Research

Objectives of this study include:

- Characterize petrophysical properties of shale core samples collected from the Horn River basin.
- Investigate effects of 1) fluid properties, and 2) shale sample properties on spontaneous imbibition rates.
- Investigate in the theoretical part, if the existing dimensionless parameters are applicable for scaling of the imbibition data measured in shales.
- Develop a simple analytical procedure to estimate the volume of fracturing fluid imbibed into the shale matrix during the shut in period after the fracturing operation.

1.4 Methodology of the Research

The following methodology was used to accomplish the thesis study objectives:

1. Determine shale petrophysical properties by direct measurement of porosity and contact angle (for wettability analysis) and interpretation of wire line well logging data.
2. Determine mineralogy and organic matter content of the shale samples by analysing XRD and TOC data, respectively.
3. Conduct spontaneous imbibition experiments using specially prepared shale samples and experimental fluids to measure the imbibed volume versus time. Examine effects of the base fluid type (aqueous vs. oleic

phase) and additives (salt, polymer, and surfactant) on the fluid intake rate into shales.

4. Analyze the results of imbibition experiments by plotting the imbibition data versus 1) actual time and 2) dimensionless time.
5. Estimate the volume of fracturing fluid imbibed into the shale matrix at the field scale soaking time (period after the fracturing operation and before flowback from the well). Conduct a sensitivity analysis by varying fluid-shale contact interface, fracture aperture and fluid leak-off to the formation. Describe methodology limitations at the field scale.

1.4 Structure of the Thesis

Chapter 1 presents brief overview and background of hydraulic fracturing in shale formations, introduces associated problems, and discusses objectives and methodology of the thesis study.

Chapter 2 provides literature review of main topics relevant to this research work and introduces the main concepts related to spontaneous imbibition in porous media. It gives detailed overview of the Horn River shale play.

Chapter 3 presents petro physical properties of core samples including porosity, contact angle, results of XRD and TOC measurements and interpretation of well logs from the two selected wells drilled in the Horn River basin

Chapter 4 provides specifics of spontaneous imbibition experiments. It describes materials used, experimental setup and procedures for conducting counter-current imbibition experiments.

Chapter 5 presents and discusses the results of conducted imbibition experiments. It explains the effect of fluid and shale properties on the observed imbibition behaviour.

Chapter 6 tests the application of the dimensionless time formulation, existing in the literature, for scaling the measured imbibition data, and discusses the limitations. It also presents a methodology for estimating spontaneous fluid loss at the field scale during the soaking time by using the imbibition data measured in the lab.

Chapter 7 summarizes the important findings of the thesis and provides recommendations for further research.

CHAPTER 2

LITERATURE REVIEW

2.1 Overview of Unconventional Resources

Although we are seeing an increasing role of renewable energy, the foreseeable future continues to indicate a heavy reliance on hydrocarbons with increasing role for unconventional crude oil and natural gas (Nash, 2012). Unconventional oil and gas resources present significant potential for meeting world's ever increasing energy demand. Proven shale gas reserves, for example, are estimated over 6622 trillion cubic feet which is 40% of world's technically recoverable gas reserves (NIAG, 2012). However, unconventional gas resources have traditionally been considered difficult or costly to produce. Advances in hydraulic fracturing technology were one of the keys to unlocking these resources, which would otherwise have been left economically stranded.

Unconventional gas is a collaborative term which refers to a natural gas that is recovered from the coalbed methane, tight gas, methane hydrate and shale gas. Shale gas is contained within a commonly occurring rock classified as shale. Shale formations are characterized as fine grained, low permeable, sedimentary rocks composed of variable amounts of clay minerals and quartz grains (Crain, 2012). These formations are often rich in organic matter and, unlike most hydrocarbon reservoirs, are typically the original source of the gas, *i.e.* shale gas is gas that has remained close to its source rock. Currently, there are 28 North American shale basins with 56 identified shale plays (EIA report, 2011). **Fig. 2.1**

shows location of major commercial shale plays including Horn River, Montney, Barnett, Haynesville, Fayetteville, Marcellus, and Eagle ford.

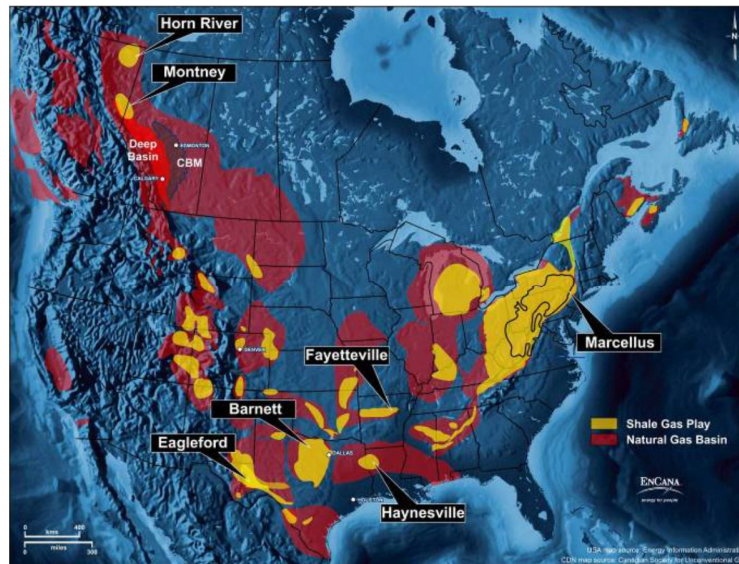


Fig. 2.1 - North American shale plays (Source: EnCana and CAPP Combined Report, 2012)

However, economic gas production requires using stimulation techniques such as hydraulic fracturing that enhances flow of gas to the wellbore.

2.1.1 Hydraulic Fracturing Technique

Horizontal wells combined with multistage hydraulic fracturing have enhanced recovery of hydrocarbons from shale formations. During hydraulic fracturing specially designed fracturing fluids are pumped in a controlled and monitored manner into the target shale formation at a pressure above the formation fracture pressure (Harper, 2008). Injected fluid, which consists of a mixture of base fluid, sand and chemical additives, transmits pressure to the hydrocarbon bearing rock

formation to create cracks in the rock or to open existing cracks (**Fig, 2.2**). The fractures are kept open by sand or other “proppant”, and serve as pathways for flow of gas towards the wellbore.

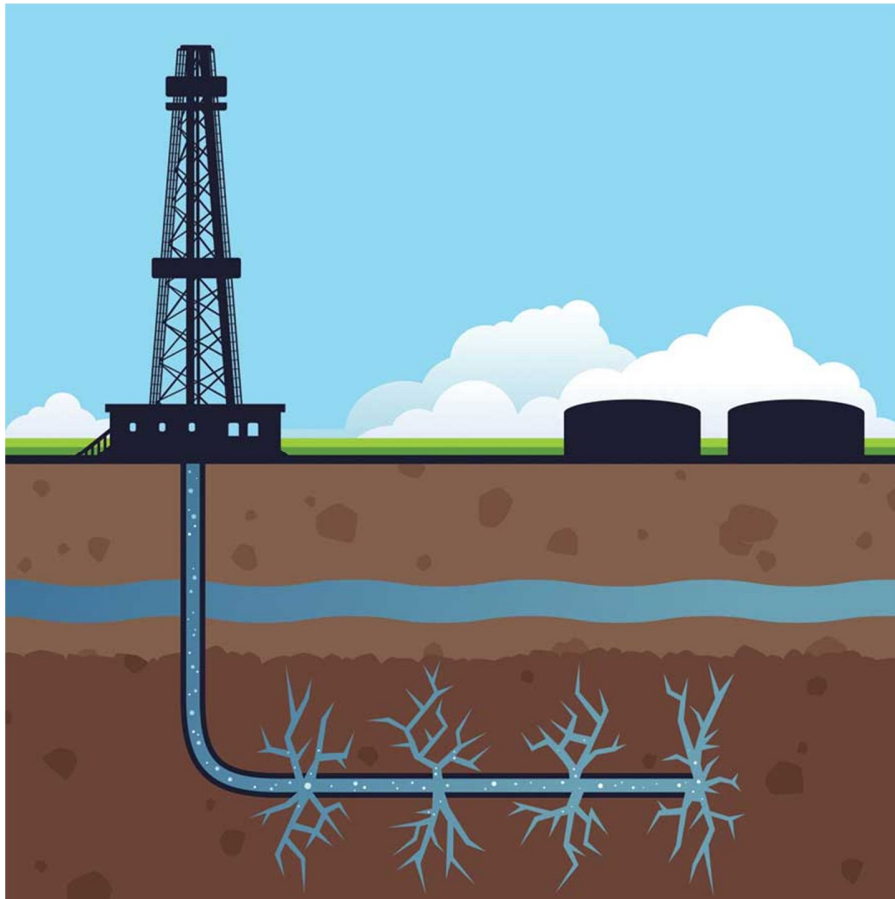


Fig. 2.2-Schematics of hydraulic fracturing (Source: Brandon Laufenberg, 2012)

2.1.2 Problems Associated with Hydraulic Fracturing of Shale Formations

Recent advances in shale gas recovery, through mostly hydraulic fracturing, encouraged number of ambitious projects, although the commercial approach is

still hindered by several issues. One of them is that hydraulic fracturing operations are subject to increased water consumptions (Oduşina *et al.*, 2011; Soeder, 2011). For instance, up to 5 000 m³ of frac fluid is needed to be injected for each fracture stage (Chapman, 2012). Typically, there are 10-20 stages per well and 10-20 wells per pad. Therefore, field operations may require up to 1M tons of frac fluids per pad. However, only around a quarter of it can be recovered during the “flowback” operation (Soeder, 2011). Such a low recovery of fracturing fluid yields in high project cost and environmental concerns.

Despite the recent surge of investigations of the problem, one major question still remains: what happens to the fracture fluid that is not recovered? Does it stay in the fracture or does it go into the matrix? In case of both mechanisms are responsible for fracture fluid retention, what fraction of fracture fluid stays in the propped fracture and what fraction is transferred from fracture to matrix. It has been reported (Roychaudhuri *et al.*, 2011; Oduşina *et al.*, 2011) that spontaneous imbibition to the formation matrix at least, partly, is responsible for high volumes of water loss in the field. Water imbibition into rock matrix does not only lead to water management issues, but also causes capillary blockages and hinders gas recovery (Dutta *et al.* 2011, Agrawal *et al.* 2013).

It is critical for the industry to quantify amount of fluid transfer to the matrix for designing better hydraulic fracturing operations. Therefore, factors causing the very low fracture fluid recovery need to be well understood and properly addressed, in order to get full benefits from costly hydraulic fracturing jobs conducted in unconventional reservoirs.

2.2 Overview of the Horn River Shale

The massive unconventional shale gas reserves have been discovered in the Horn River Basin, positioning it as major producer of shale gas in North America. It is located in northeastern British Columbia and extends northward into the Northwest Territories (Fig. 2.3).



Fig. 2.3-Location of the Horn River basin (Source: National Energy Board Report, 2011)

2.2.1 Origins and Geology

The Horn River Formation is a stratigraphical unit of Devonian age in the Western Canadian Sedimentary Basin. Skeletal debris from dead planktons, and clays, fine siliceous (silica-rich) muds were deposited in the poorly oxygenated

waters of the Horn River Basin and were converted into shale deposits over time (BC MEM and NEB, 2011). The Horn River Formation consists of the several subsurface members, from the bottom up:

I-) the Evie Member (the deepest part) is black micritic, silty limestone, which consists of dark grey to black, radioactive, organic-rich, pyritic, variably calcareous (calcite-rich), and siliceous shale (Gray and Kassube, 1963; Johnson *et. al.*, 2011).

II -) Otter Park Member (middle) is grey calcareous shale. The Otter Park Shale reaches a maximum thickness of over 270 m in the southeast corner of the Horn River Basin, where it consists of medium to dark grey calcareous shale. (Johnson *et. al.*, 2011).

III-) Muskwa Member (the upper member) is bituminous highly radioactive shale. The Muskwa consists of grey to black, radioactive, organic-rich, pyritic, siliceous shales, and is characterized on well logs by high gamma ray readings and high resistivity. Muskwa is overlaid by the thick, clay rich, low TOC Fort Simpson formation (Johnson *et. al.*, 2011; NEB report, 2006).

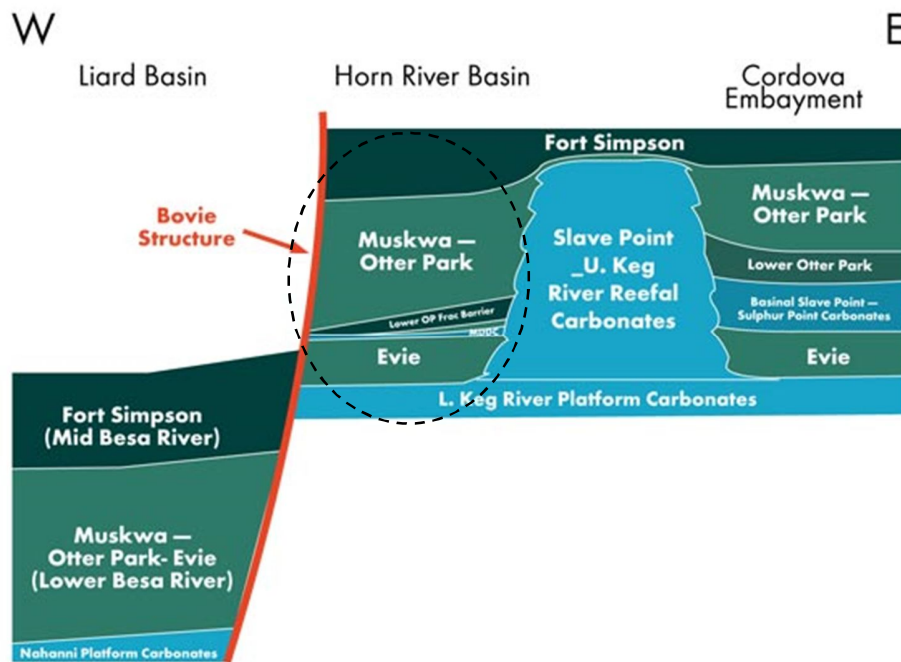


Fig. 2.4-Depositional cross-section of the Horn River basin (Source: Ross and Bustin, 2008)

Studies of shale reservoirs highlight that each shale formation requires individual approach based on local characteristics (Hu *et al.*, 2010; Roychaudhuri *et al.*, 2011). In this study, we have worked with actual core samples collected from Muskwa and Otter Park members of the Horn River formation as well as samples from Fort Simpson formation.

2.2.2 Marketable Reserves

Substantial shale gas resources were found in the Horn River basin. Total organic carbon (TOC) has been reported to be up to 5 wt.% (Reynolds and Munn, 2010; Chalmers *et al.*, 2012). The original-gas-in-place and recoverable gas in place volumes are estimated to be up to 529 Tcf and 96 Tcf, respectively (Johnson *et.*

al., 2011), making it the third largest North American natural gas accumulation discovered prior to 2010 (Mauger and Bozbiciu, 2011). Marketable resources may increase as more information is gained from longer term production data. Marketable resources may also increase if the cost of further development falls, or gas prices increase substantially.

2.3 Specific Shale Properties

Directional Anisotropy. In shales, fluid flow rate is higher parallel to the bedding plane (Chalmers *et al.*, 2012). It can be related to the effects of anisotropy. The anisotropic properties of shales are determined by the volume fraction of clay, organic matter and the degree of compaction (Sondergeld *et al.*, 2010). During the process of consolidation, clay minerals tend to align in the direction perpendicular to overburden pressure (Li, 2006). Preferred alignment of clay minerals and organics can create barriers or pathways for fluid flow depending on direction of flow.

Shale Clay. Clays are aluminosilicates in which some of the aluminum and silicon ions have been replaced by elements with different valence, or charge (Crain, 2012). For example, aluminum may be replaced by iron or magnesium, leading to a net negative charge. The clay minerals can accommodate positively charged ions (cations) on its negatively charged surface.

Clay minerals in shales are directly related to important properties such as “swelling” phenomenon, adsorption, anisotropy etc. Depending on the type of the

mineral group including the kaolin group, smectite group, illite group and chlorite group, clays can demonstrate “swelling” or “non-swelling” properties. The common “swelling” clays belong to smectite group, which induce expansion of clay platelets when contacts with water (Caenn *et al.*, 2011). Clay swelling causes fluid loss to the formation and inhibits fluid flow by blocking porous spaces (Schlumberger Oilfield Glossary, 2013).

Organic matter. Organic matter in shale is the fragments of ancient plants and planktons, which under high pressure and temperature converted into hydrocarbon compounds over time (Hayes *et al.*, 1987). Organic matter in shale forms a separate porous media and affects petrophysical properties, pore connectivity and fluid flow (Wang *et al.*, 2009). Porosity in organic matter can be higher than that of inorganic part and reach up to 25 % (Reed, 2007). The organic part is hydrophobic, thus it inhibits water flow in pores. Wang *et al.* (2009) speculated that organic matter in shales can form range of nanotubes for hydrocarbon flow.

2.4 Fracturing Fluid Compositions

The proper selection of base fracturing fluid is one of the most critical elements in fracture completion services (Chemtotal, 2012). Fluid-loss control, fracture conductivity, formation damage, and proppant transport are some of the factors that need to be considered in making the best fluid selection for a given well.

2.4.1 Water Based Fluids

Aqueous-based fracturing fluids have been widely used in the oil and gas wells because of their low cost, high performance, greater particles suspending ability, environmentally acceptable and ease of handling (Chemtotal, 2012). The fracturing fluids used for gas shale stimulations consist primarily of water but also include a variety of additives. The number of chemical additives used in a typical fracture treatment varies depending on the conditions of the specific well being fractured (Ketler *et al.*, 2006). Overall the concentration of additives in most fracturing fluids is a relatively consistent 0.5% to 2% with water making up 98% to 99.5% (Arthur *et al.*, 2009). **Fig. 2.5** shows the average volumetric percentages of additives used for hydraulic fracturing treatments.

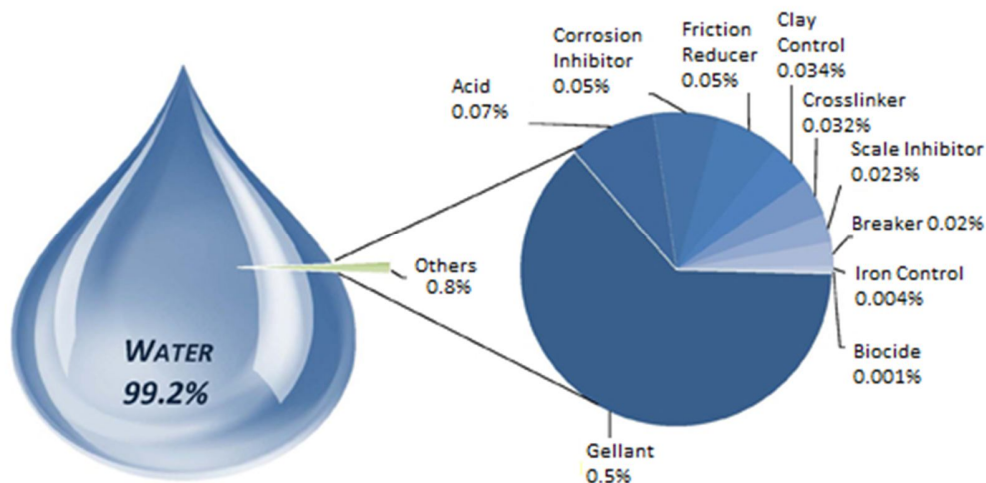


Fig. 2.5-Average Hydraulic Fracturing Fluid Composition (Source: Chemical disclosure registry, 2012)

These groups of additives represent the major compounds used in hydraulic fracturing of gas shales. In practice, fracturing companies select chemicals for each shale reservoir individually. Thus, the compounds may vary depending on properties of water and the target formation.

Each component of fracturing fluid serves for a specific purpose. **Table 2.1** below shows different types of fracturing fluid additives and their purpose in the field (Arthur *et al.*, 2008).

Table 2.1-Fracturing Fluid Additives		
Additive Type	Main Compounds	Purpose
Diluted Acid (15%)	Hydrochloric acid or muriatic acid	Help dissolve minerals and initiate cracks in the rock
Biocide	Glutaraldehyde	Eliminates bacteria in the water that produce corrosive byproducts
Breaker	Ammonium persulfate	Allows a delayed break down of the gel polymer chains
Corrosion Inhibitor	N,n-dimethyl formamide	Prevents the corrosion of the pipe
Crosslinker	Borate salts	Maintains fluid viscosity as temperature increases
Friction Reducer	Polyacrylamide	Minimizes friction between the fluid and the pipe
	Mineral oil	
Gel	Guar gum or hydroxyethyl cellulose	Thickens the water in order to suspend the sand
Iron Control	Citric acid	Prevents precipitation of metal oxides
KCl	Potassium chloride	Creates a brine carrier fluid
Oxygen Scavenger	Ammonium bisulfite	Removes oxygen from the water to protect the pipe from corrosion
pH Adjusting Agent	Sodium or potassium carbonate	Maintains the effectiveness of other components, such as crosslinkers
Proppant	Silica, quartz sand	Allows the fractures to remain open so the gas can escape
Scale Inhibitor	Ethylene glycol	Prevents scale deposits in the pipe
Surfactant	Isopropanol	Used to increase the emulsifying properties of the fracturing fluid

2.4.2 Additives to Water Based Fluids

Clay Inhibitors. Depending on type of clay and counter ions clay swelling in shale formations can be mitigated. For fracture treatments in shale formations, water based fluids are enriched with potassium salts (Boek *et al.*, 1995). The role of potassium counter ion as an inhibitor of clay swelling in the borehole is extensively described in the drilling engineering context (Caenn *et al.*, 2011; Anderson *et al.*, 2010).

Surfactants. Specially designed surfactants can significantly reduce fluid surface tension and shale wettability (Penny *et al.*, 2012). Wang *et al.* (2011) examined various surfactant formulations to enhance hydrocarbon recovery by altering shale wettability. However, not all surfactants can be useful in shale reservoirs. For example, negatively charged shale surface can either rapidly adsorb anionic surfactants within the first few inches of the formation or negatively impact reservoir wettability, thus reducing their effectiveness in lowering capillary pressure (Paktinat *et al.*, 2006). Hence, application of costly surfactants can be limited in shale reservoirs. In addition, cationic surfactants tend to be toxic and therefore their wide use in petroleum industry is restricted (Muherei and Junin, 2009). However, anionic and non-ionic surfactants are widely used in industry. They are relatively non-toxic and good surface tension reducers. The performance of anionic surfactants can be sensitive to the presence of salts in solutions (Kueper *et al.*, 1997).

Viscosifiers. Viscosifiers are used to thicken the frac fluids and improve proppant transportation (LaFollette, 2010). Xanthan Gum is the common polymer for preparing aqueous-based frac fluid. The polymer has a very high affinity for water. Xanthan Gum easily dissolves in water and readily establishes hydrogen bond with the water molecules and gets hydrated. The hydration of the polymer continues till each XG molecule is well bonded with water molecules (Chemtotal, 2012). Hydrogen bonds in the XG polymer chain structure result in a stable configuration that resists to a flow (Song *et. al.*, 2006). Moreover, the resistance to flow increases, when the polymer concentration is increasing.

2.4.3 Oil Based Fluids

Oil-based fracturing fluids are primarily used for water sensitive formations (Rajagopalan, 2012). Aluminium salts of organic phosphoric acids are generally used to raise viscosity, proppant carrying capability, and improve temperature stability (Chemtotal, 2012). Recently Hlidek *et. al.* (2012) reported that 100% of the frac oil is recovered from the well from the Montney gas play in Western Canadian Sedimentary basin. However, compared to aqueous-based fluids, they are more expensive and more difficult to handle. Oil-based fluids are also more hazardous because of flammability and also possess environmental concerns (Rajagopalan, 2012).

2.5 Scaling of Spontaneous Imbibition

In a porous medium spontaneous imbibition is a capillary pressure dominated process (Balcerak, 2012). Capillary pressure is a function of interfacial tension, rock wettability and pore radius. It is, also, related to the difference of wetting phase pressure and non-wetting phase pressure. For example, capillary pressure driven imbibition occurs when a wetting fluid such as water displaces a non-wetting fluid like oil or gas from porous space. When wetting phase and non-wetting phase move in opposite directions, the process is called counter current imbibition (**Fig. 2.6a**). When wetting phase flows in the same direction as non-wetting phase, the process is called co-current imbibition (**Fig. 2.6b**).

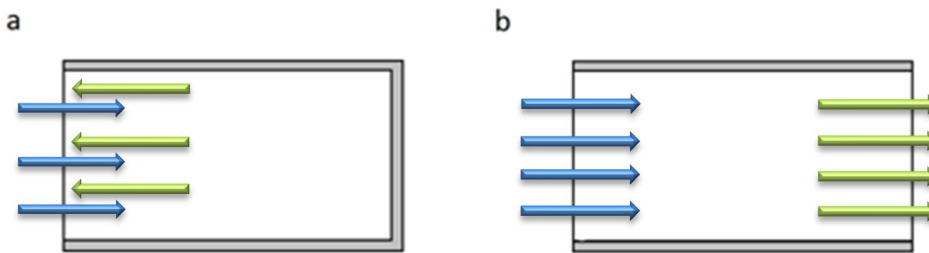


Fig. 2.6- Schematics of Counter-current (a) and Co-current (b) imbibition

The imbibition rate is strongly influenced by (1) rock properties including permeability, porosity and wettability (Mattax and KYTE, 1962); (2) fluid properties including viscosity, interfacial tension (Shouxiang et al., 1995; Li and Horne, 2002); (3) geometrical parameters such as sample shape, size and boundary conditions (Kazemi et al., 1992; Zhang et al., 1996). Extensive numerical and experimental investigations of spontaneous imbibition in oil-water-rock systems have been performed on various tight rocks (Shouxiang *et al.*, 1997; Zhang *et al.*, 1996; Schembre *et al.*, 1998; Babadagli and Hatiboglu, 2007).

However, there are few methods developed to characterize spontaneous imbibition in gas bearing rocks.

2.5.1 Handy Models

One of the earliest models of spontaneous imbibition was presented by Handy (1960). The model proposed by Handy (1960) was for water-air, co-current imbibition where volume of imbibed water was assumed to be proportional to square root of imbibition time.

$$N_w^2 = \left(\frac{2p_c \phi k_w S_{wf} A_c^2}{\mu_w} \right) t \quad (2.1)$$

where A_c and N_w are the cross-section area of the core and the volume of water imbibed into the core, respectively; ϕ is the porosity, μ_w is the viscosity of water and t is the imbibition time; k_w is the effective permeability of water, P_c is the capillary pressure, S_{wf} is usually defined as the front water saturation, when piston like displacement is assumed. The gravity effects are not considered in deriving the Handy equation.

2.5.2 Li and Horne Models

Li and Horne (2004a) used an empirical equation to scale the experimental data of water imbibition in gas-saturated rocks as a function of dimensionless time:

$$(1 - R^*)e^{R^*} = e^{t_d} \quad (2.2)$$

This equation shows the relationship between the normalized recovery (R^*) and dimensionless time (t_d), which is formulated as:

$$t_d = \frac{c^2 k k_{rw} P_c (S_{wf} - S_{wi})}{\varphi \mu_w L_c^2} t \quad (2.3)$$

Where c is the ratio of the gravity forces to the capillary forces, k is the rock permeability, k_{rw} is relative permeability, S_{wi} and S_{wf} are initial saturation and saturation behind the imbibition front, respectively. P_c is capillary pressure at S_{wf} , φ is porosity, μ_w is viscosity of water and L_c is characteristic length defined as (Ma et al., 1995):

$$L_c = \sqrt{\frac{V}{A_i/d_i}} \quad (2.4)$$

V is a bulk volume of the matrix, A_i is the area open to imbibition with respect to the i -th direction, and d_i is the distance traveled by the imbibition front from the open face to the no-flow boundary. Thus L_c compensates for different size, shape and experimental boundary conditions. The characteristic length formula was (Eq. 2.4) modified from the shape factor formula suggested by Kazemi *et al.* (1992).

2.5.3 Schmid and Geiger Models

Since analytical models heavily rely on dimensionless scaling groups, Schmid and Geiger (2012) proposed a formulation of dimensionless time for imbibition in water wet systems. Authors suggest that Handy model and subsequent attempts

following the similar approach may not be suitable for modeling spontaneous imbibition. Handy's approach is based on characterization of spontaneous imbibition by the frontal movement of the wetting phase. However authors claim spontaneous imbibition systems are best characterized by the total volume of the wetting phase imbibed rather than scaling based on the piston-like frontal movement. It was proposed that cumulative water imbibed (Q_w) is proportional to $t^{1/2}$ with characteristic parameter A that accounts for rock-fluid properties:

$$Q_w(t) = \int_0^t q_w(0, t) dt = 2At^{1/2} \quad (2.5)$$

Scaling of imbibition with \sqrt{t} was first proposed by Lucas (1918) and Washborn (1921) and has been broadly discussed in the literature (Alava, 2004; Cai and Yu, 2011; Hall, 2007; Schmid and Geiger, 2012). According to Schmid and Geiger deviations from \sqrt{t} scaling take place, first, when imbibing porous medium is not rigid enough. It occurs when fluid imbibes into paper, textile or clay-rich formations. The second reason of deviations is non-stable wetting front affected by gravity, evaporation etc.

The dimensionless group is derived from **Eq. 2.5** by relating the cumulative water phase imbibed to sample porosity, characteristic length and time:

$$t_d = \left[\frac{Q_w(t)}{\phi L_c} \right]^2 = \left[\frac{2A}{\phi L_c} \right]^2 t \quad (2.6)$$

To demonstrate the validity of the proposed version of dimensionless time, authors correlated results of 42 published experiments. These experiments were performed on different porous materials including synthetic materials, Berea sandstone and diatomite. To fit the experimental data exponential model

originally proposed by Aronosky et al., (1958) $R = 1 - e^{-\alpha t d}$ with $\alpha=70$ was applied.

2.6 Estimation of Water Loss at the Field Scale

Based on lab imbibition data, Odusina *et al.* (2011) calculated amount of water loss to the formation assuming 500 ft. symmetrical bi-wing fracture and height of 50 ft. For this geometry, it would require only 1 ft. penetration to account for 85 % of fluid loss at the field scale. Roychaudhuri *et al.* (2011) adopted the rectangular slab fracture geometry to estimate fluid loss to the formation matrix within reasonable fracture aperture sizes. Based on the lab results, authors state that spontaneous imbibition is a viable mechanism that can be responsible for major portion of water loss in the field.

Lab imbibition data can be used for rough quantification of fracturing fluid loss at the field scale (Hu *et al.*, 2010; Roychaudhuri *et al.*, 2011). However, imbibition rates at the field can be influenced by reservoir conditions including water saturation, wettability of rock-fluid systems, interfacial tension between imbibing and resident fluids, fluid viscosities, confining pressure, boundary conditions and high temperature (Li and Horne, 2006; Wang and Reed, 2009; Bennion and Thomas, 2005).

CHAPTER 3

PETROPHYSICAL CHARACTERIZATION OF SHALE CORES

This chapter provides detailed petrophysical and mineralogical analyses of shale cores from the Horn River basin. Results of wireline log analyses, XRD, Total Organic Content (TOC), porosity and contact angle measurements are presented.

3.1 Wire Line Log Interpretations

Conventional open hole logs including gamma ray, density, neutron, and array resistivity logs from wells drilled in the Horn River basin were analysed. The depths where the actual core samples collected from are marked on the well-log as shown in **Fig. 3.1**.

In Fort Simpson formation, high values of gamma ray (GR), relatively low values of Resistivity (R), and the large separation between neutron porosity (ϕ_N) and density porosity (ϕ_D) indicate the presence of brine-saturated shale. ϕ_D values are computed in sandstone unit. However, the shale matrix density, determined from XRD analysis, is higher than the sandstone matrix density. Therefore, the porosity values obtained from density log readings would be underestimated. The neutron log is sensitive to hydrogen atoms in the formation. In addition to the liquid phase, the hydroxyl groups of clay minerals contain significant number of hydrogen atoms. Therefore, the neutron log readings overestimate the shale porosity.

The same log measurements were also obtained in Muskwa formation. As the depth increases along with transition from Fort Simpson to Muskwa formation, the resistivity increases, and the separation between φ_D and φ_N decreases. Increasing resistivity and decreasing the gap between neutron and density porosity values indicate that hydrocarbon saturation increases as the formation changes from Fort Simpson to Muskwa. The presence of hydrocarbon increases the true formation resistivity. The increasing trend of φ_D and decreasing trend of φ_N indicate that the hydrocarbon phase is gas and its saturation increases with the increasing depth. Furthermore, the GR response of Muskwa formation is on average higher than that of in Fort Simpson formation. This can be explained by the presence of the organic material emitting natural gamma ray in Muskwa formation.

Log measurements in Otter Park interval show the overlap of φ_D and φ_N , and high values of resistivity, which indicate the presence of a gas-bearing shale formation. The behavior of the logs in this interval is very similar to that in the bottom of Muskwa interval.

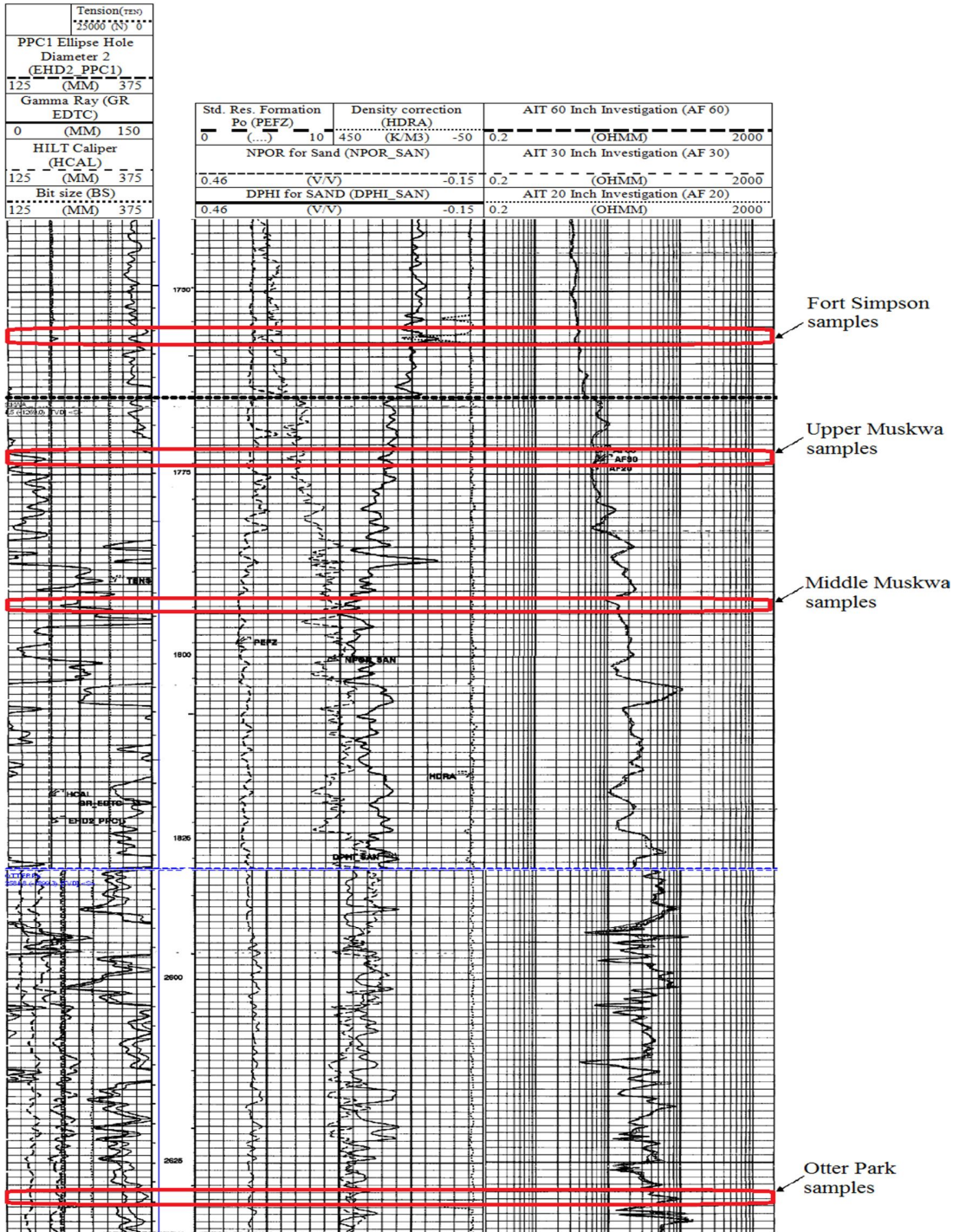


Fig. 3.1-Well Logs Recorded in Fort Simpson and the Horn River Formations and the locations of samples selected for imbibition experiment.

3.2 Total Organic Carbon (TOC) Measurement

Total Organic Carbon (TOC) of shale samples was determined by using specialized laboratory service company. Four samples representing four different depths along the well were selected for petrographical studies. **Table 3.1** shows formations, depths and TOC of selected samples. FS-group samples belong to the bottom part of the Fort Simpson formation, which is just 12 m above Muskwa formation. It is relatively young shale with very low organic content (1.7%). Two shale samples (MW1 and MW2) were taken from different depths in Muskwa deposition. In the upper zone of Muskwa formation, TOC content is only slightly higher (2.25%) than that of Fort Simpson formation. The shale samples from Middle of the Muskwa member contains up to 4% of TOC. The TOC of the shale samples from the Otter Park formation was found to be around 3%.

<u>Sample groups</u>	<u>Formation</u>	<u>Depth, m</u>	<u>TOC, %</u>
FS	Fort Simpson	1756.45	1.73
MW1	Upper Muskwa	1772.57	2.25
MW2	Middle Muskwa	1792.94	3.91
OP	Otter Park	2631.3	3.01

3.3 XRD Analysis

Mineralogical composition of the shale samples were determined by XRD analysis. Four samples representing four different depths along the well were selected for the bulk and clay XRD mineralogy analyses, which were conducted by a laboratory, specialized in rock characterization. Results of XRD analyses are presented in **Table 3.2**.

<u>Samples</u>	FS	MW1	MW2	OP
<u>Type of analysis</u>	Bulk & Clay	Bulk & Clay	Bulk & Clay	Bulk & Clay
<u>Weight %</u>	100	100	100	100
<u>Quartz</u>	35	43	61	50
<u>Plagioclase feldspar</u>	2	2	3	3
<u>Calcite</u>	0	0	0	5
<u>Dolomite</u>	0	0	0	9
<u>Pyrite</u>	4	4	7	10
<u>Clays</u>				
<u>Kaolinite</u>	1	1	0	0
<u>Chlorite</u>	27	13	0	0
<u>Illite</u>	30	36	29	23
<u>Mixed-Layer</u>	1	1	0	0
<u>Total clay</u>	59	51	29	23

The XRD analyses indicate that these shale samples consist mainly of quartz, mixture of non-swelling (illite, kaolinite) and swelling (chlorite/smectite and mixed-layer clays) clays, with moderate to minor amounts of iron sulfide (pyrite - formation cement). Amount of quartz content tends to increase with depth.

However, amount of total clay noticeably drops towards the deeper sections of the Horn River formation. Minor amount of dolomite and calcite are also present in Otter Park. Complex mineralogy greatly influence fluid flow processes in shale media and will be discussed later.

3.4 Porosity Determination

Application of standard helium porosimeter can give misleading porosity values in such a tight formation. Clarkson et al., (2012) proposed N₂ adsorption method for sample characterization based on dominant pore size distribution in tight gas reservoirs. Pore accessibility is greatly affected by the sample pore size, which is expected to be in nano-meter scale in fine grained shales. Therefore, porosities of shale samples were measured by using bulk volume and matrix volume (i.e., mass/density).

$$\emptyset = \frac{V_b - \frac{m_{ma}}{\rho_{ma}}}{V_b} \quad (3.1)$$

V_b is bulk volume of the sample, measured using Archimedes' principle. m_{ma} is sample total mass. ρ_{ma} is the matrix density of a sample, which was calculated by using the weight fractions of each mineral component as obtained from XRD analysis and their matrix density.

$$\rho_{mat} = \sum_{i=1}^n \omega_i * \rho_i \quad (3.2)$$

Where, ω_i is mass fraction of i-component, ρ_i is density of i-th component and ρ_m is matrix density of the rock sample.

Initially, shale matrix density values were calculated by using the mineral fractions given by XRD analysis. Initial matrix density values were then adjusted by considering TOC wt. fraction and density results. Density of TOC is similar to that of water (Crain, 2012) and ranges between (0.94-0.98 g/cm³). After the adjustment for TOC content, the matrix densities of shale samples were found to be varying within the range of 2.7 to 2.9 g/cm³. In total, 12 samples were selected for porosity studies. Correspondingly, averaged absolute porosity values were estimated to be varying from 6.5% to 8.7%, as shown in **Table 3.3**.

<u>Sample group</u>	<u>Formation</u>	<u>Depth, m</u>	<u>ρ g/cm³</u>	<u>\emptyset</u>
FS	Fort Simpson	1756.45	2.71	0.065
MW1	Upper Muskwa	1772.57	2.75	0.084
MW2	Middle Muskwa	1792.94	2.78	0.071
OP	Otter Park	2631.3	2.91	0.087

3.5 Contact Angle Measurements

Contact angle measurements for various rock-fluid combinations were conducted by using the droplet profile on the rock surface. Tangent line to the droplet profile from vertex point characterizes fluid contact angle against the rock surface. After capturing the droplet profile by a camera, a special software (Image J) was used to measure the contact angles. Examples of pictures used for contact angle measurements are shown in the **Fig 3.2**.

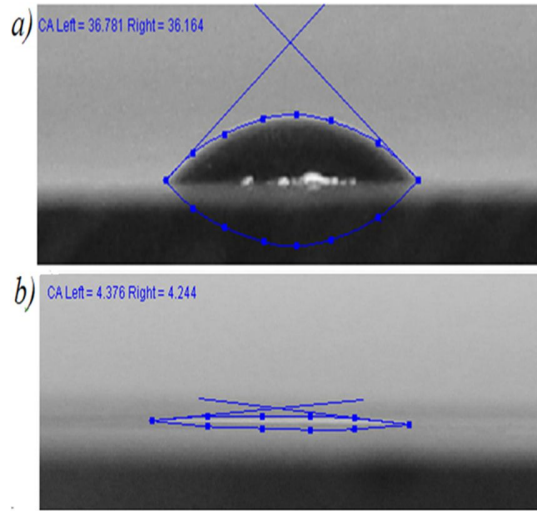


Fig. 3.2-Contact angle by *Image J* software: a- KCl brine drop profile; b-Mineral oil drop profile.

Summary of the results from contact angle measurements of 8 fluid-shale systems is presented in **Table 3.4**. The results show that the shale samples are more oil wet than water wet in all cases investigated. Otter park formation samples are slightly more hydrophobic than other samples.

Table 3.4-Static Contact Angle Measurements		
<u>Shale samples</u>	<u>2 wt. % KCl brine</u>	<u>Mineral Oil</u>
Ft. Simpson (FS)	35.6	4.2
Muskwa (MW1)	36.1	4.2
Muskwa (MW2)	36.4	4.3
Otter Park (OP)	63.1	6.4

CHAPTER 4

SPONTANEOUS IMBIBITION EXPERIMENTS

This chapter provides information on how spontaneous imbibition experiments were conducted. It describes materials used, experimental setup and procedures for conducting counter-current imbibition in the lab conditions.

4.1 Materials Used

Ten sets of imbibition fluids were prepared to examine specific factors that influence spontaneous imbibition. Water based and oil based solutions were prepared with specific formulations. Shale samples from various formation members coated with epoxy polymer were also used.

4.1.1 Imbibing Fluids

First set of experiments were conducted with fresh water. It is critical to examine effects of pure water to determine effects of additive ingredients. Therefore, resulting imbibition curves from water experiments served as benchmark and compared with other enhanced solutions.

KCl brine solution was used to mitigate clay swelling effects in shale (set-2). Imbibition rates can be influenced by clay swelling in shales. The effectiveness of KCl brine as an inhibiting agent was examined in organic and non-organic shales of the Horn River basin. The concentration of KCl salt in water was 2 % by weight. It is a common concentration that is used for the well treatment.

Both non-ionic and anionic surfactants solutions were used to examine effects of surface tension reduction. Tergitol 15-S-7, a Secondary Alcohol Ethoxylate (AE)

and Sodium Dodecylbenzenesulfonate (DDBS) represented non-ionic and anionic surfactants respectively. Critical Micelle Concentrations (CMC) was selected as the optimum surfactants concentrations in both cases. Combined salt/surfactant solutions were prepared by first adding surfactants to fresh water and then, adding 2 wt. % KCl. Thus four sets of fluid systems were created:

- non-ionic (AE) and fresh water (set-3);
- anionic (DDBS) and fresh water (set-4);
- non-ionic (AE) and 2 wt. % KCl brine (set-5);
- anionic (DDBS) and 2 wt. % KCl brine (set-6).

Xanthan Gum (XG) polymer was used to examine the effect of viscosity on imbibition rates. Two different concentrations of XG polymer in the solutions were prepared as: i-) 1 g of XG polymer in 350 ml of water, which is 0.28 wt. % (set-7); ii-) 2 g of XG polymer in 350 ml of water, which is 0.56 wt. % (set-8).

Viscosity of XG solutions was determined at the specific shear rate at 0.01 s^{-1} .

Imbibition of oleic phase was also examined by using two sets of fluids: i-) Kerosene (set-9); ii-) Mineral Light Oil (set-10). Density and surface tension of oleic base fluids varied slightly. The viscosity values, however, were significantly different. Physical properties of all the fluids used in imbibition experiments are summarized in **Table 4.1**.

Set #	Fluids	ρ (g/cc)	μ (cP)	σ (N/m)
1	DI Water	0.998	1	0.072
2	2 wt. % Brine	1.015	1	0.074
3	Tergitol+DI	0.998	1	0.029
4	DDBS+DI	0.998	1	0.035
5	Tergitol+brine	0.998	1	0.029
6	DDBS+brine	0.998	1	0.028
7	XG (0.28 wt.%)	0.987	47500	0.073
8	XG (0.56 wt.%)	0.993	252000	0.075
9	Kerosene	0.81	2.5	0.03
10	Mineral oil	0.85	24	0.028

4.1.2 Epoxy Seal

Impermeable epoxy polymer was used to coat the samples. The rock face parallel to the bedding plane was exposed to the fluid while the other surfaces were covered by epoxy to make sure that fluid could imbibe only through designated shale surface. The similar procedure was used for the imbibition experiments, where the open face exposed to imbibition was orthogonal to the bedding plane.

4.2 Shale Samples

Small samples. Shale samples were cut into rectangular shapes and coated with impermeable epoxy all around except one flat face open for imbibition. This is to ensure fluid could imbibe only through designated shale surface. **Fig. 4.1** illustrates pictures of epoxy covered shale samples.

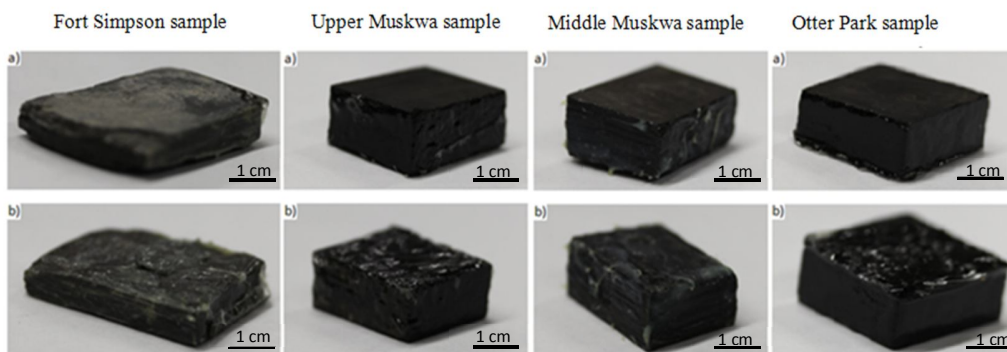


Fig. 4.1-Photopictures of shale samples: a-surface open to imbibition; b-reverse sides covered by epoxy.

Because the influx of water and the out flux of gas occur in the opposite direction, these samples are designed to represent counter-current imbibition.

Large samples. The samples were covered with epoxy polymer the same way as small samples. However, sample geometry differs from the small sample shape (**Fig. 4.2**).

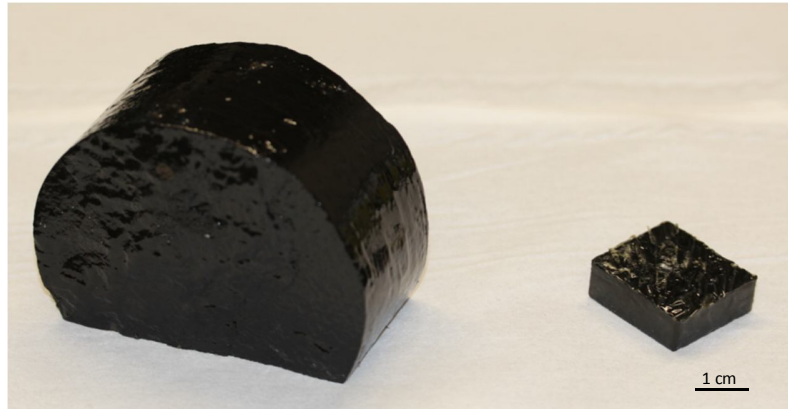


Fig. 4.2-Comparative pictures of large and small shale samples covered by epoxy all over except one designated surface.

Physical characteristics of each group of shale samples are shown in **Table 4.2**.

Imbibing fluids	<i>Fort Simpson</i>			<i>Upper Muskwa</i>			<i>Middle Muskwa</i>			<i>Otter Park</i>		
	Sample names	Area, A_i , cm ²	Volume, V_i , cm ³	Sample names	Area, A_i , cm ²	Volume, V_i , cm ³	Sample names	Area, A_i , cm ²	Volume, V_i , cm ³	Sample names	Area, A_i , cm ²	Volume, V_i , cm ³
DI Water	FS-1	20	151.3	MW1-1	11.2	96.8	MW2-1	28	199.8	OP-1	24	181.6
2% KCl Brine	FS-2	15.2	115	MW1-2	15.3	108.9	MW2-2	15.3	108.9	OP-2	38.3	272.4
2% KCl Brine	FS-2a	65.4	121	MW1-2a	65.4	133	MW2-2	65.4	139	OP-2a	65.4	151
Tergitol+DI	FS-3	22.9	163.5	MW1-3	26.4	187.7	MW2-3	11.2	96.8	OP-3	46.7	333
DDBS+ DI	FS-4	9.1	78.5	MW1-4	25.5	181.6	MW2-4	28.7	211.9	OP-4	46.7	333
Tergitol+brine	FS-5	17.8	127.2	MW1-5	24.6	175.6	MW2-5	31.2	230	OP-5	32	242.2
DDBS+ brine	FS-6	19.5	139.3	MW1-6	18.7	133.2	MW2-6	13.5	108.9	OP-6	34	242.2
XG-0.28 wt.%	FS-7	11.9	102.9	MW1-7	21.3	151.3	MW2-7	10.5	90.8	OP-7	40	302.7
XG-0.56 wt. %	FS-8	12.6	108.9	MW1-8	26.4	199.8	MW2-8	25.5	181.6	OP-8	40	302.7
Mineral oil	FS-9	22.1	157.4	MW1-9	30.6	217.9	MW2-9	30	302.7	OP-9	42.5	302.7
Kerosene	FS-10	8.8	78.7	MW1-10	18	121.1	MW2-10	12	121.1	OP-10	40	302.7
DI Water	FS-1s	3.6	3.6	MW1-1s	9	9	MW2-1s	7.35	7.35	OP-1s	11	11.2
2% KCl Brine	FS-2s	4.3	12.9	MW1-2s	9.8	13.7	MW2-2s	8.75	12.25	OP-2s	9.9	9.9

Due to the layered nature, the shale samples present strong structural anisotropy.

Fig. 4.3 illustrates the possible orientations of rock/fluid contact surfaces with respect to direction of bedding plane and how these surfaces can be positioned within the fractures encountered in a typical hydraulically fractured horizontal well.

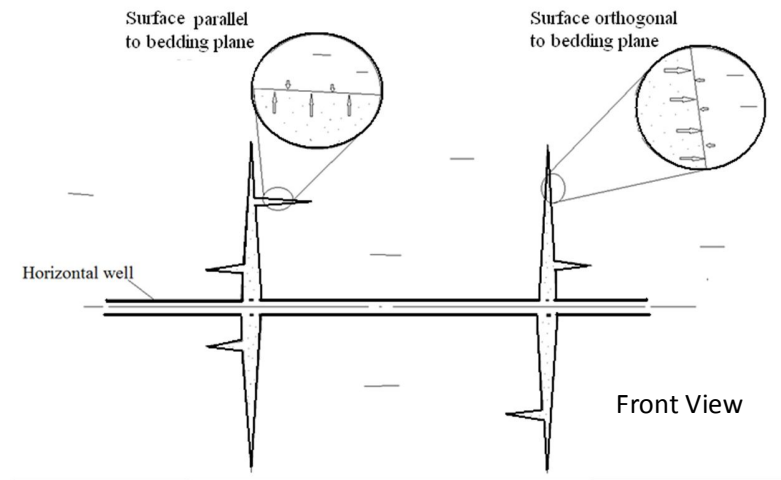
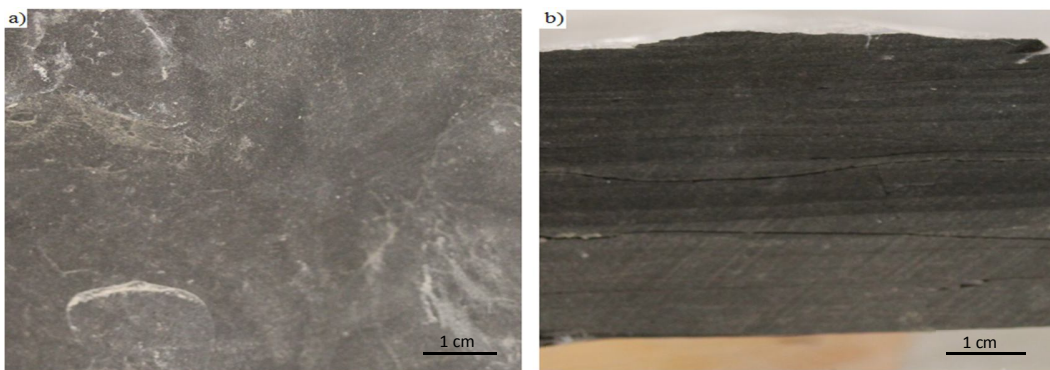


Fig. 4.3- Orientation of rock/fluid contact surface area with respect to bedding plane and how it might relate to actual fractures in hydraulically fractured horizontal well.

Since the Horn River formation samples are clay rich and extracted from deeply buried formations, they are subject to directional anisotropy. **Fig. 4.4** illustrates the photos of actual core samples obtained from Fort Simpson, Muskwa and Otter Park formations where the structural differences of the surfaces parallel vs. orthogonal to the bedding plane are clearly visible. In all cases the rock surfaces orthogonal to the bedding plane are clearly layered and show vertically heterogeneous structure. Micro fractures parallel to the bedding plane direction are observed in the pictures.



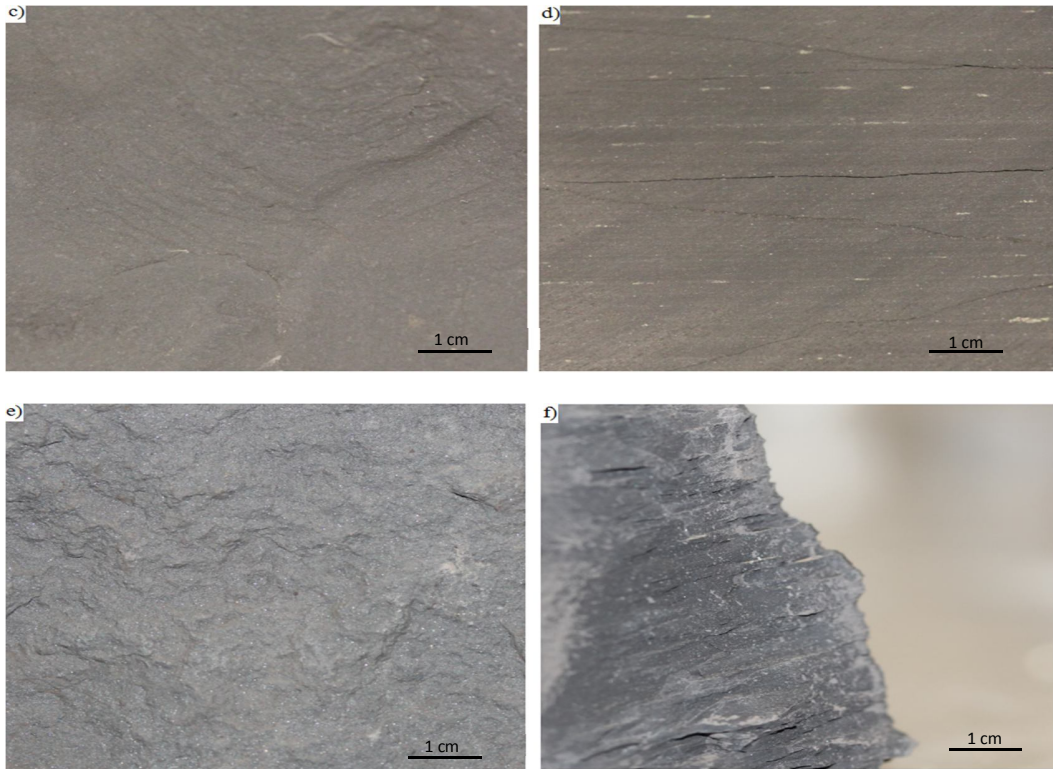


Fig. 4.4-Images of rock samples indicating directional anisotropy: a-Fort Simpson Formation, surface parallel to bedding plane; b-Fort Simpson Formation, surface orthogonal to bedding plane; c-Muskwa Formation, surface parallel to bedding plane; d-Muskwa Formation, surface orthogonal to bedding plane; e-Otter Park Formation, surface parallel to bedding plane; f-Otter Park Formation, surface orthogonal to bedding plane.

4.3 Experimental Setup

An experimental set-up was designed to measure the change in sample weight as a function time. The accurate measurement of mass change was determined by analytical balance with readability of 0.0001g. The obtained data was automatically transmitted to the computer using Wedge Link software package.

The weight change with time data was recorded and plotted in MS Excel program.

The schematic of experimental set-up is illustrated on the **Fig. 4.5**.

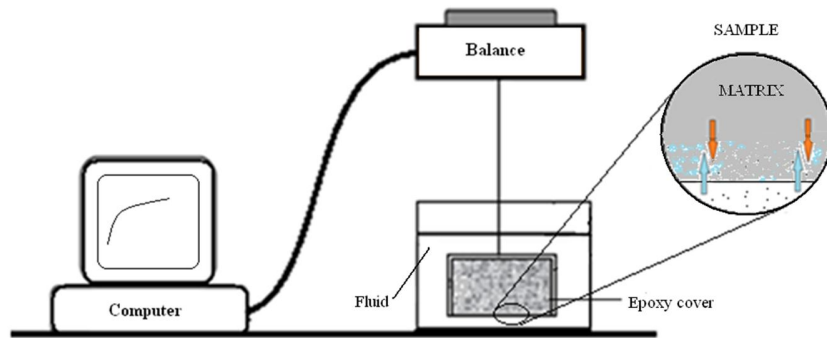


Fig. 4.5-Schematic of set-up used for counter-current imbibition experiments.

4.4 Experimental Procedure

We have worked with actual core samples collected from the Horn River basin, North-East of British Columbia. When the shale surface touches a wetting liquid, the liquid will spontaneously imbibe into pores and displace non-wetting phase under the force of capillary pressure.

4.4.1 Sample Preparation Procedure

Due to the high vertical heterogeneity, samples were chosen from the similar depths. In addition, samples were carefully selected to avoid any visual microfractures on the sample surface. Each shale sample has been used only once during the experiments.

4.3.2 Core Imbibition Procedure

Procedure for spontaneous, counter-current imbibition experiments is as follows:

- The shale sample was cleaned and dried in the oven at 105 °C for 24 hours or until there is no further weight loss.
- Initial weight, surface area and volume of samples were measured prior to the experiments.
- The shale sample was sealed with epoxy all around except one face open for imbibition.
- The shale sample was connected to an electronic balance by a thread and submerged to the test fluid.
- As test fluid imbibed into the pores, the change of shale sample weight with time was recorded.
- Mass of fluid imbibed was calculated by subtracting the initial mass of the shale sample from mass of the shale samples measured instantaneously. Knowing the density of the imbibing fluid, the volume of the imbibed fluid was estimated.
- Normalized imbibed volume was calculated as the volume of fluid (cm³) that passed through unit area (cm²) of rock face open to the flow.
- Cumulative normalized imbibed volume was recorded and plotted against square root of time (SQRT).

CHAPTER 5

IMBIBITION EXPERIMENTS: RESULTS AND DISCUSSION

This chapter presents results and detailed discussions of imbibition experiments. It also explains the effect of fluid and shale properties on the observed imbibition behaviour.

5.1 Imbibition of Aqueous Solutions

Results of imbibition tests using fresh water, brine, aqueous surfactants, and aqueous polymer solutions are presented in this section.

5.1.1 Fresh Water Imbibition Tests

Fig 5.1 shows normalized volume data for deionized water imbibition into shale samples versus square root of time. Fresh water imbibition volume was much higher in Fort Simpson (FS) samples than that of Muskwa and Otter Park samples. As seen from XRD analyses, Fort Simpson formation is richer in clay content than Muskwa and Otter Park samples. Higher water intake rate in Fort Simpson formation can be explained by the fact that negatively charged clay layers adsorb polar water molecules. It creates water adsorption force, which causes an additional driving force for capillary pressure driven suction.

Another explanation is related to clay swelling and micro fracture generation. Depending on the mineral type, clays swell when contact with water (Caenn *et al.*, 2011). It is a common phenomenon in drilling engineering, when reactive shales

are drilled with water based mud (Boek *et al.*, 1995;; Anderson *et al.*, 2010). Clay swelling or expansion causes disintegration of sample structure and generation of micro fractures along the lamination. Created micro fractures significantly increase sample permeability and initial pore volume.

Importantly, there are two distinct slopes in imbibition data of DI water in Fort Simpson samples. In region (1), the higher slope indicates the water imbibition into micro fractures until water front reaches the end of the sample. Permeability of micro fractures significantly higher than that of matrix, which results in rates of fluid influx (indicated by higher slope) at initial times. In region (2), the lower slope indicates the water imbibition from micro fractures to the ultra-low permeability matrix. Similar behavior also reported by Roychaudhury *et al.*, (2011). The lower slope of water imbibition at later periods can be explained by the very low permeability values in matrix pores ranging in nano Darcy scale. However, in Muskwa and Otter Park samples, we observe only the region (2), which represents fluid imbibition into shale matrix.

Apart from the mineralogy, the organic content may also influence imbibition rate. Wang *et al.*, (2009) reported that organic matter could inhibit advance of aqueous front in porous media. TOC measurements and the log analyses indicate that organic material content in Muskwa and Otter Park formation is higher than that in Fort Simpson formation. This may be another reason why low imbibition rates were observed in Muskwa and Otter Park formation in comparison to Fort Simpson formation. The absolute porosity values are noted to be very similar among all the samples tested, therefore, porosity is not likely to be the reason for

the differences seen in spontaneous imbibition results for Fort Simpson, Muskwa and Otter Park formations.

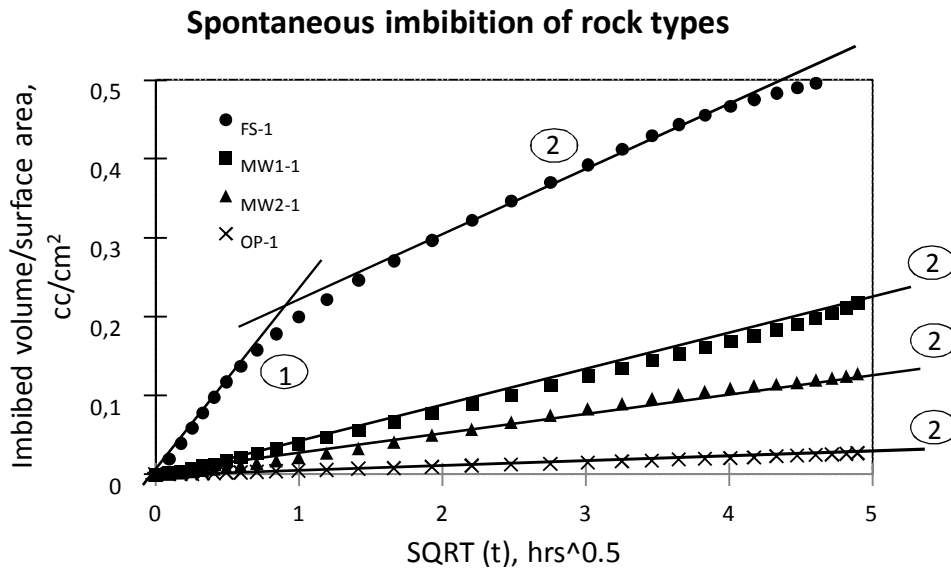
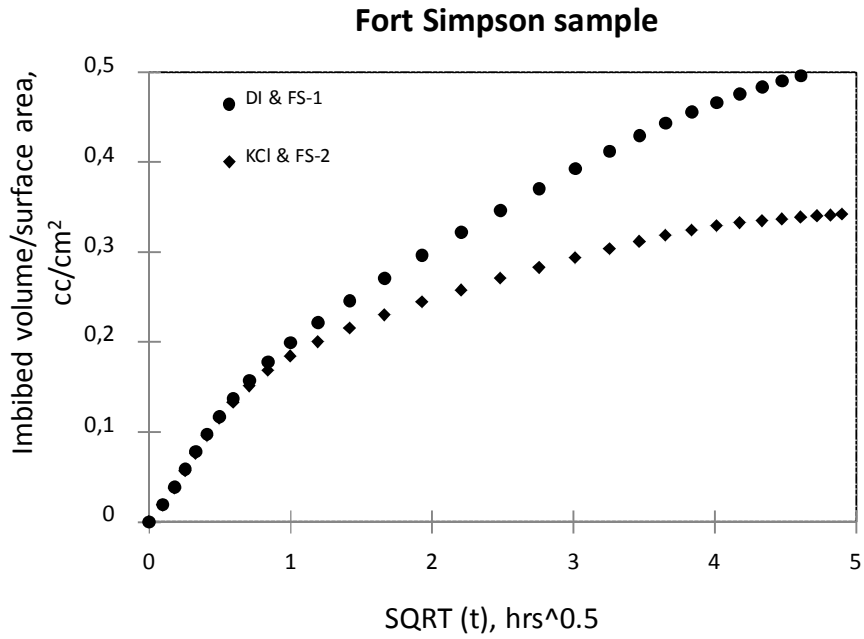


Fig 5.1-Spontaneous imbibition curves of different rock types

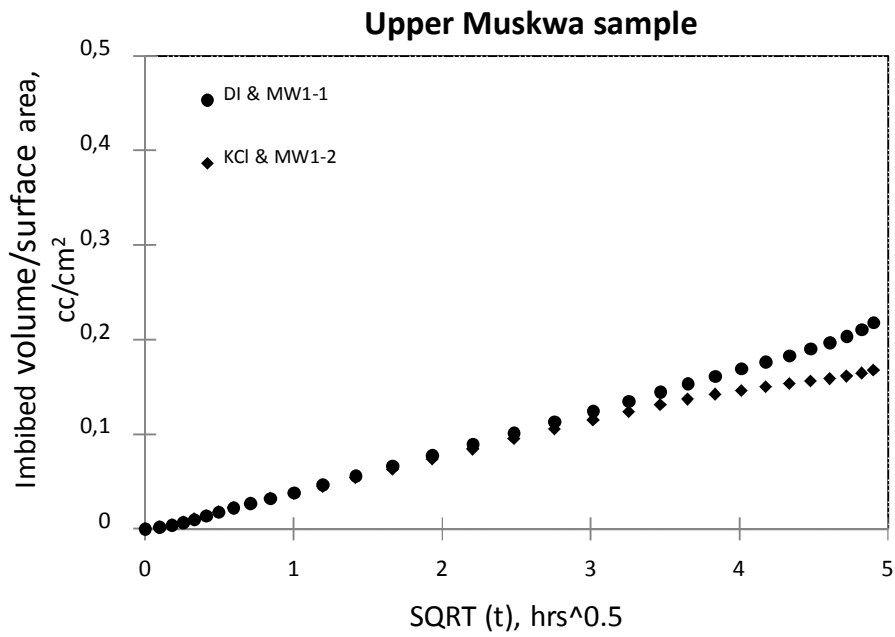
5.1.2 Effects of Brine Solution Imbibition

The effect of salinity on imbibition process was examined with 2 % wt. KCl brine solution. Fig. 5.2 shows comparative imbibition curves of fresh water and brine solutions. As seen in Fig. 5.2 (a) KCl brine reduces imbibition rate in Fort Simpson samples and the gap between fresh water and brine solution intake rates significantly increases with time. The imbibition rate of KCl brine in clay rich shale is higher than that of fresh water. According to XRD results, clay content in Fort Simpson samples reaches up to 59 % as compared to 29 % and 23 % in Muskwa and Otter Park formation samples. Due to the specific behavior of potassium ion (known as Potassium Fixation), KCl brine prevents excessive water intake of shale clay layers (Caenn *et al.*, 2011; Anderson *et al.*, 2010). In Muskwa

and Otter Park samples (Fig. 5.2 b, c, and d), the effect of KCl salt is considerably less compared to Fort Simpson samples. It indicates that the effect of KCl salt is limited in shales with less clay content (Fig. 5.2d).

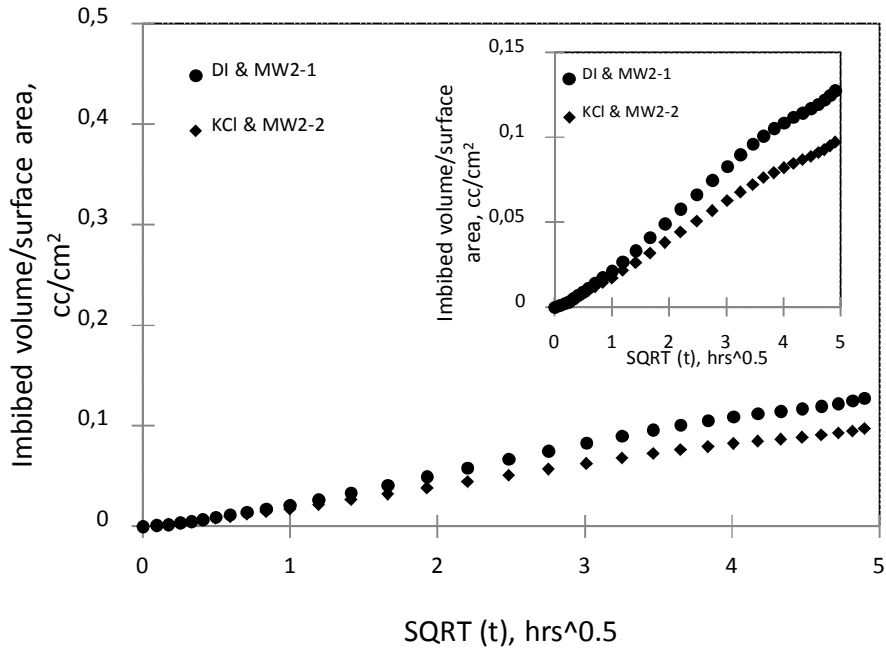


a)



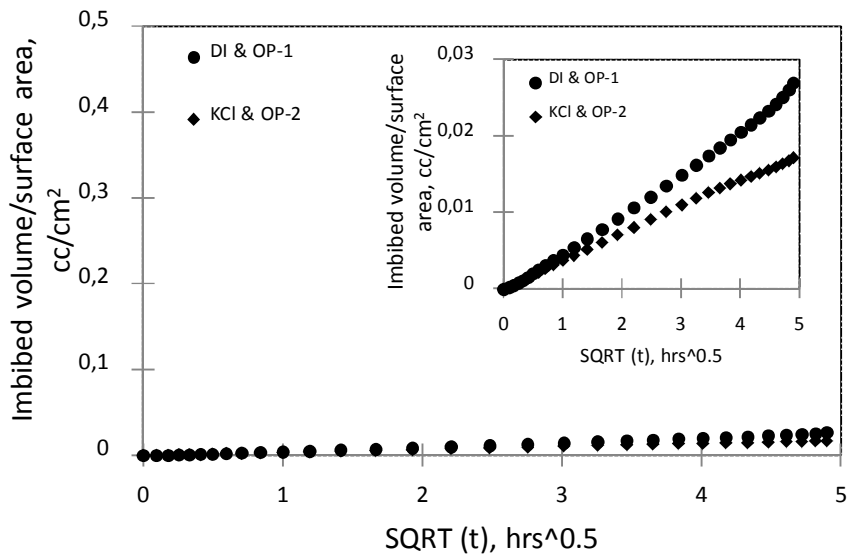
b)

Middle Muskwa sample



c)

Otter Park sample



d)

Fig. 5.2- Effect of Salinity on imbibition of various shale samples: a-Fort Simpson; b-Upper Muskwa; c-Middle Muskwa; d-Otter Park.

5.1.3 Effects of Surfactant Solutions Imbibition

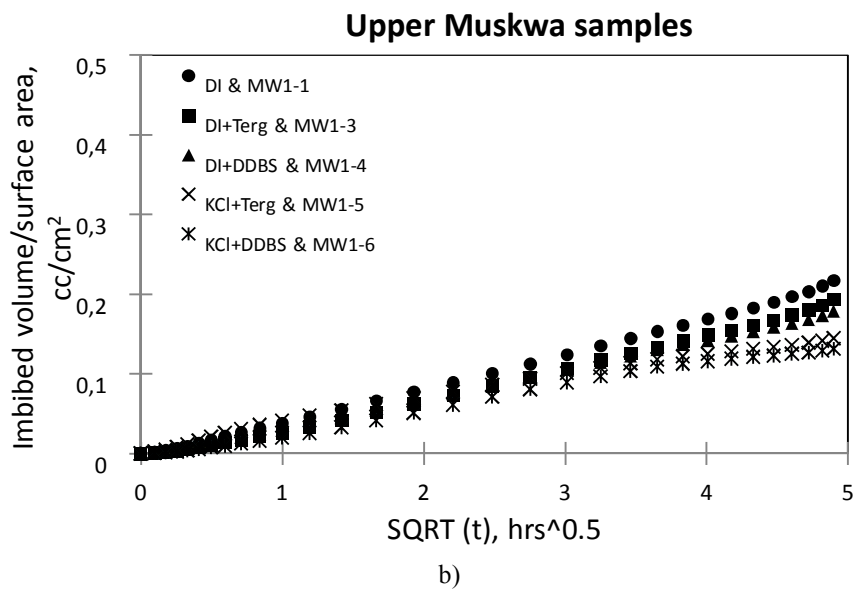
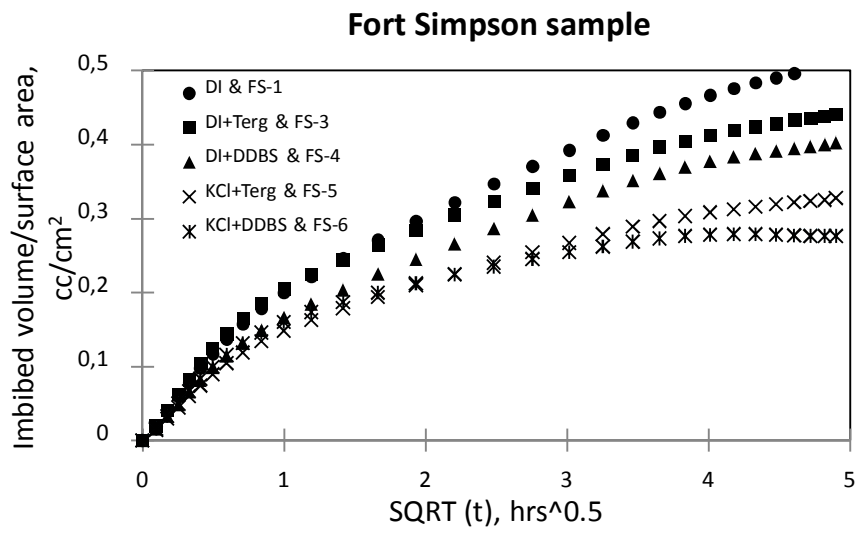
The effects of surfactant on the imbibition rate were examined by using DI water 2wt. % KCl brine and several surfactants solutions. **Fig. 5.3** shows how the use of surfactants affects imbibition rates into various shale samples. The general trend shows that imbibition rate of pure water is greater than that of the surfactant solutions both in organic and non-organic shales. Addition of surfactants reduce the interfacial tension between wetting phase and non-wetting phases in porous media, which in turn, causes reduction in capillary pressure as the major driving force for the imbibition. Therefore, use of surfactant solutions generally reduces the rate of imbibition into the shale formations. As shown in **Table 4.1**, all four sets of surfactant solutions have significantly low surface tension values. While all surfactant solutions tend to decrease imbibition rate (Lakia *et al.*, 2011), some are more effective than others in a shale media.

Nonionic Tergitol (AE) surfactant results in slightly higher imbibition rates than anionic DDBS in Fort Simpson samples. This tendency remains the same in both cases where fresh water and brine solution are used as base fluids. Even though nonionic Tergitol (AE) has lower surface tension values than DDBS in fresh water, it still has higher imbibition rates. It indicates that imbibition is affected not only by capillary pressure change, but also by the electrostatic properties of rock and fluid systems. Commonly, shale surface is negatively charged and can cause an electrostatic repulsion of negatively charged anionic surfactants (Muherei *et*

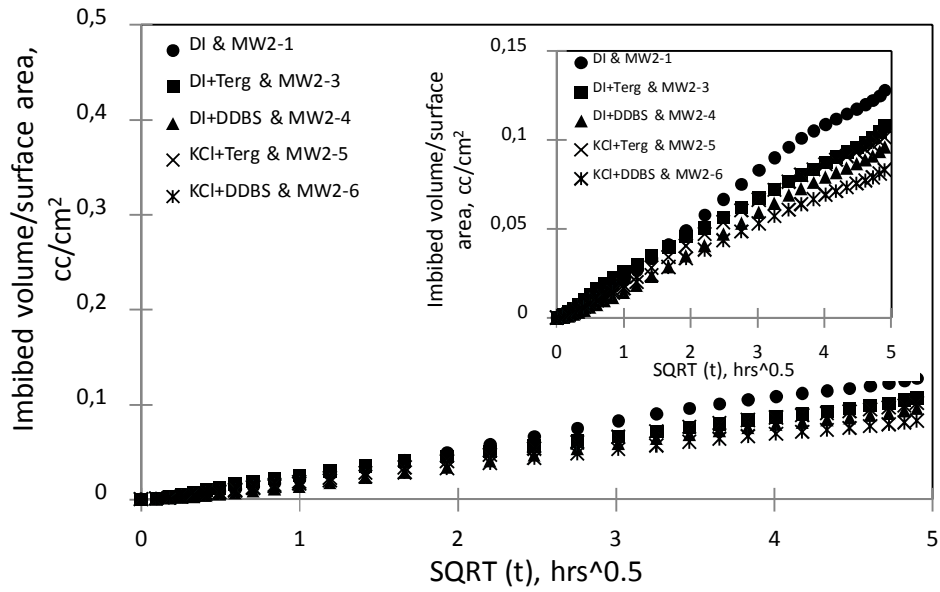
al., 2009; Blatt *et al.*, 1996), which could decrease overall adsorption of surfactant solutions on the clay surface.

In addition, DDBS surfactant in brine solution results in the lowest imbibition rate of all four cases. Imbibition rate is further reduced when 2 wt. % KCl brine is added to anionic surfactant solutions. **Table 4.1** shows that combination of KCl brine with DDBS solution results in further reduction of the surface tension. While non-ionic Tergitol surfactant show reaction to salt addition. Takaya *et al.* (2005) observed that addition of KCl salt decreases electrostatic repulsion among surfactant molecules which causes accumulations of surfactants at the interface. Thus greater amount of surfactants at the interface causes, first, further decrease of surface tension and second, higher electrostatic repulsion between anionic surfactants and shale clay surface. As a consequence, the lowest imbibition rates are observed among all four types of surfactants solutions.

Muskwa and Otter Park formation samples expresses linear dependence with square root of time with surfactants solutions. However, the deeper sections of Muskwa and Otter Park formations imbibition data show only slight difference among aqueous fluids (**Fig. 5.3 c & d**).

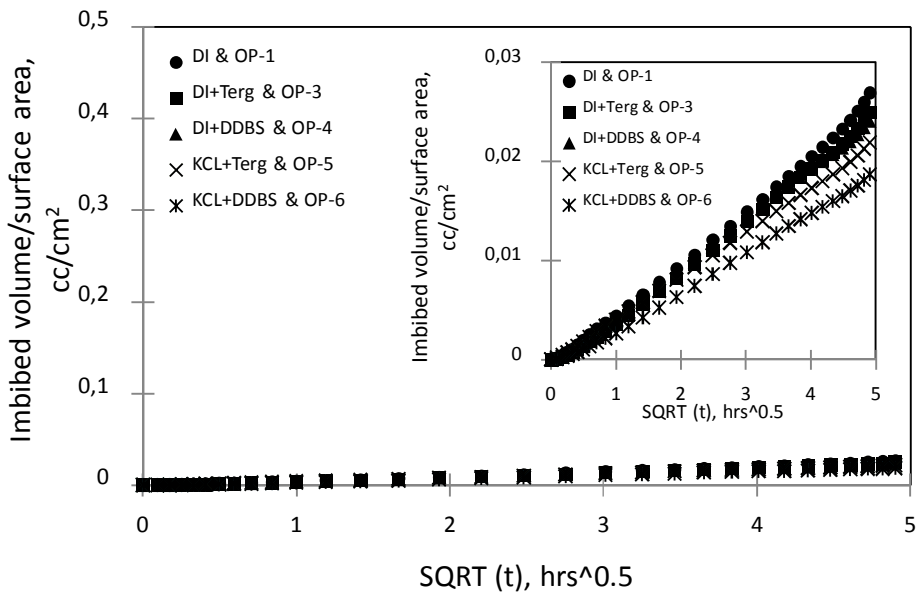


Middle Muskwa samples



c)

Otter Park samples



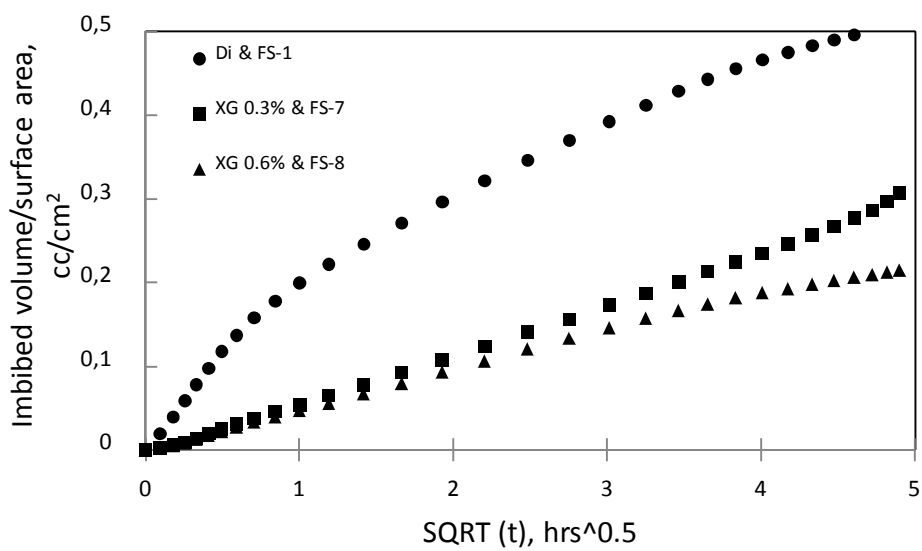
d)

Fig. 5.3- Imbibition of surfactants solutions in various shale samples: a-Fort Simpson; b-Upper Muskwa; c-Middle Muskwa; d-Otter Park.

5.1.4 Effects of Xanthan Gum Polymer Solutions Imbibition

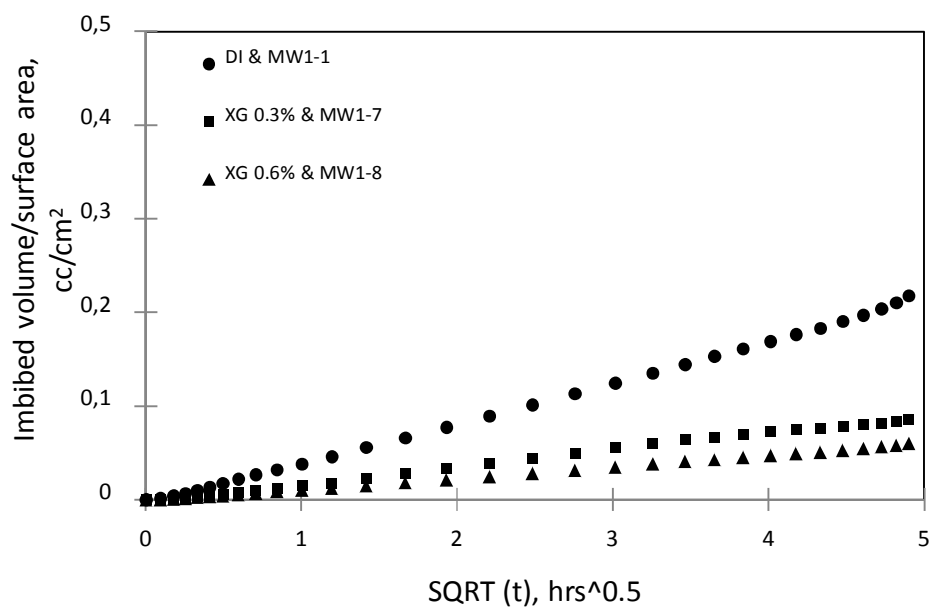
As shown in **Table 4.1**, increase in XG polymer concentration increases the viscosity of water. The effects of viscosity on phase mobility and imbibition characteristics are extensively described in the literature (Zhou *et al.*, 2002; LaFollette, 2010; AlQuraishi *et al.*, 2012). Effect of fluid viscosity on imbibition rate was examined by using aqueous polymer (XG) solutions of 1g/350 ml (0.28 wt.%) and 2g/350 ml (0.56 wt.%) concentrations. Fresh water imbibition results were used as benchmark to compare the imbibition rate observed when using polymer solutions. As shown in **Fig.5.4**, imbibition rate of XG polymer solution was lower than that of pure water in all cases. However, increasing the polymer concentration from 0.28 wt.% to 0.56 wt.% decreases the imbibition rate only slightly. This observation shows that solution viscosity does not have much impact on imbibition rate of XG solution, because water molecules are preferentially adsorbed. Largest separation of imbibition data was observed in Fort Simpson shale (**Fig.5.4a**), while Muskwa and Otter Park samples demonstrate very similar results for both polymer concentrations (**Fig. 5.4 -b, c and d**).

Fort Simpson samples



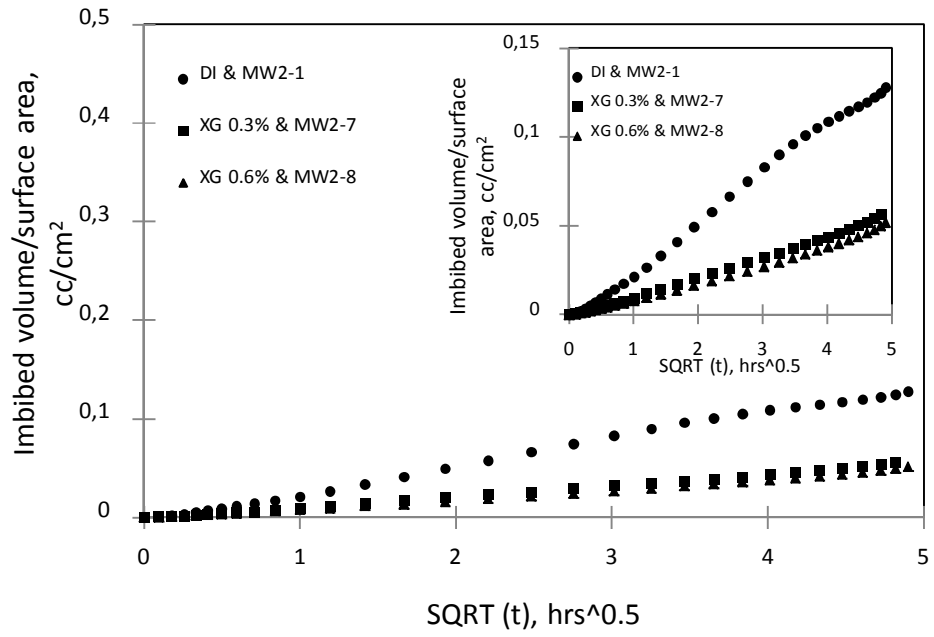
a)

Upper Muskwa samples



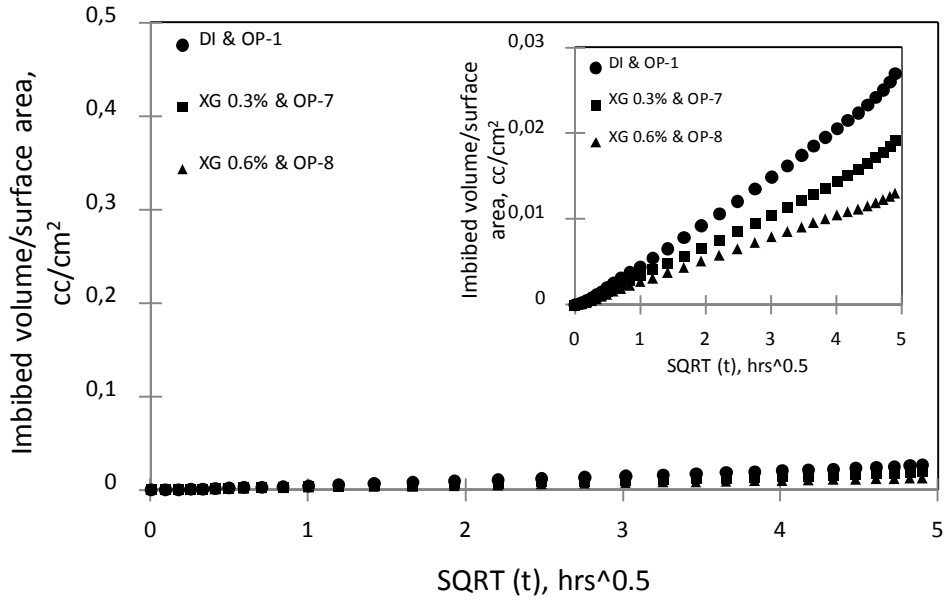
b)

Middle Muskwa samples



c)

Otter Park samples



d)

Fig. 5.4- Effects of viscosity on imbibition of various shale samples: a-Fort Simpson; b-Upper Muskwa; c-Middle Muskwa; d-Otter Park.

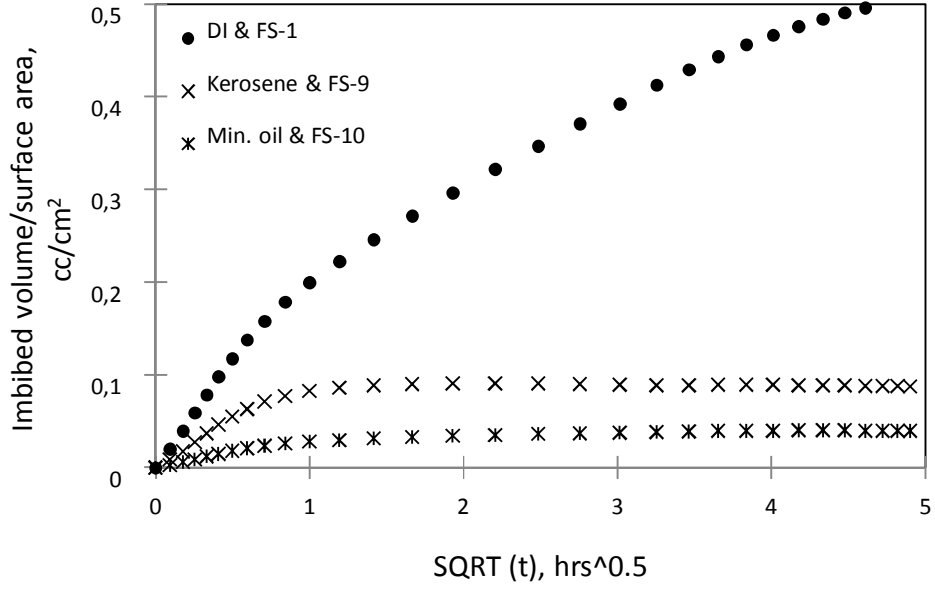
5.2 Imbibition of Oleic Phase

Kerosene and Mineral oil were used for investigating the imbibition of oleic phase into shales. As shown in **Fig. 5.5**, both Kerosene and Mineral oil had significantly lower imbibition rates compared with fresh water. The imbibition rate of oleic phase into Fort Simpson formation samples (**Fig. 5.5a**) is significantly higher than that in the Muskwa and Otter Park shales (**Fig.5.5 b, c and d**).

In organic rich shales (Muskwa and Otter Park) imbibition rates of kerosene seems to be slightly higher than that of mineral oil, which could probably be explained by the fact that kerosene viscosity is less than that of mineral oil.

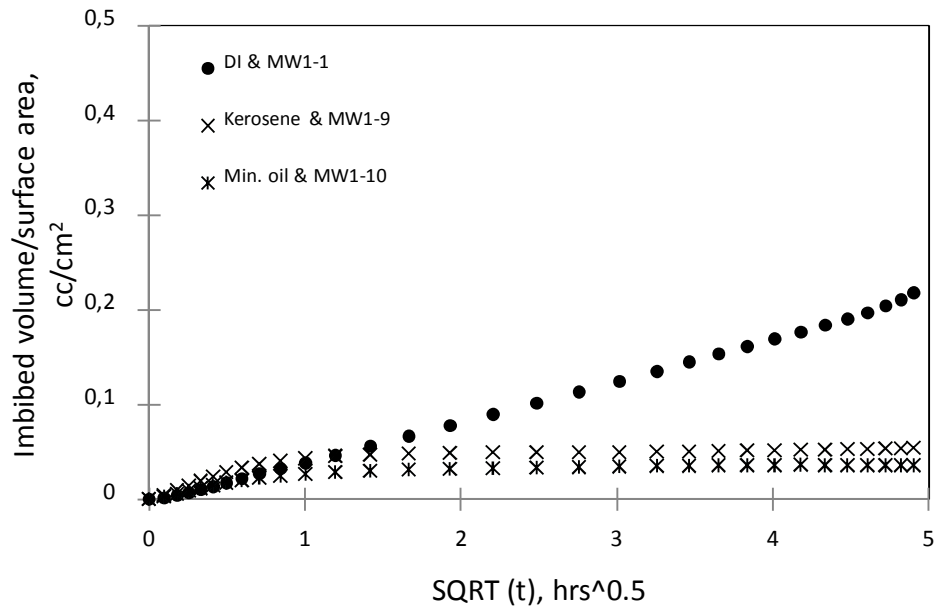
Earlier contact angle measurements (both on bulk and crushed powdered shale samples) showed that the shales under investigation were more oil wet than water wet. However, despite the favorable wettability condition, both kerosene and mineral oil show low imbibition values compared with fresh water. These results suggest that the total amount of water intake might not solely be due to capillarity. Other effects might be present such as adsorption of water molecules by clays. Water adsorption depends on rock mineralogy and water salinity. Similar studies conducted on Barnett, Eagle Ford, and Floyd shale samples showed that water imbibition rate is higher than oil imbibition rate (Odusina *et al.*, 2011).

Fort Simpson samples



a)

Upper Muskwa samples



b)

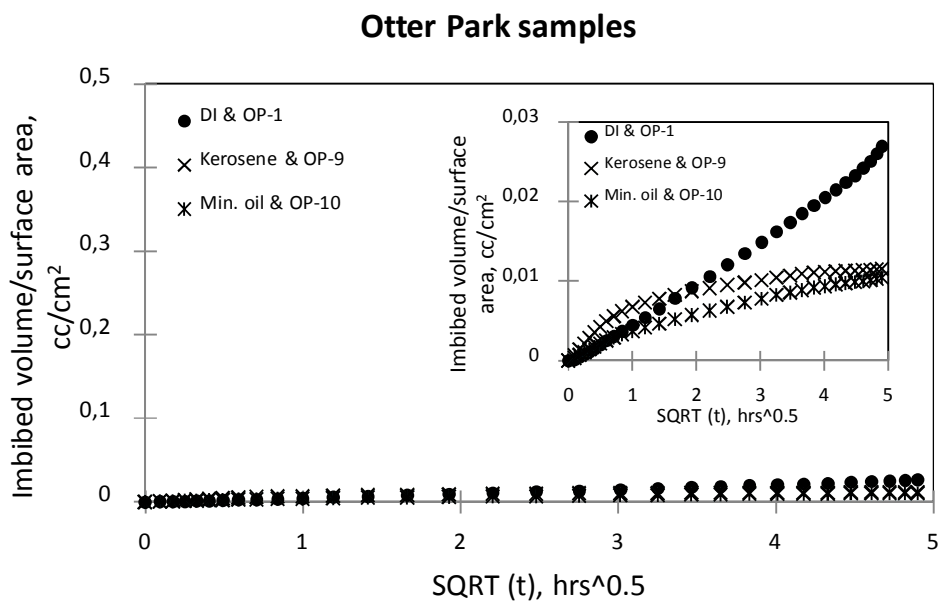
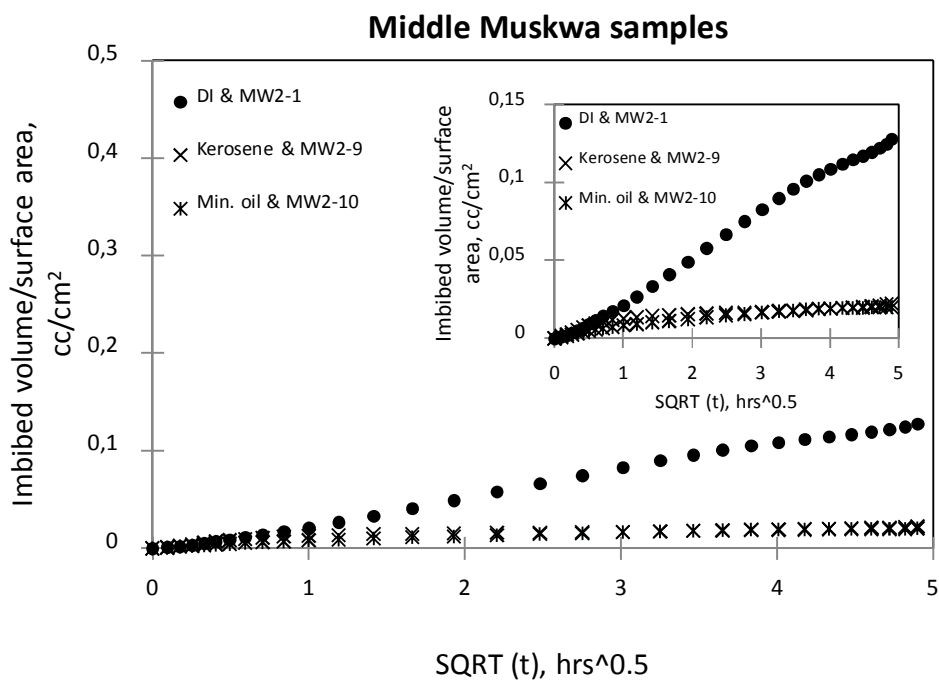
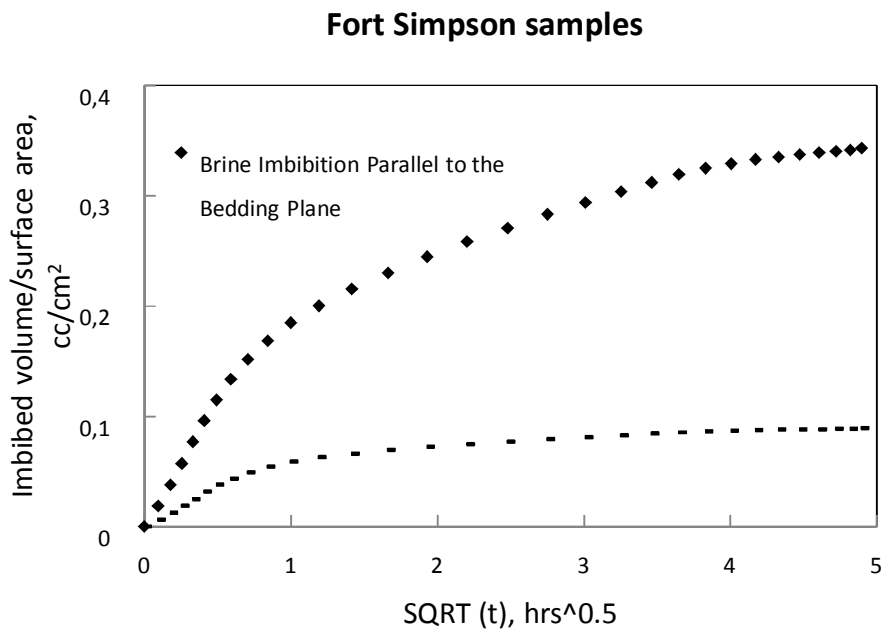


Fig. 5.5-Imbibition of aqueous and oleic fluids in shale samples: a-Fort Simpson; b-Upper Muskwa; c-Middle Muskwa; d-Otter Park.

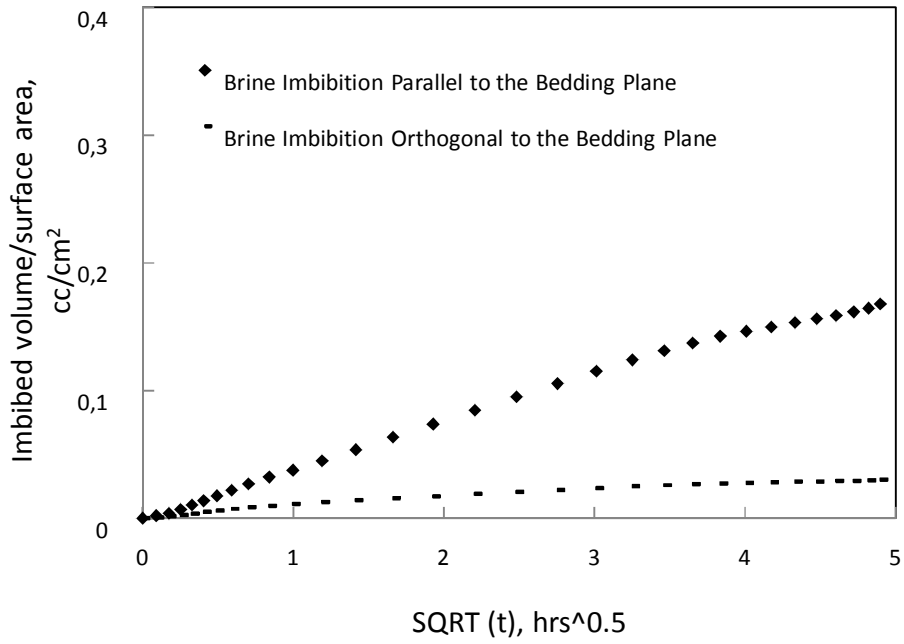
5.3 Anisotropy in Shale Samples

We have conducted several imbibition experiments to see if the orientation of rock-fluid contact surface with respect to bedding plane has any bearing on the imbibition rate. These experiments were conducted using KCl 2 wt. % solution only. **Figs. 5.6** shows brine imbibition data in parallel to bedding plane direction (in the plots shown as KCl) and orthogonal to the bedding plane direction (in the plots shown as KCl ax.) in for Fort Simpson, Upper Muskwa, Middle Muskwa and Otter Park samples, respectively. In case of Fort Simpson (**Fig. 5.6a**), the imbibition rate through the rock surface orthogonal to bedding plane is significantly higher than that through the rock surface parallel to the bedding plane. In deeper sections of the Horn River formation, the difference between imbibed volume of brine per unit surface area in directions parallel and orthogonal to the bedding plane decrease significantly.



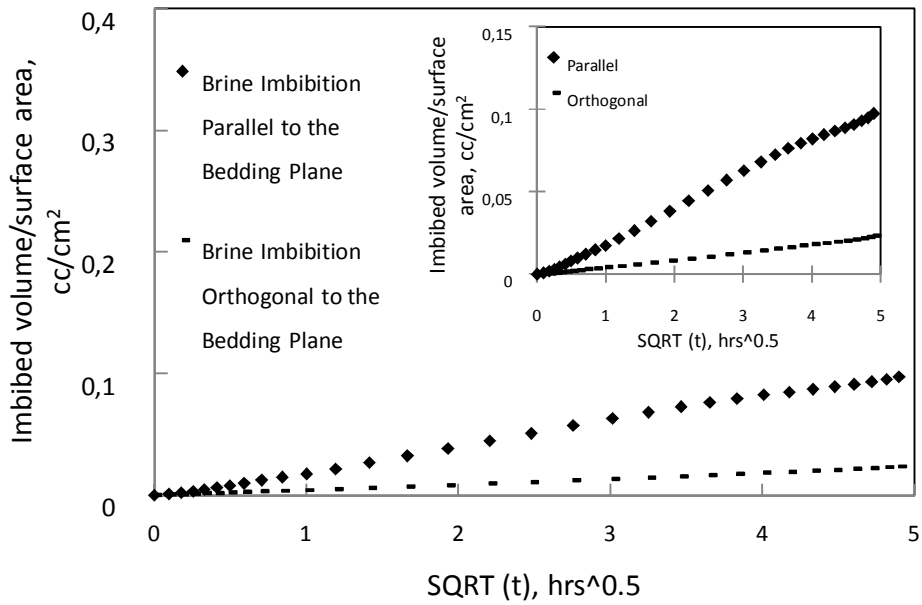
a)

Upper Muskwa samples



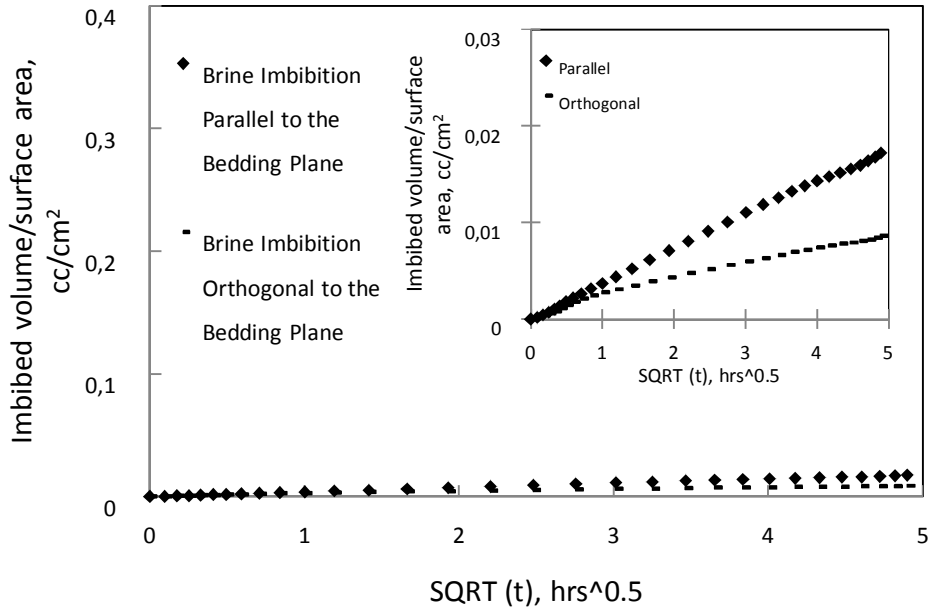
b)

Middle Muskwa samples



c)

Otter Park samples



d)

Fig. 5.6-The effect of anisotropy on spontaneous imbibition rate: a-Fort Simpson formation sample; b-Upper Muskwa formation samples; c-Middle Muskwa formation samples; d-Otter Park formation samples.

Effects of directional anisotropy on spontaneous imbibition were studied using anisotropy index. It is measured based on the amount of brine intake after 24 hours of imbibition experiments. Anisotropy index is calculated for each group of samples using **Eq. 5.1** and ranges from 0 to 1. If the calculated index equals to 0 there is no difference between the volume imbibed parallel to the bedding plane and volume imbibed orthogonal to the bedding plane. The calculation method is adopted from Moseley *et al.* (1990) and modified as following:

$$I_A = \frac{V_{wp} - V_{wo}}{V_{wp}} = 1 - \frac{V_{wo}}{V_{wp}} \quad (5.1)$$

Where V_{wp} is volume of water imbibed parallel to the bedding plane and V_{wo} volume of water imbibed orthogonal to the bedding plane.

Fig. 5.7 shows degree of directional anisotropy with depth. Results show the anisotropy index decrease with depth. The highest index belongs to the samples from Upper Muskwa and the lowest index belongs to the samples from Otter Park member. The layering nature of shales due to the significant clay content and degree of compaction (Li, 2006; Sondergeld *et al.*, 2010), can significantly contribute to directional anisotropy effects in our samples.

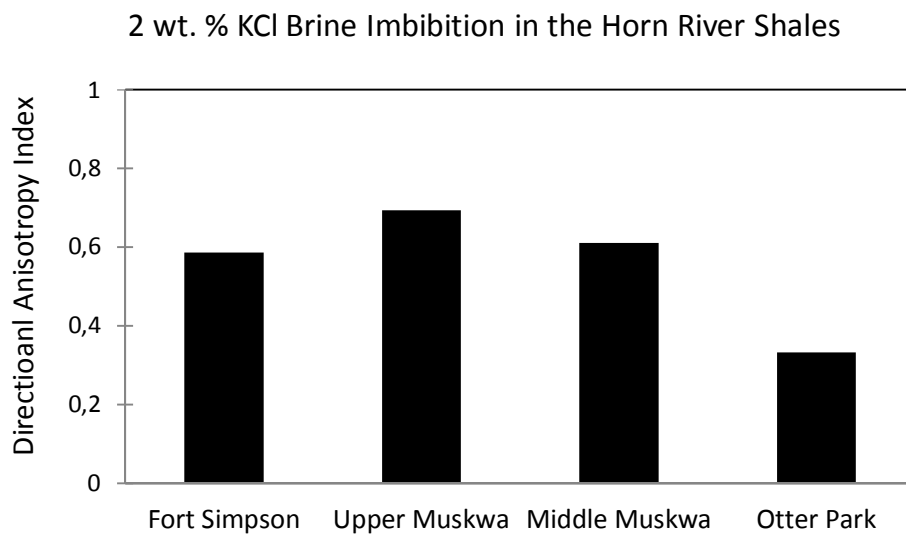


Fig. 5.7-The directional anisotropy index in shale samples.

CHAPTER 6

IMBIBITION SCALING RESULTS

This chapter presents an analytical study of spontaneous imbibition in shales. Dimensionless scaling has been applied to investigate spontaneous imbibition of various fluids in Fort Simpson, Muskwa and Otter Park shales. Moreover, a procedure is proposed to estimate spontaneous fluid loss at the field scale during the soaking time (shut-in time) by using the imbibition data measured in the lab.

6.1 Dimensionless Scaling of Spontaneous Imbibition

The dimensionless analysis is an essential tool for interpretation of laboratory results and predicting the field performance from lab measurements. In conventional rocks imbibition rate is mainly affected by (1) rock properties including permeability, porosity and wettability; (2) fluid properties including viscosity, interfacial tension (IFT); and (3) geometrical parameters such as sample shape, size and boundary conditions (Li and Horne, 2002). Various dimensionless scaling groups have been developed to characterize the spontaneous imbibition in rocks. We applied the dimensionless scaling approach to understand the factors controlling imbibition process in fluid-shale systems.

6.1.1 Dimensionless Time Formulation

Several formulations have been proposed to scale imbibition in gas saturated rocks (Li and Horne, 2006). The frequently used dimensionless time is a function of rock-fluid properties and imbibition time (Mattax and KYTE, 1962; Ma *et al.*, 1995):

$$t_d = \sqrt{\frac{k}{\phi}} \frac{\sigma}{\mu_w L_c^2} t \quad (6.1)$$

where, t_d is dimensionless time, k is matrix permeability, ϕ is porosity, σ is interfacial tension, μ_w water viscosity, t is the imbibition time and L_c is the characteristic length.

The dimensionless time (**Eq. 6.1**) accounts for the rock, fluid and sample's geometrical properties. However, the dimensionless time proposed for air/water rock systems ignores viscosity of resident gas and honors only water viscosity (Handy, 1960; Li and Horne, 2004). Moreover, the dimensionless time formulation does not account for rock wettability.

The characteristic length (L_c) compensates for the different size, shape and boundary conditions and is defined as (Ma et al., 1995):

$$L_c = \sqrt{\frac{V}{S_A/d_i}} \quad (6.2)$$

V is a bulk volume of the matrix, S_A is the area open to imbibition with respect to the i -th direction, and d_i is the distance from the rock face open for flow to the no-flow boundary.

6.1.2 Analyses of the Lab Data by Using Dimensionless Time

The systematic analyses of imbibition data obtained from air/water/shale and air/oil/shale systems were conducted by using the dimensionless time (**Eq. 6.1**). Effects of boundary conditions, permeability, porosity, viscosity and surface tension were investigated for both non-organic and organic shales. **Table 6.1** shows the parameters used for calculation of dimensionless time (t_d).

Table 6.1-Parameters used for the dimensionless scaling						
Samples	Imbibing Fluid	Lc (cm)	K (mD)	\emptyset (-)	μ_w (cP)	σ (N/m)
Fort Simpson Samples						
FS-1	DI Water	7	8.0E-05	0.065	1	0.072
FS-2	2 wt. % KCl Brine	7.1	8.0E-05	0.065	1	0.074
FS-2a	Brine (axial)	3.1	8.0E-05	0.065	1	0.074
FS-3	Tergitol+DI	7.3	8.0E-05	0.065	1	0.029
FS-4	DDBS+DI	7.4	8.0E-05	0.065	1	0.035
FS-5	Tergitol+brine	7.3	8.0E-05	0.065	1	0.029
FS-6	DDBS+brine	7.3	8.0E-05	0.065	1	0.028
FS-7	XG (0.28 wt.%)	7.4	8.0E-05	0.065	237	0.073
FS-8	XG (0.56 wt.%)	7.1	8.0E-05	0.065	279	0.075
FS-9	Mineral oil	7.5	8.0E-05	0.065	24	0.03
FS-10	Kerosene	7.2	8.0E-05	0.065	2.5	0.028
FS-1s	2 wt. % KCl Brine	3.8	8.0E-05	0.065	1	0.074
FS-2s	DI Water	1.1	8.0E-05	0.065	1	0.072
FS-3s	Mineral oil	2.3	8.0E-05	0.065	24	0.03
FS-4s	XG (0.28 wt.%)	1.0	8.0E-05	0.065	237	0.073
Muskwa						
<i>Upper Muskwa</i>						
MW1-1	DI Water	7.4	1.0E-04	0.084	1	0.072
MW1-2	2 wt. % KCl Brine	7.3	1.0E-04	0.084	1	0.074
MW1-2a	Brine (axial)	2.2	1.0E-04	0.084	1	0.074
MW1-3	Tergitol+DI	7.2	1.0E-04	0.084	1	0.029
MW1-4	DDBS+DI	7.4	1.0E-04	0.084	1	0.035
MW1-5	Tergitol+brine	7.1	1.0E-04	0.084	1	0.029
MW1-6	DDBS+brine	7.5	1.0E-04	0.084	1	0.028
MW1-7	XG (0.28 wt.%)	7.2	1.0E-04	0.084	606	0.073
MW1-8	XG (0.56 wt.%)	7.2	1.0E-04	0.084	738	0.075
MW1-9	Mineral oil	7.3	1.0E-04	0.084	24	0.03
MW1-10	Kerosene	7.1	1.0E-04	0.084	2.5	0.028
MW1-1s	2 wt. % KCl Brine	2.9	1.0E-04	0.084	1	0.074
MW1-2s	DI Water	1.0	1.0E-04	0.084	1	0.072
MW1-3s	Mineral oil	1.3	1.0E-04	0.084	24	0.03
MW1-4s	XG (0.28 wt.%)	1.0	1.0E-04	0.084	606	0.073
<i>Middle Muskwa</i>						
MW2-1	DI Water	7.7	9.2E-05	0.071	1	0.072
MW2-2	2 wt. % KCl Brine	7.2	9.2E-05	0.071	1	0.074
MW2-2	Brine (axial)	2.1	9.2E-05	0.071	1	0.074
MW2-3	Tergitol+DI	7.4	9.2E-05	0.071	1	0.029
MW2-4	DDBS+DI	7.5	9.2E-05	0.071	1	0.035
MW2-5	Tergitol+brine	7.3	9.2E-05	0.071	1	0.029
MW2-6	DDBS+brine	7.1	9.2E-05	0.071	1	0.028
MW2-7	XG (0.28 wt.%)	7.4	9.2E-05	0.071	606	0.073
MW2-8	XG (0.56 wt.%)	7.3	9.2E-05	0.071	738	0.075
MW2-9	Mineral oil	7.3	9.2E-05	0.071	24	0.03
MW2-10	Kerosene	7.1	9.2E-05	0.071	2.5	0.028
MW2-1s	2 wt. % KCl Brine	2.5	9.2E-05	0.071	1	0.074
MW2-2s	DI Water	1.0	9.2E-05	0.071	1	0.072
MW2-3s	Mineral oil	1.6	9.2E-05	0.071	24	0.03
MW2-4s	XG (0.28 wt.%)	1.0	9.2E-05	0.071	606	0.073
Otter Park						
OP-1	DI Water	7.5	1.1E-04	0.087	1	0.072
OP-2	2 wt. % KCl Brine	7.4	1.1E-04	0.087	1	0.074
OP-2a	Brine (axial)	2.3	1.1E-04	0.087	1	0.074
OP-3	Tergitol+DI	7.1	1.1E-04	0.087	1	0.029
OP-4	DDBS+DI	7	1.1E-04	0.087	1	0.035
OP-5	Tergitol+brine	7.2	1.1E-04	0.087	1	0.029
OP-6	DDBS+brine	7.3	1.1E-04	0.087	1	0.028
OP-7	XG (0.28 wt.%)	7.2	1.1E-04	0.087	829	0.073
OP-8	XG (0.56 wt.%)	7.1	1.1E-04	0.087	879	0.075
OP-9	Mineral oil	7.1	1.1E-04	0.087	24	0.03
OP-10	Kerosene	7.4	1.1E-04	0.087	2.5	0.028
OP-1s	2 wt. % KCl Brine	4.1	1.1E-04	0.087	1	0.074
OP-2s	DI Water	1.1	1.1E-04	0.087	1	0.072
OP-3s	Mineral oil	2.1	1.1E-04	0.087	24	0.03
OP-4s	XG (0.28 wt.%)	1.0	1.1E-04	0.087	829	0.073

Samples. There are 60 samples representing Fort Simpson, Muskwa (Upper zone and Middle zone) and Otter Park stratigraphic units. Selected samples have a different size and orientation with respect to the bedding plane. Samples are coated using impermeable epoxy, so that the fluid could imbibe only through the designated surface. Physical properties of used samples are listed in **Table 4.2**.

Fluids. In total, 10 different fluids were used as imbibing fluids including aqueous and oleic phases. Aqueous phase consisted of fluids that have different level of salinity, surface tension and viscosity:

- Fresh water
- 2 wt. % KCl brine
- Anionic surfactant in fresh water
- Non-ionic surfactant in fresh water
- Anionic surfactant in KCl brine water
- Non-ionic surfactant in KCl brine
- XG polymer solution with concentration of 0.28 wt. %
- XG polymer solution with concentration of 0.56 wt. %

Oil phase consists of mineral oil and kerosene, which have different viscosities.

Characteristic length. Characteristic length represents the distance traveled by the imbibition front from the open face to the no-flow boundary (**Eq. 6.2**). There is only one surface open in our experimental samples; hence, L_c is equal to the sample width. The characteristic length differs in small and large samples. Although the large samples have cylindrical segmented shapes, the geometry of large samples has been simplified to the rectangular shape. Therefore, L_c in large samples also equals to the sample width.

Porosity. Porosity values were calculated based on the estimation of shale matrix density using XRD and TOC data. Porosity calculation methodology and details are explained in Chapter 3. Porosity values are listed in **Table 3.3**.

Permeability. Permeability values of the shale samples have been estimated from the correlations proposed by Aguilera *et al.*, 2013:

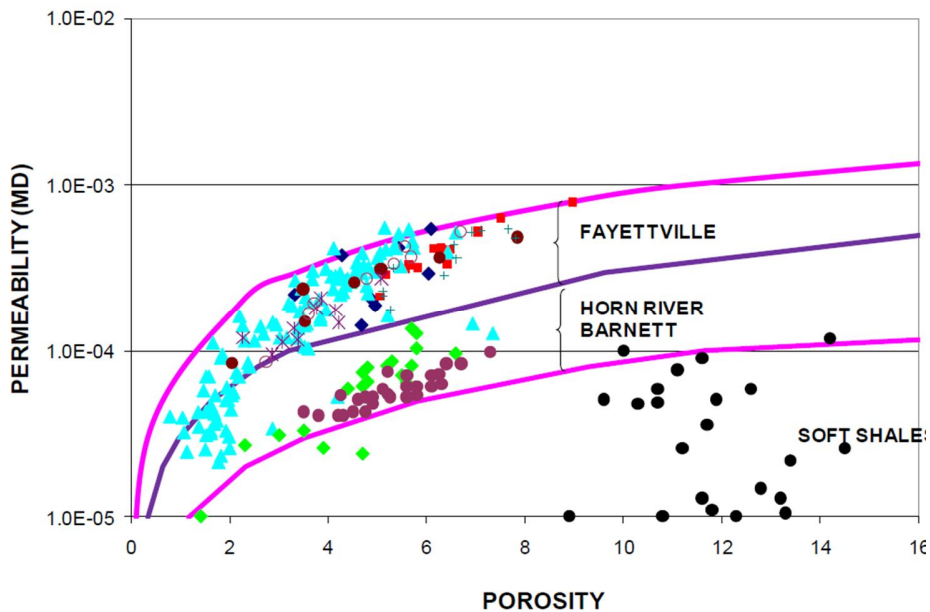


Fig. 6.1-Permeability vs. porosity cross plot for various shales (Aguilera *et al.*, 2013)

Fig. 6.1 demonstrates the permeability- porosity cross plot for various shales including the Horn River Formation. Although presented data are for Muskwa member of the Horn River formation, it was assumed that the Fort Simpson and Otter Park member samples have the similar permeability-porosity correlations.

Viscosity. Viscosity of both Xanthan Gum solutions corresponds to the calculated shear rate in porous media. Xanthan gum solutions show a non-Newtonian shear-thinning behavior which is described by a power law flow model (Song *et al.*,

2006). Christopher and Middleman (1965) proposed an expression that could be used for predicting shear rate in porous media:

$$\gamma = \frac{3n+1}{4n} \frac{4Q}{S_A(8k\phi)^{0.5}} \quad (6.3)$$

where γ is shear rate, 1/s; n is a non-Newtonian correction factor for power-law fluids; Q is flow rate, cm³/s; S_A is the cross sectional area of the core, cm²; k is permeability, cm²; and ϕ is the porosity.

Flow rate is related to imbibition rates in our experiments. Imbibition rate is not constant in porous media, but decreasing with time. We calculated flow rate based on average values of imbibition rates for each fluid-shale system. Average imbibition rate was calculated from the integral of imbibition rate function. In simple, it is the area under the imbibition rate curve in the interval from 0 to 24 hours divided by the experimental time.

Interfacial tension. The interfacial tension between imbibing fluids and air was measured using the Du Nouy ring method at the ambient conditions. This technique works by slowly lifting a platinum ring from the surface of a liquid in presence of air or other gases. The force required to raise the ring from the liquid's surface is measured and related to the interfacial tension.

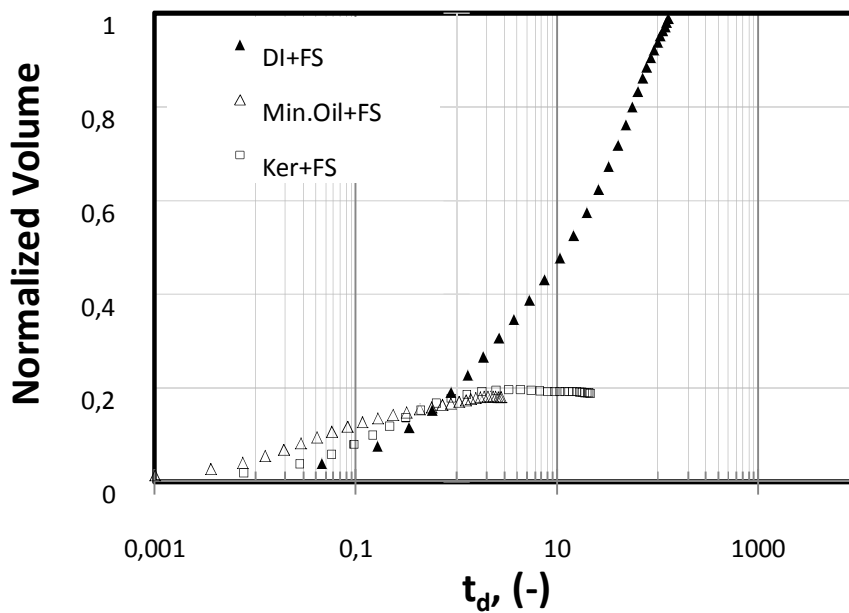
6.1.3 Results of Spontaneous Imbibition Scaling

This section presents dimensionless scaling results for fluid imbibition in shales. The results are presented in the form of normalized volume versus dimensionless time plots in a semi log scale. The normalized volume is defined as the ratio of imbibed volume to the initial sample pore volume. Dimensionless time is

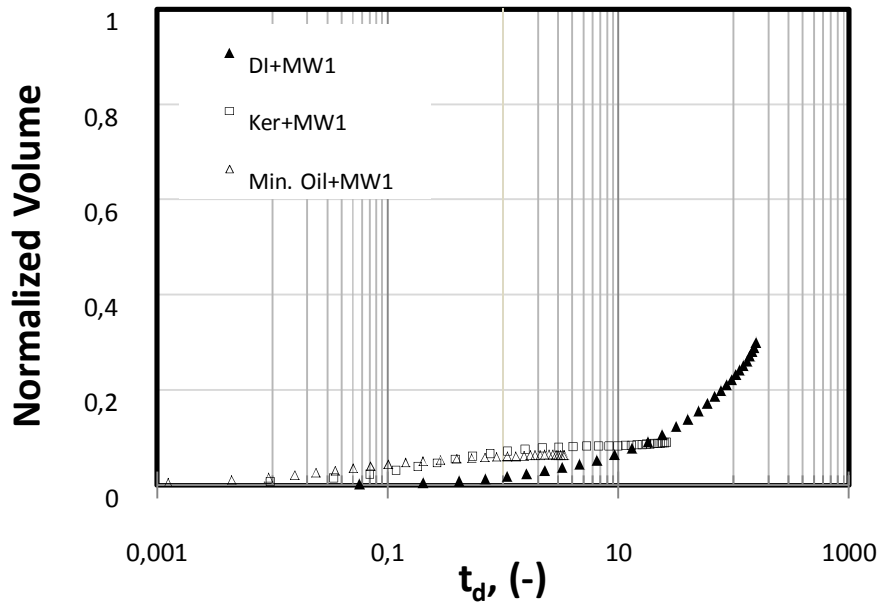
calculated using Eq. 6.1. According to the existing theory, all of the data that scale spontaneous imbibition in shale samples from the same depth should sit around one single curve. Although Eq. 6.1 does not account for the wettability, we assume that imbibition data should have the similar results for samples from the same stratigraphic units.

Comparison of Aqueous and Oleic Phase Imbibition.

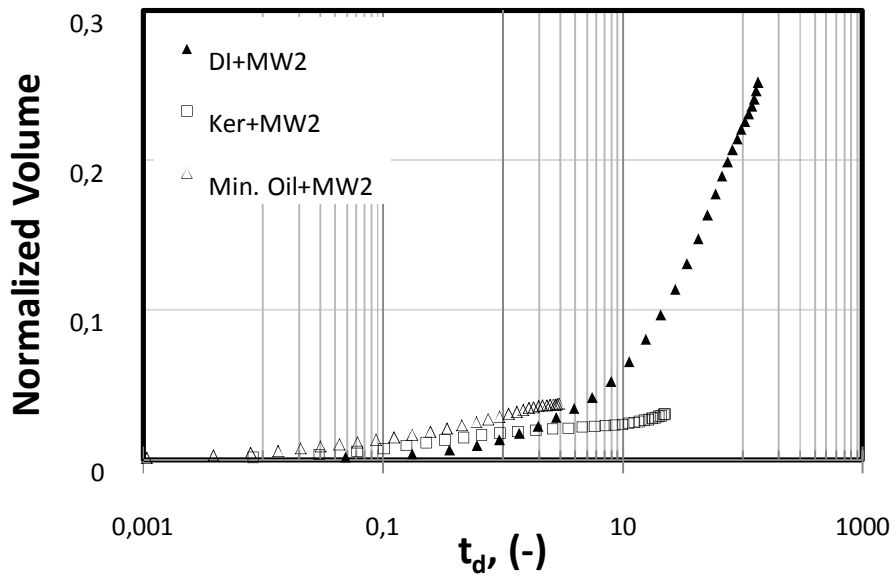
Fig. 6.2 shows plots of normalized deionized water, mineral oil and kerosene imbibition data versus the corresponding dimensionless time.



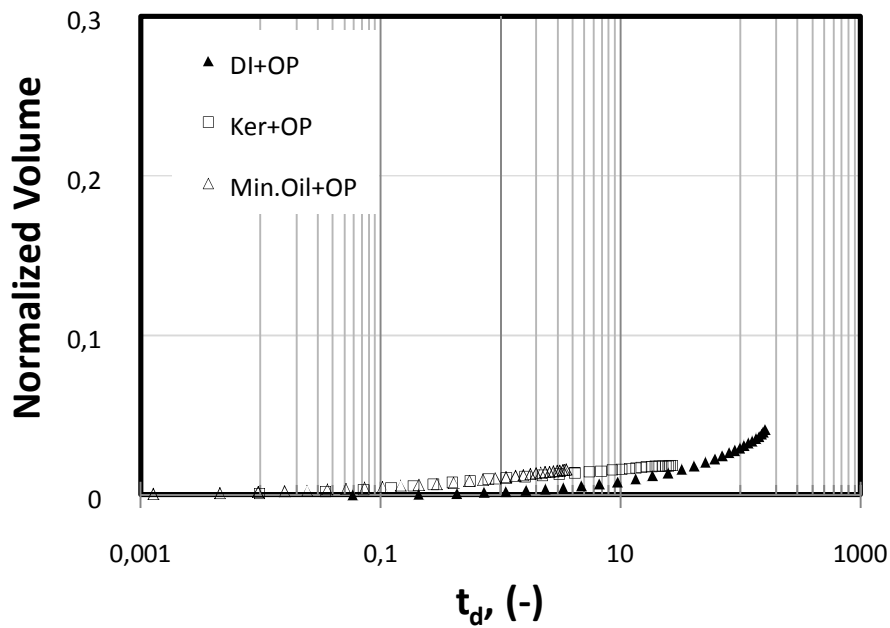
(a)



(b)



(c)



(d)

Fig. 6.2- Normalized volume of aqueous and oleic phase imbibition in large shale samples versus dimensionless time: a-Fort Simpson, b- Upper Muskwa, c- Middle Muskwa and d- Otter Park samples

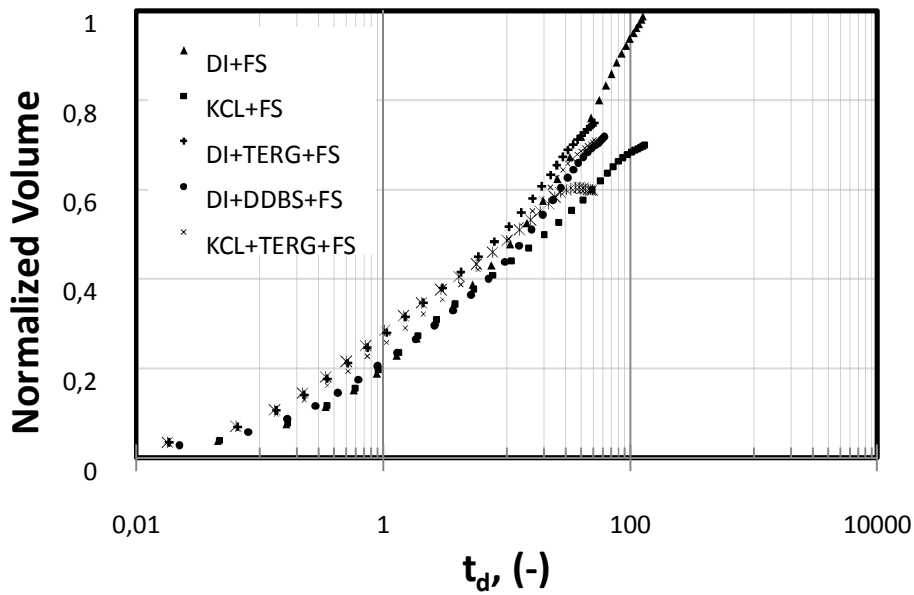
It is observed that water imbibition data are much higher than mineral oil and kerosene data in Fort Simpson samples. In Upper Muskwa and Middle Muskwa samples aqueous phase imbibition data is also higher than that of oil phase although they have less separation between aqueous and oil phase imbibition. Otter Park samples have relatively close data for both aqueous and oil phase's imbibition.

It is also observed that, at initial times, normalized imbibed volume of oleic phase is higher than that of aqueous phase in all of the samples. Oil imbibition gradually decreases and will reach plateau at some point. Although imbibition of aqueous phase is lower comparing at oil imbibition at initial times, it significantly increases after certain point in t_d scale.

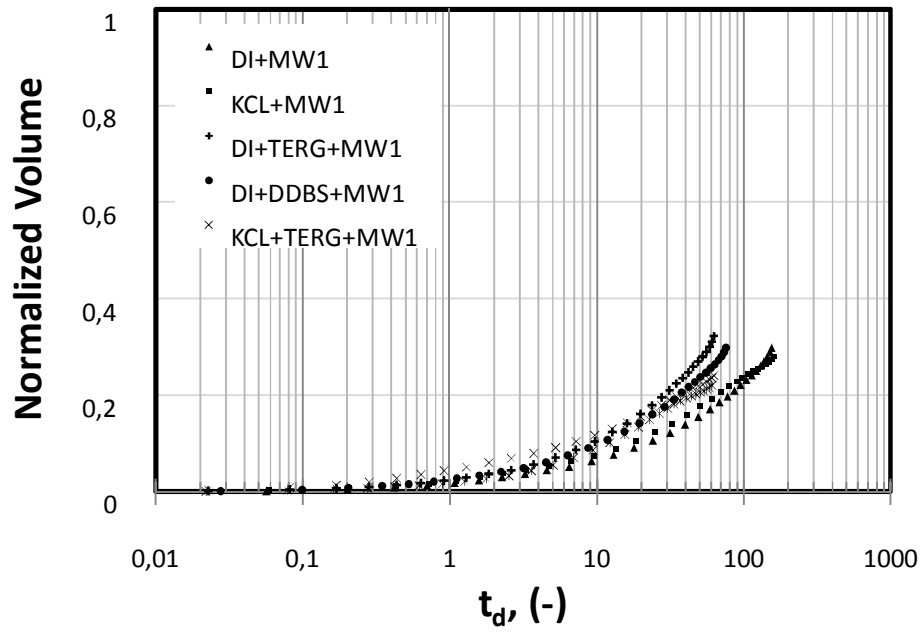
Results also show that normalized fluid imbibition is significantly decreasing with depth. Fort Simpson, being from the shallowest depth, has highest normalized imbibition data for all fluids, while Otter Park samples being from the deepest depth of all the samples tested show the lowest imbibition results. Muskwa formation lies between Fort Simpson and Otter Park formation, so does the imbibition rates in Muskwa formation.

Imbibition of Fresh Water, Brine and Surfactant Solutions.

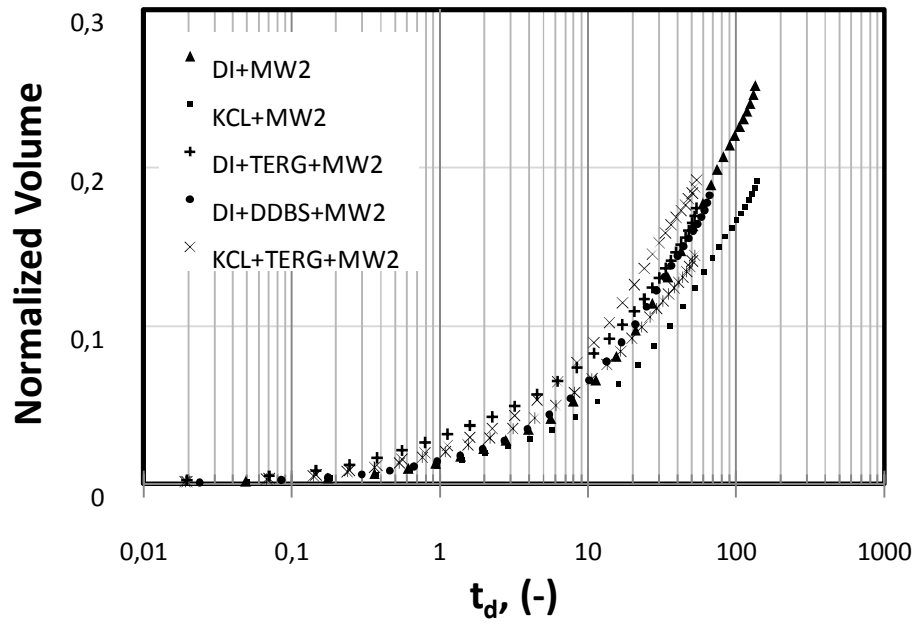
Fig. 6.3 shows normalized imbibition data for deionized water, 2 wt. % KCl brine and surfactant solutions versus the corresponding dimensionless time.



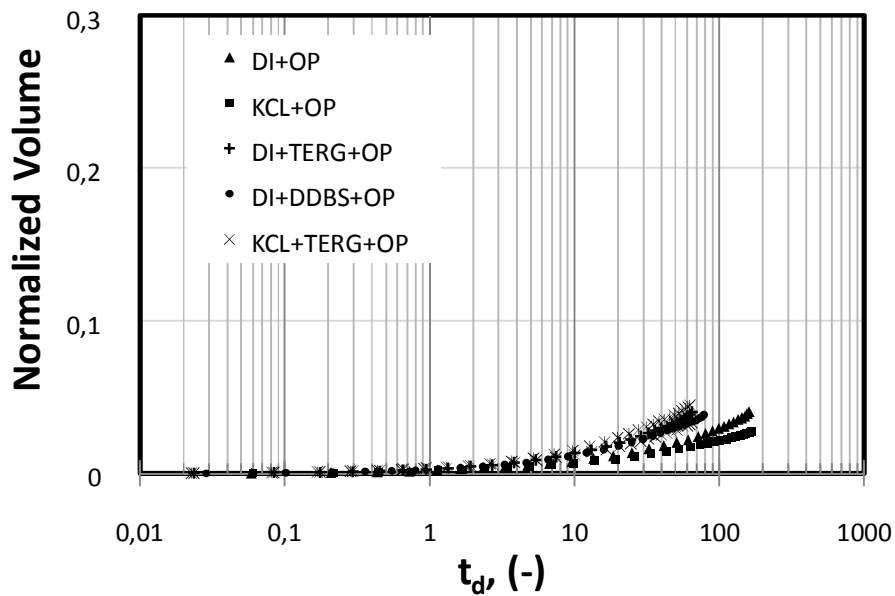
(a)



(b)



(c)



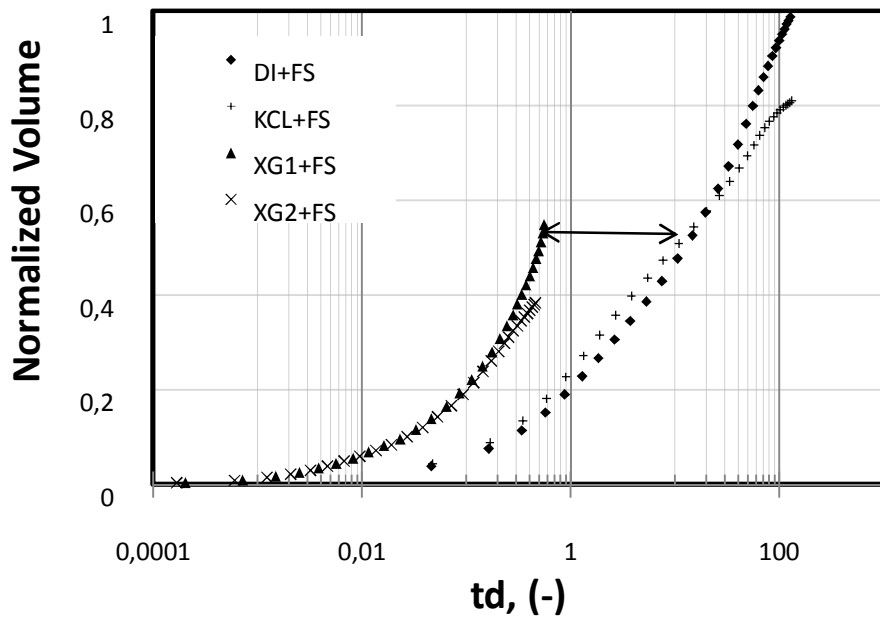
(d)

Fig. 6.3- Normalized volume of DI water, brine and surfactants solutions imbibition in large shale samples versus dimensionless time: a-Fort Simpson, b- Upper Muskwa, c- Middle Muskwa and d- Otter Park samples

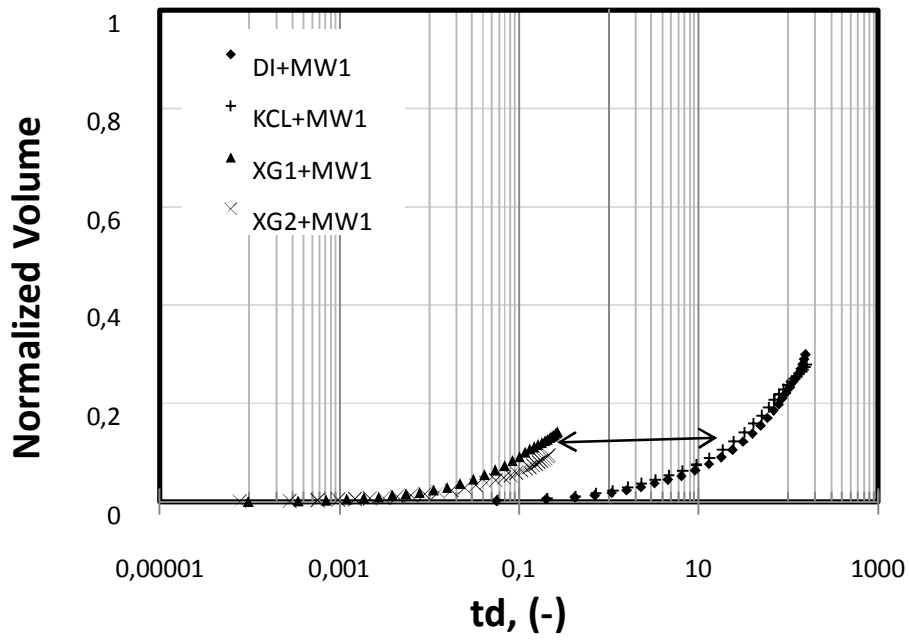
It is observed that all of the data approximately fall onto one curve for each shale type. In Fort Simpson samples, fresh water data points show the highest values reaching near sample's initial pore volume, while brine with the addition of anionic (DDBS) surfactant demonstrates the lowest imbibition rate. In Muskwa samples, fresh water has the similar imbibition data points as the brine and brine with surfactants. In Otter Park samples, similar imbibition data points were also observed for fresh water, brine and brine with surfactant.

Imbibition of Fresh Water, Brine and XG Polymer Solutions.

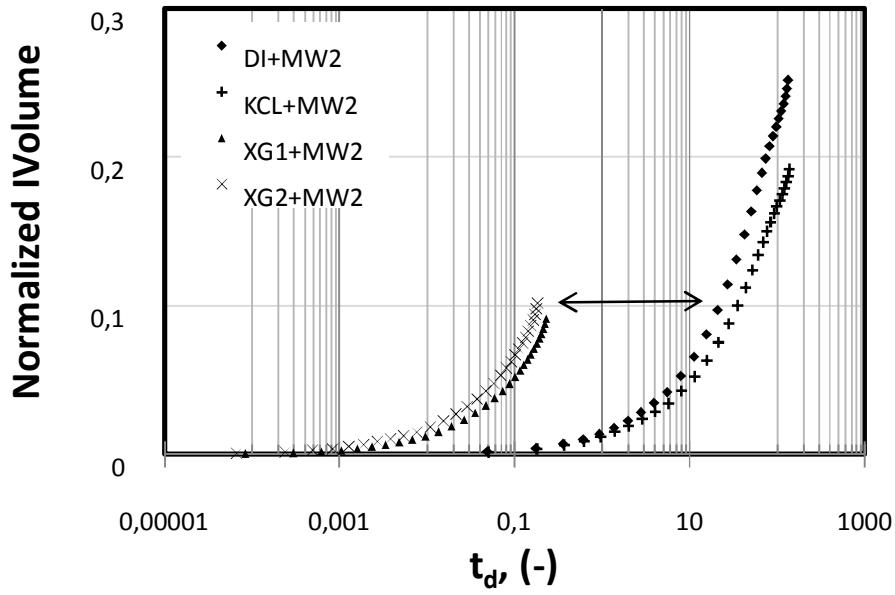
Fig. 6.4 shows normalized imbibition data for deionized water, brine, 0.28 wt. % and 0.56 wt. % of XG solutions versus the corresponding dimensionless time.



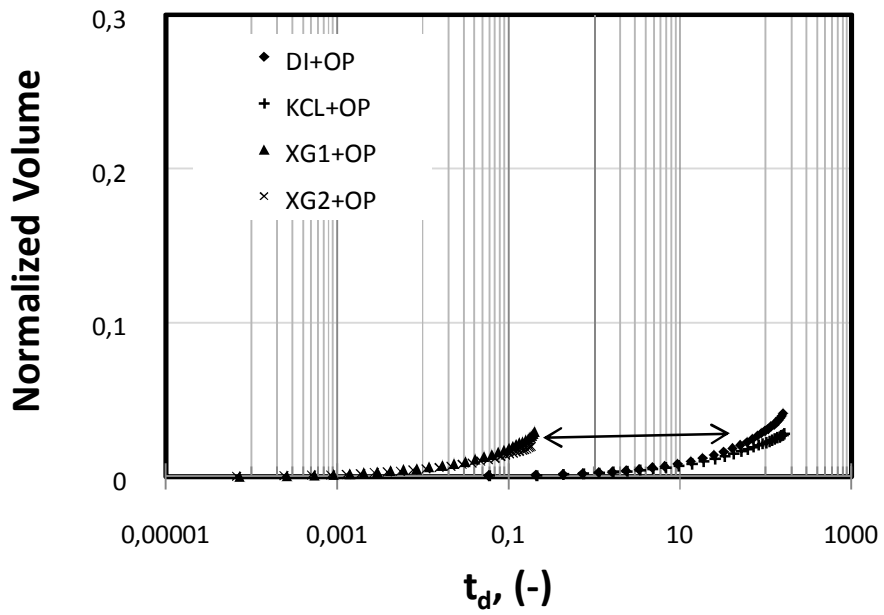
(a)



(b)



(c)



(d)

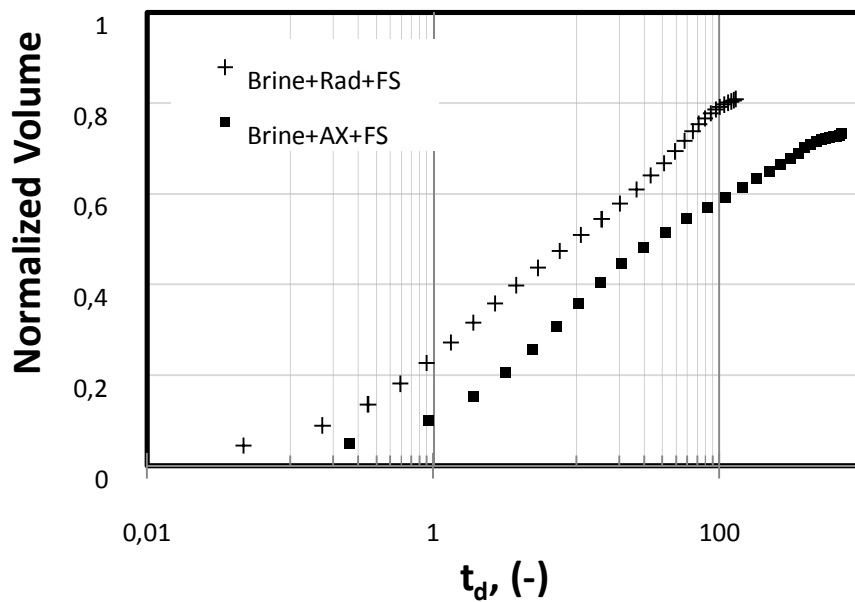
Fig. 6.4- Normalized volume of fresh water, brine and XG solutions imbibition in large shale samples versus dimensionless time: a- Fort Simpson, b- Upper Muskwa, c- Middle Muskwa and d- Otter Park samples.

The normalized imbibition data for XG polymer solutions are lower than that of deionized water and brine in all rock samples except Otter Park formation where the difference is not so significant. More concentrated 0.56 wt. % solution of XG polymer has lower intake than less concentrated 0.28 wt. % XG solution.

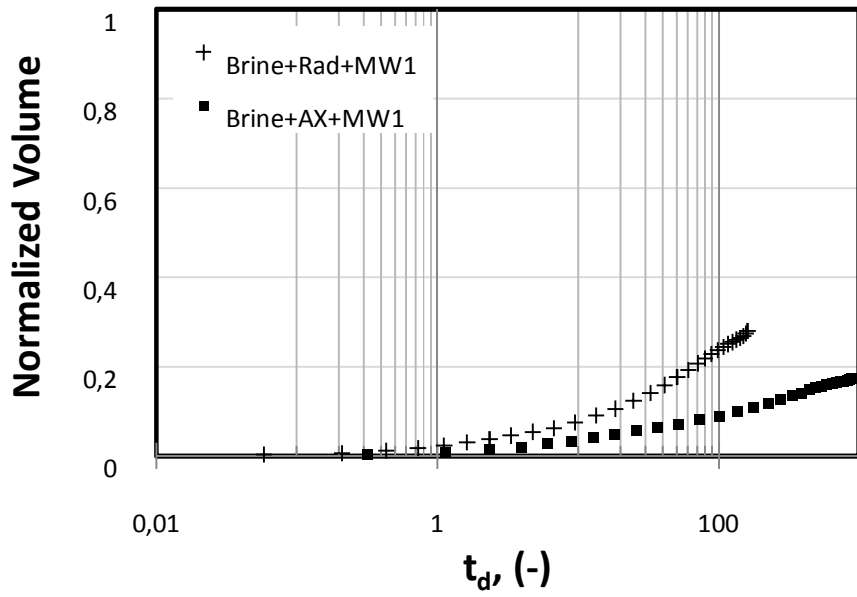
Furthermore, it can be observed that data points for XG solutions fall behind the deionized water and brine data for several orders of magnitude. This separation can be observed in all the samples.

Effect of Rock Anisotropy on Imbibition.

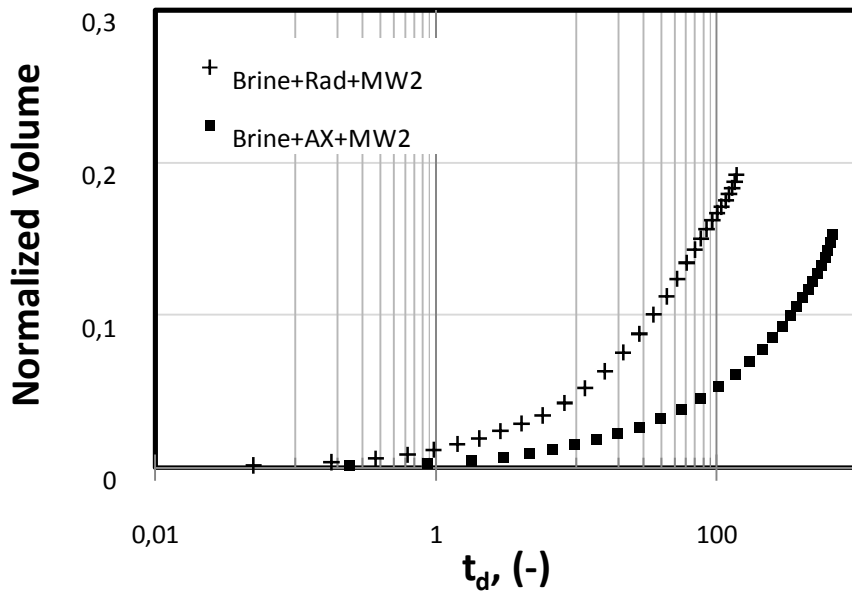
Fig. 6.5 shows imbibition data for 2 wt. % KCl brine in directions parallel (radial) and orthogonal (axial) to the bed deposition plane (lamination direction).



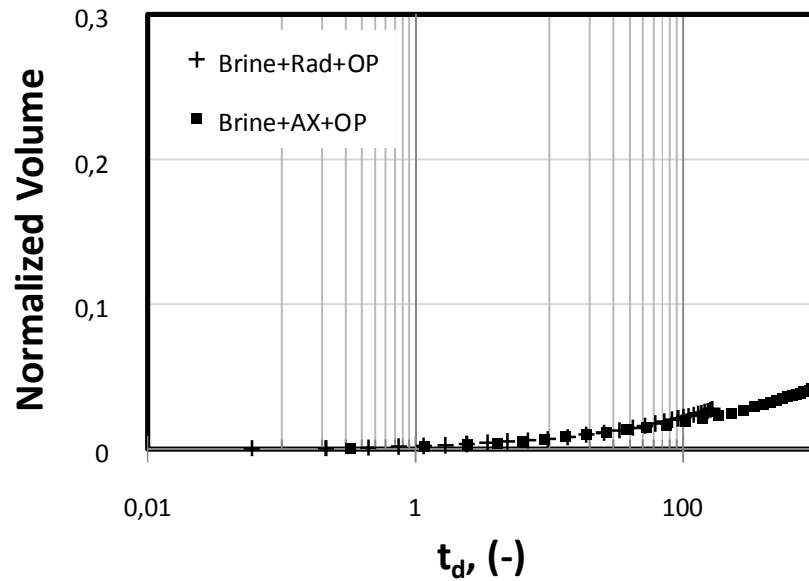
(a)



(b)



(c)



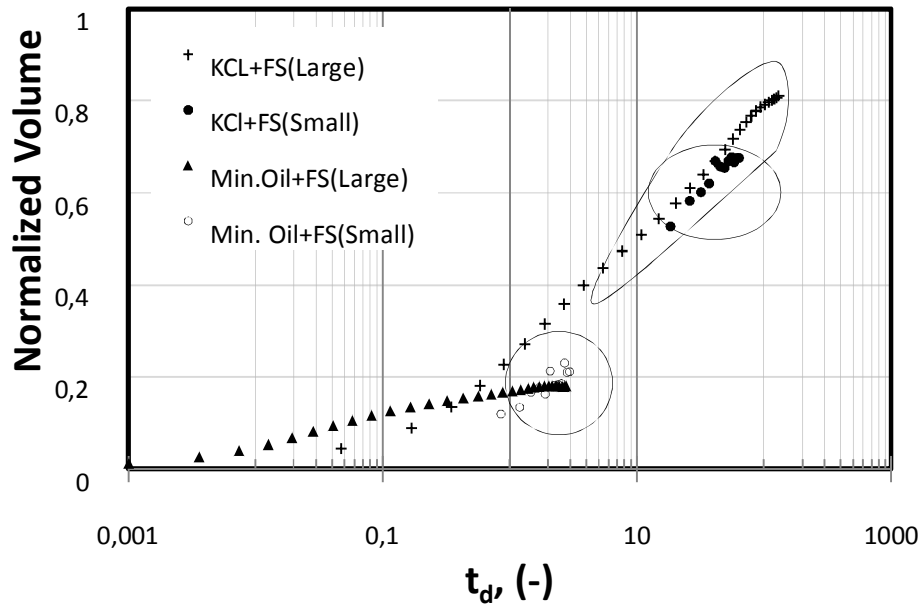
(d)

Fig. 6.5- Normalized imbibition of brine perpendicular directions in large shale samples versus dimensionless time: a- Fort Simpson, b- Upper Muskwa, c- Middle Muskwa and d- Otter Park samples

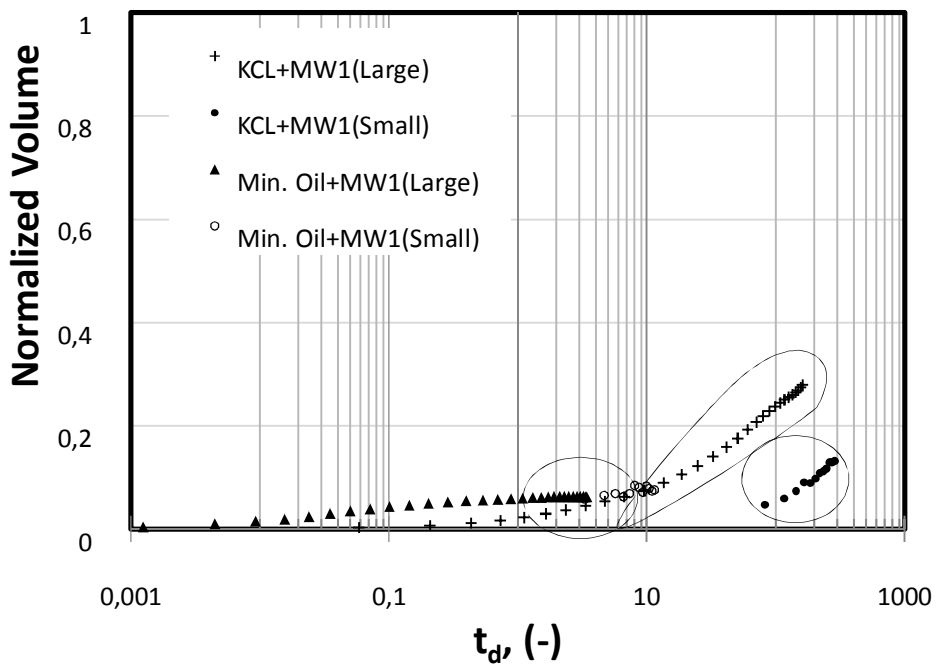
It is seen that normalized volume in the direction parallel to the bedding plane is higher than that in the direction orthogonal to the bedding plane in Fort Simpson and Muskwa samples. The difference is more pronounced in Fort Simpson samples comparing to Muskwa samples. However, in Otter park samples normalized volume is relatively the same in both directions (i.e., very little directional dependency of imbibition).

Effect of Sample Size on Imbibition of Brine and Mineral Oil.

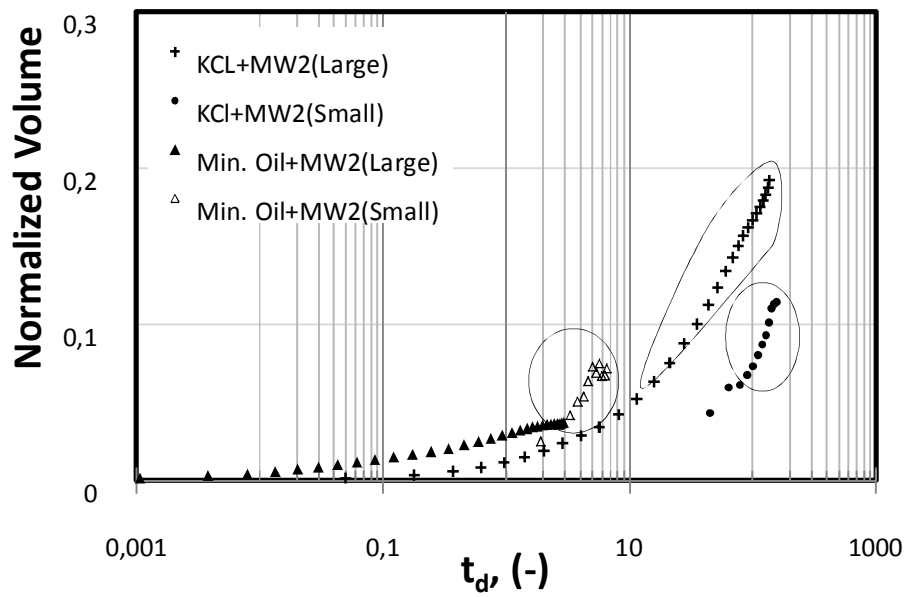
Fig. 6.6 shows normalized imbibition data of brine and mineral oil in large and small samples versus the corresponding dimensionless time. Imbibition data for large and small samples are marked as “Large” and “Small” respectively in the plot legends.



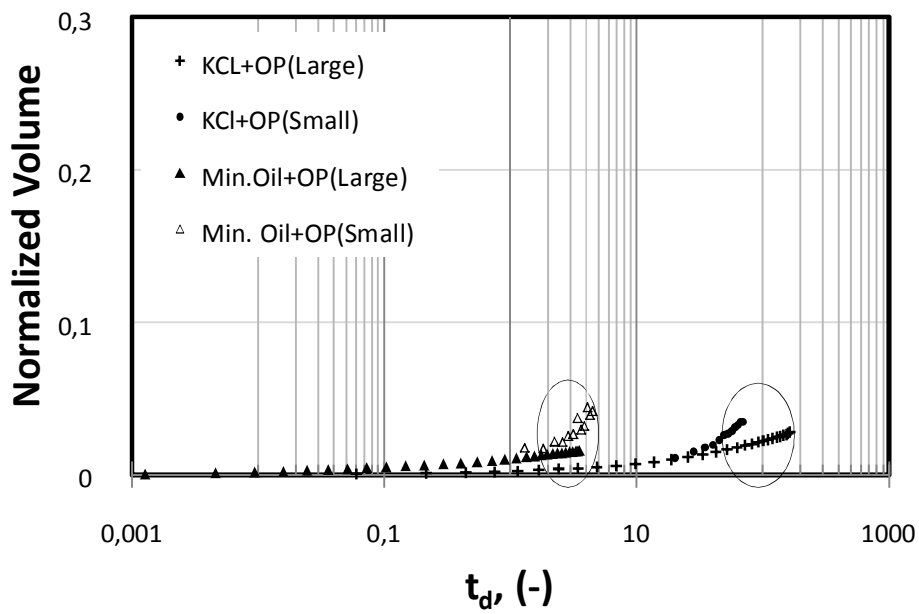
(a)



(b)



(c)



(d)

Fig. 6.6- Normalized volume of KCl brine and mineral oil imbibition in large and small shale samples versus dimensionless time: a-Fort Simpson, b- Upper Muskwa, c- Middle Muskwa and d- Otter Park samples

Three groups of scaled data are observed for each type of shale. The data groups are designated with circled lines in the plots. The highest values relate to brine imbibition in large samples. The intermediate values relate to brine imbibition in small samples, which are shifted to the right in Upper and Middle Muskwa samples. The lowest values relate to oil imbibition in both small and large samples. However, in Otter Park member, brine data points for large and small samples are close to each other.

6.1.4 Discussions of Dimensionless Scaling Results

Fresh Water vs. Oil Imbibition

According to the scaling plots imbibed volume of fresh water are higher than that of oil data (**Fig. 6.2**). These results seem to be conflicting with the fact that the rock samples under investigation are more oil wet than water wet, which should have normally resulted in more oil intake. These anomalous results may be due to the fact that total water intake is also influenced by: 1) water adsorption by clay minerals, and 2) increase in sample permeability due to micro fracture induction.

Increased water intake can be related to adsorption of water by charged clay particles in dry samples. By nature, water molecules are polarized and may be attracted to negatively charged clay platelets. This may cause additional driving force for capillary driven imbibition of water phase in shale samples.

Moreover, adsorbed water can expand the clay platelets, which generate micro fractures in the sample. These induced micro fractures increase sample

permeability and initial pore volume. **Fig. 6.7** shows an example of Fort Simpson sample before and after exposure to water for 24 hours. Shale samples break along the lamination and generate new micro fractures after exposure to water. Since samples are not confined, sample expansion increases the initial pore volume. Therefore clay-rich Fort Simpson samples may imbibe large amount of water, which may exceed sample's initial pore volume (PV). This phenomenon does not occur during the oil phase imbibition. After exposure to oil, we did not observe considerable physical alteration.

It was also observed that, at initial times, normalized imbibed volume of oleic phase is higher than that of aqueous phase in all of the samples. Being oil wet, shale samples imbibe more of oleic phase initially. Oil imbibition rate gradually decreases and reaches plateau at some point due to the very low permeability in matrix.

However, although imbibition of aqueous phase is lower compared to oil imbibition at initial times, it significantly increases after higher point in t_d scale. Significant increase in normalized imbibed volume at higher t_d can be caused by the micro fractures in shale samples, which generate after some times due to the clay swelling.

Before exposure to water



a)

After exposure to water



b)

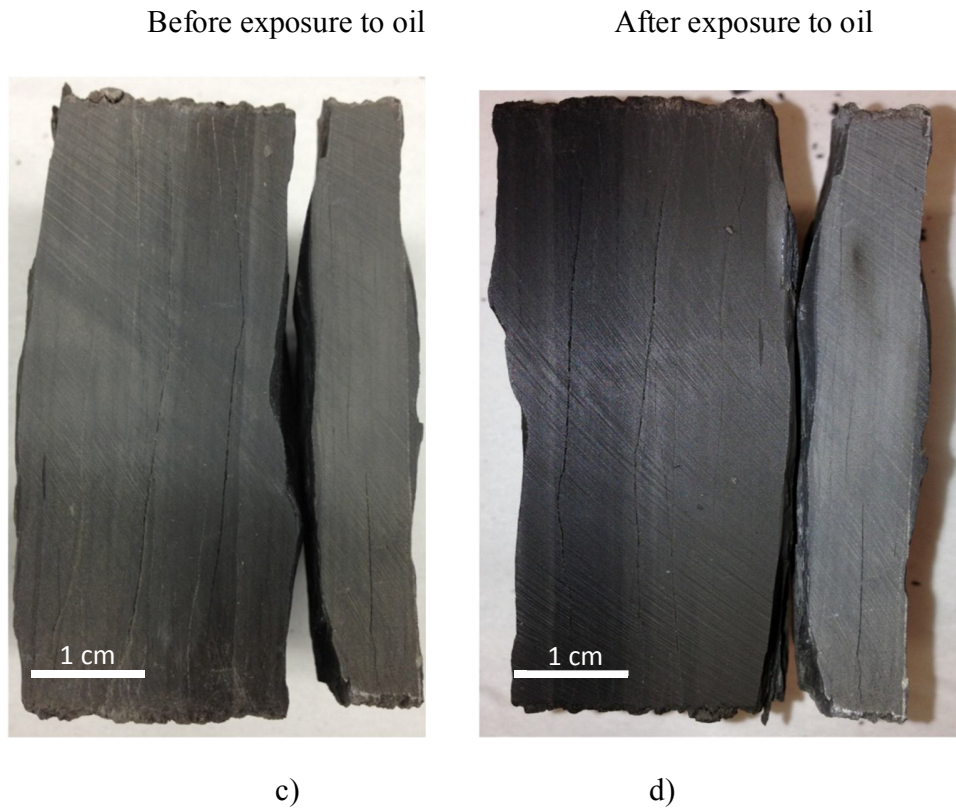


Fig. 6.7-Pictures of Fort Simpson samples before and after 1 day of fluid exposure: a-before water imbibition, b- after water imbibition, c-before oil imbibition, d- after oil imbibition.

Samples break along the lamination and generate new micro fractures after water treatment. We observe only few micro fractures after oil imbibition.

Fig. 6.8 shows pictures of Muskwa samples before and after exposing to water and oil for 24 hours. Muskwa samples demonstrate less induced micro fractures in water compared with Fort Simpson samples.

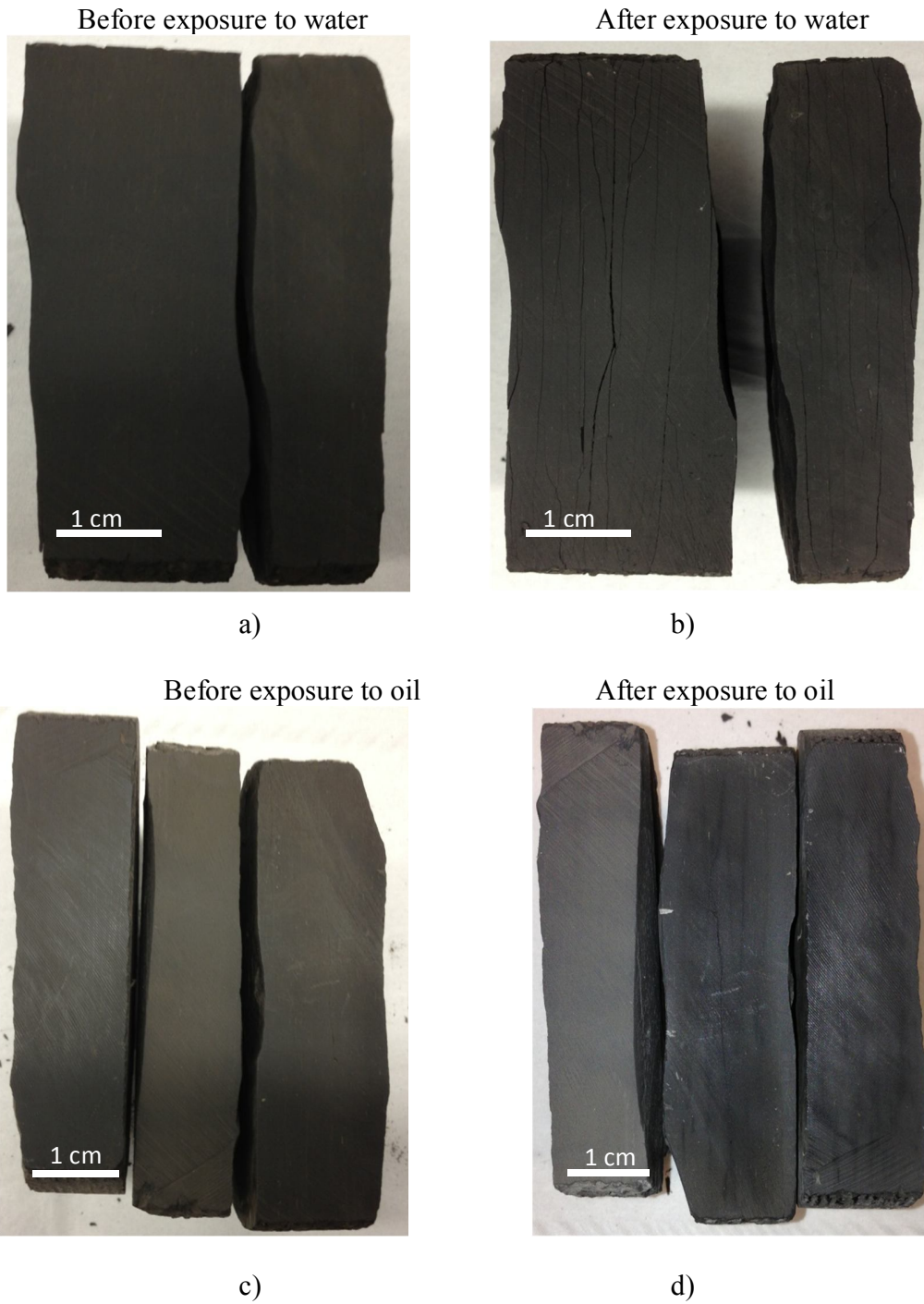


Fig. 6.8- Pictures of Middle Muskwa samples before and after 1 day of fluid exposure: a- before water imbibition, b- after water imbibition, c-before oil imbibition, d- after oil imbibition. Samples show visible cracks along the lamination after water treatment. Breakage along the lamination is significantly less pronounced after oil imbibition.

The difference between the behavior of Fort Simpson and Muskwa samples upon water intake can be related to mineralogical composition of the samples, particularly to the amount of the clay content, which decreases with depth. According to XRD results (**Table 3.2**) Fort Simpson samples have 59% of clay compared to 29% in Middle Muskwa and 23% in Otter Park. Illite is the dominant type of clay mineral in all of the samples (30% in Fort Simpson, 29% in Middle Muskwa and 23% in Otter Park samples). This type of clay mineral is believed to swell to a small degree in contact with water. The presence of “swelling” mixed layer clays is not significant and their amount decrease with depth i.e., from Fort Simpson (nearly 1%) to Muskwa and Otter Park (0%).

Commonly, illites do not swell. However, it is believed that water adsorption may induce “swelling” of illite. Hydrogen atoms of water can attack both lattice ions and interlayer potassium cation in the illite clay structure; hence, it may lead to “swelling” of illite (Chenevert, 1970; Brinkman, 1970).

In addition, chlorites (27% in Fort Simpson, 0% in Middle Muskwa and 0% Otter Park) are also known to be a non-swelling clay type, but there have been reported cases of “swelling chlorites” (Moore and Reynolds, 1997). Reeves *et al.*, (2006) speculated that swelling chlorites are most likely to be a mixed layer chlorite-smectite, which can swell to some extent. This can be a reason for high water intake for samples that collected from Fort Simpson and Upper Muskwa.

KCl Brine Imbibition

Imbibition of KCl brine is less than that of DI water. It can be observed that effect of KCl salt is more pronounced in samples with higher clay content (**Fig. 6.3**). Imbibition is affected by the presence of potassium ion, which acts as a clay swelling inhibitor. The potassium ion (K^+) can replace cations already present in the shale structure. Low hydration energy of K^+ inhibits reactions with water molecules, hence it helps to keep shale structure intact. Since KCl brine inhibits clay swelling and induced micro fracture generation, it results in a reduced imbibition rate as compared to fresh water data.

Imbibition of Surfactant Solutions

Fig. 6.3 shows that normalized imbibed volume of fresh water and brine are higher than that of surfactant solutions. Surfactants reduce imbibition rates in both non-organic and organic shales. By being adsorbed at the interface, surfactants reduce the surface tension between water and air. Reduction of surface tension decreases capillary forces, which, in turn, results in reduced intake of surfactant solutions compared to fresh water and brine.

Furthermore, anionic DDBS in brine shows lower data points comparing to non-ionic Tergitol in brine. It can be related to specific properties of anionic surfactants in the presence of salts. Takaya *et al.* (2005) speculated that salt water decreases repulsion forces between ionic surfactant molecules, which, in turn, allows to more surfactant molecules be accumulated on the interface. Greater

surfactants on the interface contribute to the reduction of surface tension and decrease of imbibition rates.

It is observed that anionic DDBS solutions show lower imbibition data points than non-ionic Tergitol solution. It can be related to adsorption properties of clay minerals. Negatively charged clay particle repulse negatively charged DDBS surfactants, which could decrease overall adsorption of surfactant solutions on the clay surface.

Imbibition of Polymer Fluids

Fig. 6.4 shows normalized volume of XG solution, which presents clear separation from the fresh water and brine imbibition data. The dimensionless time equation (**Eq. 6.1**) includes a viscosity term. High viscosity of polymer fluids results in the relatively low values of dimensionless time. It is not clear at this point what real viscosity values should be used as a representative of imbibition process. Therefore, application of **Eq. 6.1** is questionable for polymer fluid applications.

Directional Anisotropy

Fig. 6.5 shows a separation between imbibition data measured in the direction parallel and orthogonal to the bedding plane. Commonly, shale has layered structure, which yields greater permeability parallel to the bedding plane than that perpendicular to the bedding plane (Chalmers *et al.*, 2012). Therefore, imbibition rate parallel to the laminations is higher than that perpendicular to the lamination.

In addition, clay rich Fort Simpson and Upper Muskwa samples demonstrate more imbibition anisotropy. The ratio between imbibition in parallel direction and imbibition in orthogonal direction increases with clay content (Li, 2006). It indicates that clays contribute to the directional anisotropy in shale structure.

The dimensionless time given in **Eq. 6.1** does not account for the effects of anisotropy. Imbibing fluid front may move faster through the micro fractures parallel to the lamination and then reach the end of the block. This may violate the concept of boundary conditions presented in the characteristic length L_c , which assumes piston like movement of imbibition front in all directions.

Effects of Sample Size

Small and large samples were used for the experiments to study brine and oil imbibition in shales. We observed that normalized volume of imbibed brine for large samples is higher than for the small samples. By definition, all the boundary conditions should be compensated by the characteristic length parameter in the dimensionless time formula (**Eq. 6.2**). This contradiction can be explained by the fact that the chance of micro fracture generation in large samples is greater than that in small samples.

Moreover, the proposed scaling approach is more suitable for conventional reservoir rocks such as sandstones, where capillary pressure is the dominant driving force. Its application for shale reservoirs is hampered by the effects of water adsorption by clay particles and micro fracture induction. Also, the applied dimensionless time formula does not properly scale spontaneous imbibition when

non-Newtonian polymer fluids are used. Shale mineral dissolution and fingering of water front in micro fractures can affect scaling results as well. Therefore, additional investigations are required for scaling of spontaneous imbibition in shale samples.

6.2 Fluid Loss at the Field Scale

6.2.1 Introduction

Currently, the oil and gas industry is facing problems related to excessive water loss in hydraulic fracturing operations (Soeder, 2011). A significant portion of fracturing water remains unrecovered and causes environmental concerns. Typical load recovery values from multi-fractured horizontal wells completed in the Muskwa and Otter Park formations are shown in the **Fig. 6.9**. The vertical axis show load recovery, which is the amount of injected water recovered at the surface. The horizontal axis shows the time period of flowback operations. Flowback is the process when injected fracturing water is recovered at the surface facilities. Plots demonstrate that only around 25 % of injected water are recovered after nearly 40 days of flowback operations.

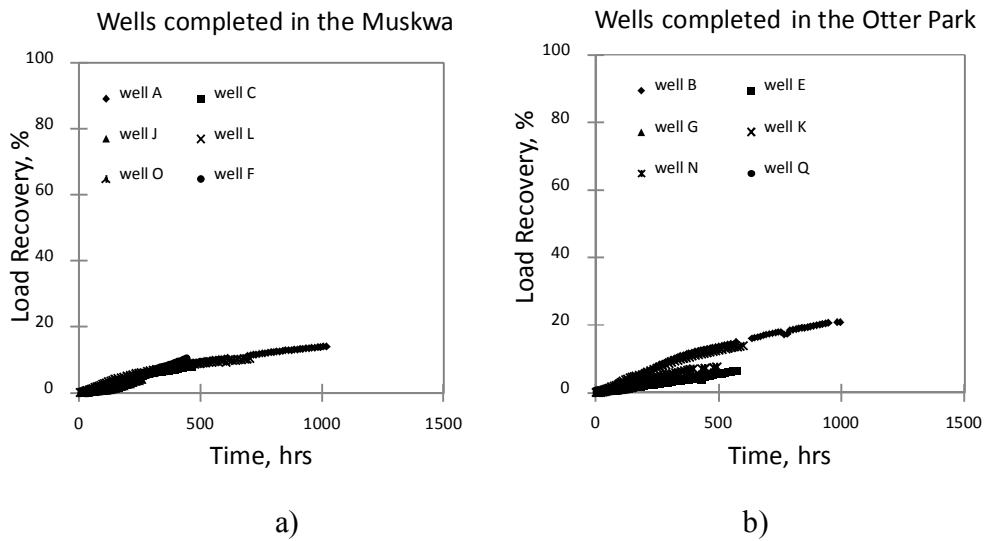


Fig. 6.9- Typical load recovery values during the flowback operations from multi-fractured wells completed in Muskwa formation (a) and Otter Park formation (b)

In addition to the water management issues, invasion of the fracturing fluid into the shale matrix may affect natural gas production (Dutta *et al.*, 2011). On one hand, due to the substantial capillary pressure, water imbibes into the matrix pores and prevents counter-current gas flow (Agrawal *et al.*, 2013). On the other hand, imbibing water may generate micro fractures in the formation matrix or release gas from pores due to counter-current flow. Therefore, understanding of spontaneous imbibition at the field scale is an important task for the shale-gas industry.

There are several reasons causing low recovery of fracturing water. One reason is related to the incomplete water drainage from the propped fractures (Parmar *et al.*, 2012) and is beyond of the scope this thesis work. Second is related to the imbibition process during and after the fracturing operation, which is, partly, responsible for high volumes of water loss in the field (Odusina *et al.*, 2011).

6.2.2 Estimation of Water Imbibition at the Field Scale

Based on the data from the laboratory imbibition experiments, the amount of frac fluid imbibed into the formation can be estimated during the soaking time. The soaking time is a period between the end of fracturing fluid injection and the beginning of the flowback operation. The following methodology is proposed to estimate the fluid loss at the field scale:

1) Based on the laboratory data, calculate the slope of cumulative imbibed volume per unit surface area versus square root of time.

$$V_{imb}/S_A = A\sqrt{t} \quad (6.8)$$

where A is the slope of the cumulative imbibed volume per unit surface area (V_{imb}/S_A) versus square root of time \sqrt{t} .

2) Estimate the total fracture-matrix interface at the field scale:

$$A_{cm} = 4n_f y_e h \quad (6.9)$$

where A_{cm} is the total fracture-matrix interface, n_f is the number of fracture stages (one fracture per stage is assumed), y_e is the fracture half-length and h is the fracture height.

3) Calculate the amount of imbibed fluid at the field scale with time:

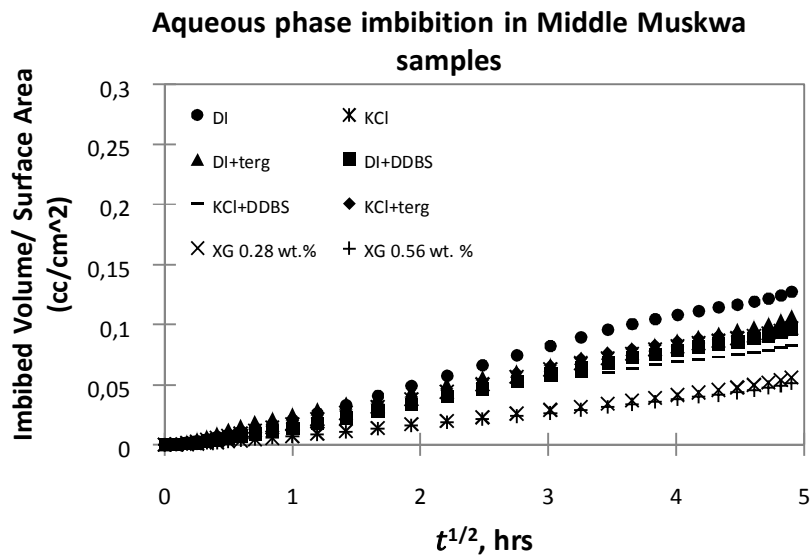
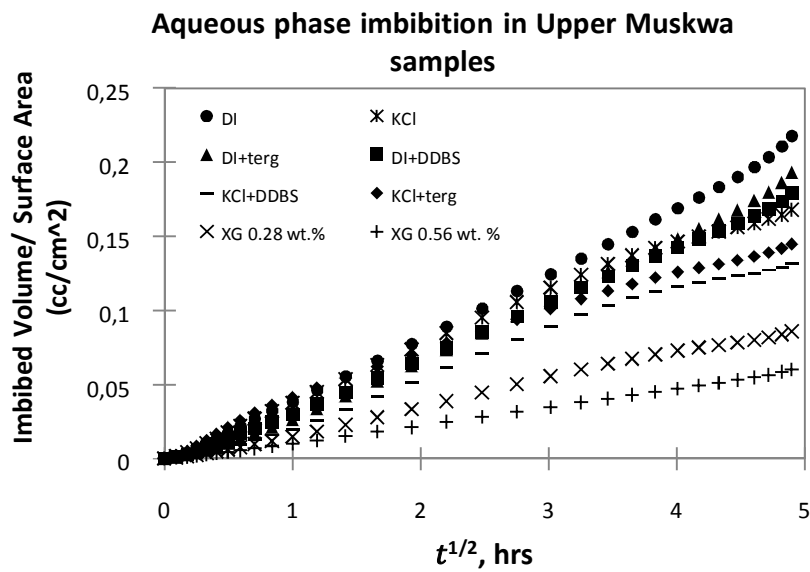
$$V_{imb} = 4n_f y_e h A\sqrt{t} \quad (6.10)$$

Where, V_{imb} is the volume imbibed into the formation, A is a parameter obtained from **Eq. 6.8** and t is the soaking time.

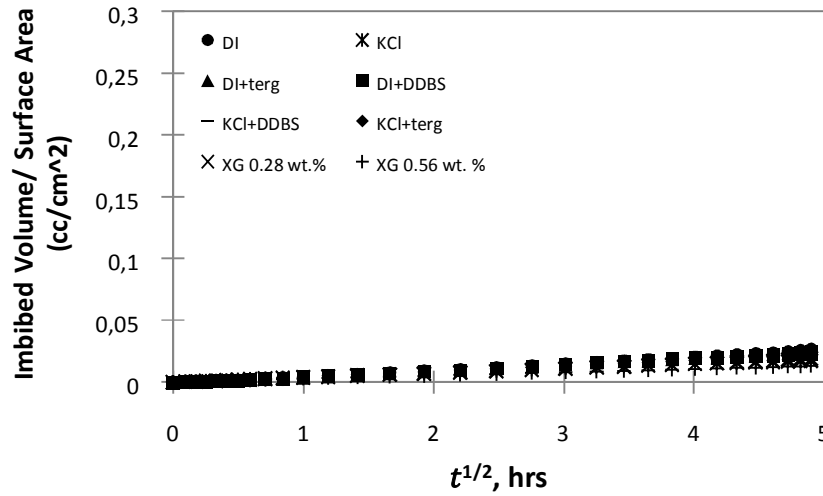
6.2.3 Determination of A-parameter from the experimental data

The A-parameter can be estimated from the slope of cumulative imbibed volume per unit surface area versus square root of time. The experimental plots for various aqueous fluids imbibing into the shale samples are shown in **Fig. 6.10**.

The vertical axis is the cumulative imbibed volume per unit area. The horizontal axis is the square root of experimental time.



Aqueous phase imbibition in Otter Park samples



c)

Fig. 6.10 -Plots of cumulative imbibed volume per unit area versus square root of time. Plots of various aqueous fluids imbibing into the Upper Muskwa (a), Middle Muskwa (b) and Otter Park (c) samples.

There is a linear relationship between the imbibed volume per unit surface area and square root of time in all of the plots. This dependence results in constant imbibition slope, which can be used to predict the imbibed amount of fluids at different times. Reasons causing such a linear dependence are extensively discussed previously in the literature (Alava, 2004; Cai and Yu, 2011; Hall, 2007; Schmid and Geiger, 2012).

A-parameter values are higher in Upper Muskwa samples compared to Middle Muskwa and Otter Park samples. It was also observed that DI water has the highest slope among all of the samples. Brine imbibition in orthogonal to the lamination direction shows the lowest A parameter value. Because A-parameter (the slope) contains all the information about hydraulic-capillary properties, it

represents a rigorous combination of all the forces acting during the imbibition process (Schmid and Geiger, 2012).

Table-6.2 shows A-parameter values that characterize imbibition of various aqueous fluids into the Upper Muskwa, Middle Muskwa and Otter Park samples.

Table 6.2- A-parameter values obtained from the experimental data			
A (m/√s)			
<u>Imbibing Fluids</u>	<u>Upper Muskwa (MW1)</u>	<u>Middle Muskwa (MW1)</u>	<u>Otter Park (OP)</u>
DI Water	3.71E-04	2.17E-04	4.58E-05
2 wt. % KCl Brine	2.86E-04	1.66E-04	2.92E-05
Brine (axial)	5.14E-05	4.01E-05	1.46E-05
Tergitol+DI	3.29E-04	1.83E-04	4.25E-05
DDBS+DI	3.05E-04	1.63E-04	4.10E-05
Tergitol+brine	2.46E-04	1.72E-04	3.73E-05
DDBS+brine	2.24E-04	1.41E-04	3.18E-05
XG (0.28 wt.%)	1.46E-04	9.56E-05	3.26E-05
XG (0.56 wt.%)	1.03E-04	8.78E-05	2.21E-05

6.2.4 Determination of the fracture-matrix interface at the field scale

The fracture-matrix interface is the critical parameter for quantification of fluid imbibition in the field (Roychaudhury *et al.*, 2011). The shape and size of hydraulic fractures are never known exactly, but can be estimated by interpretation of microseismic surveys and pressure or rate decline analysis (Clarkson *et al.*, 2011). Several methods are known that can be used to estimate the fracture-matrix interface at the field scale.

Methods for estimation of the fracture-matrix interface

Method-1. Production data analysis method can be used to estimate fracture-matrix interface at the field scale. Bello (2009) proposed a method to calculate fracture-matrix interface for the shale gas reservoirs:

$$\sqrt{k_m A_{cm}} = \frac{1262T}{\sqrt{2(\phi\mu c_t)_m}} \frac{1}{m_4} \quad (6.4)$$

Where k_m is permeability of matrix block, A_{cm} is the total interface between matrix and fractures, T is absolute temperature, ϕ is matrix porosity, μ is viscosity of gas, c_t is total matrix compressibility and m_4 is the slope of rate normalized pressure data versus square root of time,.

Figure 6.11 shows a schematic of a simplified, multistage hydraulic fracture. Single fracture per perforation cluster is assumed during each fracture stage.

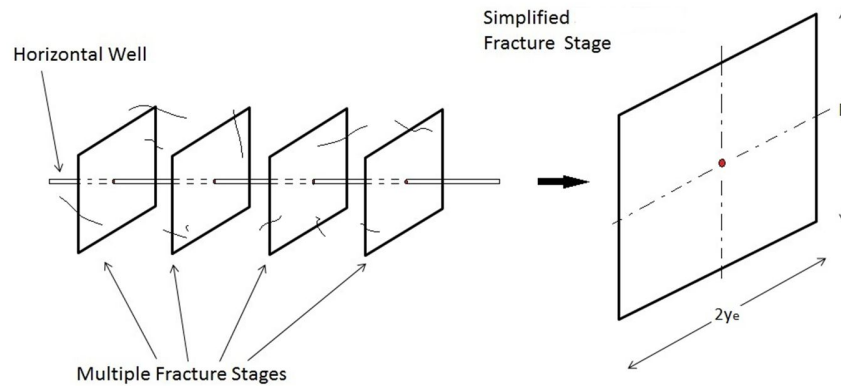


Fig. 6.11-Schematic of a multi-fractured horizontal well.

The total fracture-matrix interface (A_{cm}) can also be estimated, if fracture height, fracture half-length and number of stages are known:

$$A_{cm} = 4n_f y_e h \quad (6.6)$$

Where A_{cm} fracture-matrix interface, n_f is number of hydraulic fracture stages, y_e is fracture half-length, h is fracture height.

Method-2. The fracture-matrix interface can also be estimated using the material balance method. This method assumes that fracture volume equals to the difference between the total injected volume and fluid leak-off volume. Therefore, assuming the rectangular slab geometry of fractures, the total fracture-matrix interface (A_{cm}) can be estimated from:

$$A_{cm} = 2 \frac{V_{inj} - V_{leak}}{w} \quad (6.7)$$

Where A_{cm} is the total fracture-matrix interface, V_{inj} is the total injected volume, V_{leak} is the fluid leak-off volume and w is the fracture aperture.

During hydraulic fracturing operations, fracturing fluids are pumped under the high pressure to create fractures in the formation. Fluid leak-off volume represents how much of the injected fracturing fluid goes into the matrix and naturally existing fractures due to the high pressure pumping. It is calculated from the pressure decline data (Jones and Britt, 2009) and ranges between 10-40% for tight gas and shale reservoirs (Bai *et al.*, 2005). Rogers *et al.*, (2010) anticipated up to 30% of leak-off in the Horn River basin.

6.2.5 Estimation of Brine Imbibition at the Field Scale: a Sensitivity Analysis

To put our observations in a practical scale, we estimated the volume of imbibed brine into the Muskwa shale. Volume of imbibed brine per unit surface area was estimated by using the A-parameter value for 2 wt. % KCl solution imbibition into the Muskwa sample. Parallel to the bedding plane direction of brine imbibition was considered as the dominant imbibition direction.

The total fracture-matrix interface at the field scale was estimated using the material balance approach. The actual injected volume and the number of fracture stages are related to the fracture-matrix interface in the wells completed in the Muskwa and Otter Park formations (**Table 6.3**). Moreover, the total fracture-matrix interface was estimated by conducting a sensitivity analysis. By varying the leak-off volumes and fracture apertures, we examined how they affect the total fracture-matrix interface.

The fracture-matrix interface was estimated by considering several sets of fracture apertures. In practice, fractures are filled with proppants, which are always paved in multilayer patterns (Goa *et al.*, 2012). We estimate the average fracture apertures by the different layers of commonly used proppants. The thickness of one proppant is estimated 840 μm (20-40 mesh).

Table 6.3-Parameters used for a sensitivity analysis of the total fracture-matrix interface in Muskwa shale							
Injection V, m ³	Number of Stages, n_f	Aperture w	Interface (A_{cm}) , m ²	Aperture w	Interface (A_{cm}) , m ²	Aperture w	Interface (A_{cm}) , m ²
		<i>Leak-off, 10%</i>		<i>Leak-off, 20%</i>		<i>Leak-off, 30%</i>	
50808	18	2 prop	3020000	2 prop	2690000	2 prop	2350000
50808	18	3 prop	2016190	3 prop	1790000	3 prop	1570000
50808	18	4 prop	756000	4 prop	672000	4 prop	588000

Moreover, the leak-off percentage is varied from 10 % to 30 %, which is in agreement with the existing leak-off values in the literature (Rogers *et al.*, 2010; Bai *et al.*, 2005).

Fig. 6.12 shows the results of the sensitivity analysis conducted for brine imbibition in Muskwa shale. The left vertical axis represents actual volume of imbibed brine into the formation. The right vertical axis represents the percentage

of the injected volume that is imbibed into the formation. The horizontal axis represents the soaking time.

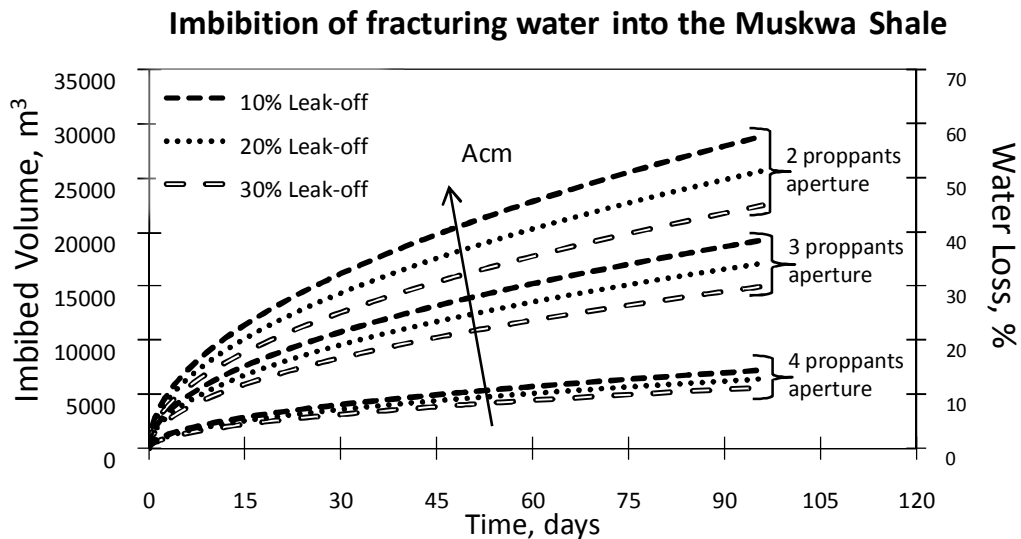


Fig. 6.12- Imbibed volume of brine into the Muskwa shale versus the soaking time. Imbibed volume increases with the increase in the soaking time. Smaller fracture aperture results in greater percentage of water loss to the formation. Moreover, higher amount of leak-off volume results in the smaller amount of imbibed volume.

Results show that the amount of imbibed brine increases with the increase in the fracture matrix interface. The greater volumes of brine imbibition into the formation matrix were observed when the smaller apertures were used. Moreover, it is also observed that lower leak-off percentages result in greater volume of brine imbibition into the formation. High leak-off into the formation hinders generation of large fractures.

Fig. 6.13 shows the dependence between water loss due to the spontaneous imbibition and the fracture aperture for various soaking times. The vertical axis shows the percentage of injected water that is imbibed into the formation matrix.

The horizontal axis shows the average fracture apertures. Fracturing water leak-off to the formation is not considered.

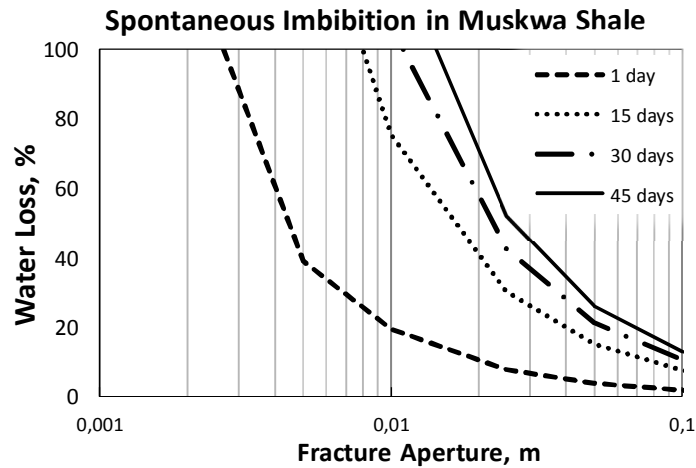


Fig. 6.13- Percentage of injected water that is imbibed into the Muskwa shale versus the fracture aperture. Imbibed volume increases with the decrease in the fracture aperture.

Imbibed volume also increases with time.

Smaller apertures create larger fracture-matrix interfaces, which can result in up to 100% water loss to the formation due to the spontaneous imbibition. The percentage of injected water that is lost to the formation is also affected by the soaking time.

The ratio of imbibed brine volume to the injected brine volume at the field scale is presented in **Fig. 6.14**. A fracture aperture size of 3 proppants and 20% leak-off were assumed.

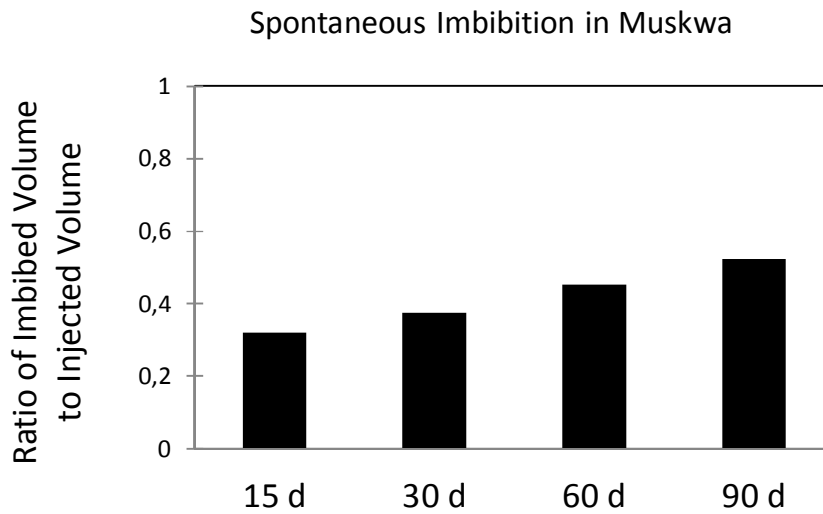


Fig. 6.14- Ratio of the imbibed volume to the injected volume for different periods of soaking time.

Results show that fluid loss in Muskwa member can reach up to 50 % of injected volume after 90 days of shut-in period.

6.2.6 Limitations of the Proposed Methodology for Fluids Loss Predictions

All the experimental data were obtained in the lab conditions. Measurements conducted at the laboratory conditions may differ from those in reservoir conditions. We anticipate that the actual imbibition rates at the field scale would be lower than those rates predicted using the laboratory results. The following discussion is provided to explain how some of the parameters involved in the imbibition process would influence the accuracy of the predictions based on the proposed methodology.

Porosity. Actual reservoir porosity values are expected to be lower than the values that are measured at the lab conditions. The absence of reservoir in-situ

stress can result in expansion of rock samples, which might induce micro fractures. Simply, the swelling pressure of clays induces micro-cracks when there is no confining pressure. These micro fractures enhance porous space in samples (Passey *et al*, 2010). Porosity measured in laboratory conditions yields in overestimated data. Moreover, the porosity of dried samples is overestimated due to the removal of capillary and clay bound water from the shale pores.

Water Saturation. Initial water saturation of the rock may reduce the imbibition rate (Li and Horne, 2006). Furthermore, the possibility of water adsorption by clay minerals can be negatively affected by initial water saturation in shale pores. Dry clays consist of layers that are closely packed. Hydration causes separation of layers; thus, reduces their density and alters electrical properties (Chenevert, 1970). In our study, the experimental shale samples are heated and dehydrated, which have a high potential for water adsorption.

Pressure drop. Natural gas trapped in shales is pressurized and inhibit water imbibition by the counter-current flow in the pores. This factor may also decrease the imbibition rates at the field scale (Dutta *et al*. 2012). In case, when pressure drawdown overcomes capillary pressure, the imbibed fluid can be displaced from shale matrix by the gas pressure (Gdanski *et al.*, 2005).

In addition, spontaneous imbibition at the field scale depends on other reservoir properties including temperature, fluid viscosities, interfacial tension between the imbibed phase and the resident phase, anisotropy, matrix size and boundary conditions.

CHAPTER 7

CONCLUSIONS AND RECOMMENDATIONS

7.1 Conclusions

In the current work we have investigated spontaneous imbibition in shale formations, which is inherent part of hydraulic fracturing. Factors that influence on imbibition phenomena in the Horn River shale were examined by various fluids and compared among the formation members. Major points have been summarized as follows:

- Imbibition rates of aqueous phase are higher than that of oleic phase in all of the samples. Adsorption by clay minerals can be the additional driving force for water phase imbibition. Reaction of water with clay minerals causes swelling of clay minerals in shale samples and generation of micro fractures.
- Addition of KCl salt reduces water imbibition rate in shale. Effects of KCl salt are more pronounced in samples with higher clay content.
- Surfactants reduce imbibition rates due to reduction of surface tension, which in turn reduces capillary driven forces. Anionic surfactants are sensitive to the presence of KCl salt in solution and causes reduction of surface tension and imbibition rate. Negatively charged surfactants may decrease effects of adsorption by clay minerals.

- Viscous XG solutions have lower imbibition rates compared to fresh water and brine. Application of **Eq. 6.1** is questionable due to the shear-thinning behaviour of polymer solution.
- Imbibition rate parallel to the laminations is higher than that of perpendicular to the lamination. Effects of directional anisotropy are more pronounced in clay rich samples.
- Water intake in large samples is higher than that in small samples. Effects of water adsorption by clay particles and induced micro fractures are more pronounced in large samples compared to small ones.
- The applied dimensionless scaling approach is more suitable for conventional rocks and requires additional investigations for scaling of spontaneous imbibition in shale samples.
- Low load recovery of frac fluids is, partly, caused by spontaneous imbibition of frac fluid in shale matrix.
- Fluid loss due to the spontaneous imbibition at the field scale is function of imbibition rates, contact interface and soaking time. Imbibition rates are the highest when fresh water imbibe in clay rich formations parallel to the lamination direction. Imbibed volume of frac fluid is proportional to the size of contact interface in hydraulic fracture. Imbibed volume of frac fluid is also proportional to the square root of soaking time.

7.2 Recommendations

Although most of the objectives set were achieved, there is still scope for further research and are recommended here:

- Effects of shale surface absorption need to be investigated separate from fluid imbibition. This will deepen understanding of water loss to the formations and find better applications for surface active substances, salts and polymers.
- Combination of anionic surfactants with salt water requires additional studies. Its application in shale reservoirs may reduce water invasion of shale pores. Optimum salt and surfactants concentration must be measured in order to meet economic and environmental constraints.
- All the experiments were conducted at room temperature and atmospheric pressure. In order to duplicate actual imbibition conditions in shale reservoirs set of experiments should be conducted in heated and pressurized tubes with actual fracturing fluids. Furthermore, it is recommended to use preserved cores so that obtained results would represent actual downhole processes.
- Scaling and modelling of spontaneous imbibition in shales needs further investigations. Due to the specific shale properties, scaling and consequently modelling can be affected by natural or induced micro fractures, fluid types, anisotropy etc. The applied model is restricted to

laboratory use; therefore, imbibition model that can be used in field scale for various shale and fluid types needs to be developed.

- Upscaling of dynamic imbibition processes needs to be studied. Impact of water loss due to imbibition in the actual multistage hydraulically fractured wells can be quantified in the field scale. Ultimately, water recovery technique needs to be developed that combines knowledge of fluid retention in the both formations matrix and propped fractures.

REFERENCES

- Aguilera, R. 2013. Flow Units: From Conventional to Tight Gas to Shale Gas to Tight Oil to Shale Oil Reservoirs. In SPE Western Regional & AAPG Pacific Section Meeting, 2013 Joint Technical Conference.
- Alava, M., Dubé, M., & Rost, M. 2004. Imbibition in disordered media. *Advances in Physics*, 53(2), 83-175.
- Alquraishi, A. A., & Alsewailem, F. D. 2012. Xanthan and guar polymer solutions for water shut off in high salinity reservoirs. *Carbohydrate Polymers*, 88(3), 859-863
- Akin, S., Schembre, J. M., Bhat, S. K., & Kovscek, A. R. 2000. Spontaneous imbibition characteristics of diatomite. *Journal of Petroleum Science and Engineering*, 25(3), 149-165.
- Anderson, R. L., Ratcliffe, I., Greenwell, H. C., Williams, P. A., Cliffe, S., & Coveney, P. V. 2010. Clay swelling—A challenge in the oilfield. *Earth-Science Reviews*, 98(3), 201-216.
- Anuj, G., & Faruk, C. 1994. An improved model for laboratory measurement of matrix to fracture transfer function parameters in immiscible displacement. In SPE Annual Technical Conference and Exhibition.
- Arthur, J. D., Bohm, B., & Layne, M. 2009. Hydraulic fracturing considerations for natural gas wells of the Marcellus Shale.
- Arthur, J.D., B. Bohm, and M. Layne. 2008. ALL Consulting. Hydraulic Fracturing Considerations for Natural Gas Wells of the Marcellus Shale. Presented at the GWPC Annual Forum in Cincinnati, OH. September 2008.
- Babadagli, T., & Hatiboglu, C. U. 2007. Analysis of counter-current gas–water capillary imbibition transfer at different temperatures. *Journal of Petroleum Science and Engineering*, 55(3), 277-293.
- Bai, M., Green, S., & Suarez-Rivera, R. 2005. Effect of Leakoff Variation on Fracturing Efficiency for Tight Shale Gas Reservoirs. In Alaska Rocks 2005, The 40th US Symposium on Rock Mechanics (USRMS).

- Balcerak, E. 2012. A general approach to spontaneous imbibition. *Eos, Transactions American Geophysical Union*, 93(16), 168-168.
- Bello, R.O. 2009. Rate Transient Analysis in Shale Gas Reservoirs with Transient Linear Behavior. Ph.D. Dissertation, Texas A&M U., College Station, Texas.
- Bennion, D. B., & Thomas, F. B. 2005. Formation damage issues impacting the productivity of low permeability, low initial water saturation gas producing formations. *Journal of energy resources technology*, 127(3), 240-247.
- Blatt, Harvey and Tracy, R.J. 1996. *Petrology: Igneous, Sedimentary and Metamorphic*, 2nd ed., Freeman, pp. 281–292
- Bear, J. 1972. *Dynamics of Fluids in Porous Media*, Dover, New York.
- Boek, E. S., Coveney, P. V., & Skipper, N. T. 1995. Monte Carlo molecular modeling studies of hydrated Li-, Na-, and K-smectites: Understanding the role of potassium as a clay swelling inhibitor. *Journal of the American Chemical Society*, 117(50), 12608-12617.
- Bourbiaux, B., & Kalaydjian, F. 1990. Experimental study of cocurrent and countercurrent flows in natural porous media. *SPE Reservoir Engineering*, 5(3), 361-368.
- Brinkman, R. 1970. Ferrolysis, a hydromorphic soil forming process. *Geoderma*, 3(3), 199-206.
- British Columbia Ministry of Energy and Mines and National Energy Board. 2011. BC MEM/NEB Report: Ultimate Potential for Unconventional Natural Gas in Northeastern British Columbia's Horn River Basin. <http://www.neb-one.gc.ca/clf-nsi/rnrgynfimt/nrgyrprt/ntrlgs/hrnrvr/hrnrvrm-eng.html>
- Caenn, R., Darley, H.C.H., Gray, G.R. 2011. Clay Mineralogy and the Colloid Chemistry of Drilling Fluids. *Composition and Properties of Drilling and Completion Fluids (Sixth Edition)*, Pages 137-177
- Cai, J., and B. Yu. 2011. A discussion of the effect of tortuosity on the capillary imbibition in porous media, *Transp. Porous Media*, 89, 1–13, doi:10.1007/s11242-011-9767-0.
- Canadian Geoscience Knowledge network. 2004. *Lexicon of Canadian Geologic Units*, http://cgkn1.cgkn.net/weblex/weblex_litho_detail_e.pl?00053:016853 (accessed 17 July 2012).

- Chalmers, G. R., Ross, D. J., & Bustin, R. M. 2012. Geological controls on matrix permeability of Devonian Gas Shales in the Horn River and Liard basins, northeastern British Columbia, Canada. *International Journal of Coal Geology*.
- Champagne, L., Zelenev, A., Penny, G., & Travis, K. 2011. Critical Assessment of Microemulsion Technology for Enhancing Fluid Recovery from Tight Gas Formations and Propped Fractures. In SPE European Formation Damage Conference.
- Chapman, A. 2012. Managing surface water use for hydraulic fracturing, BC oil and gas commission <https://www.bcwwa.org/resourcelibrary/Allan%20Chapman%20%20%20March%202012.pdf> (accessed 19 October 2012).
- Chemical disclosure registry (CDR). 2012. What is hydraulic fracturing, <http://fracfocus.ca/hydraulic-fracturing-process/what-hydraulic-fracturing> (accessed 19 October 2012).
- Chemtotal Pty Ltd website. 2013. Fracturing Fluid Systems. <http://www.chemtotal.com/fracturing-fluid-systems.html>
- Chen, J., Miller, M. A., & Sepehrnoori, K. 1995. Theoretical investigation of countercurrent imbibition in fractured reservoir matrix blocks. In SPE Reservoir Simulation Symposium.
- Chenevert, M. E. 1970. Shale control with balanced-activity oil-continuous muds. *Journal of Petroleum technology*, 22(10), 1309-1316.
- Cheng, Y. 2012. Impact of water dynamics in fractures on the performance of hydraulically fractured wells in gas-shale reservoirs. *Journal of Canadian Petroleum Technology*, 51(2), 143-151.
- Cheng, Y., McVay, D. A., & John Lee, W. 2009. A practical approach for optimization of infill well placement in tight gas reservoirs. *Journal of Natural Gas Science and Engineering*, 1(6), 165-176.
- Christopher, R. H., & Middleman, S. 1965. Power-law flow through a packed tube. *Industrial & Engineering Chemistry Fundamentals*, 4(4), 422-426.

Clarkson, C. R., Jensen, J. L., & Blasingame, T. A. 2011. Reservoir Engineering for Unconventional Gas Reservoirs: What Do We Have to Consider?. In Paper SPE 145080 presented at SPE North American Unconventional Gas Conference and Exhibition held in The Woodlands, Texas(pp. 14-16).

Clarkson, C. R., Jensen, J. L., Pedersen, P. K., & Freeman, M. 2012. Innovative methods for flow-unit and pore-structure analyses in a tight siltstone and shale gas reservoir. AAPG bulletin, 96(2), 355-374.

Crain's petrophysical handbook. 2012. Shale basics. <http://www.spec2000.net/11-vshbasics.htm> (accessed 29 January 2013).

Cui, X., Bustin, A. M. M., & Bustin, R. M. 2009. Measurements of gas permeability and diffusivity of tight reservoir rocks: different approaches and their applications. Geofluids, 9(3), 208-223.

Ding, M., & Kantzas, A. 2004. Estimation of residual gas saturation from different reservoirs. In Canadian International Petroleum Conference.

Dutta, R., Lee, C. H., Odumabo, S., Ye, P., Walker, S., Karpyn, Z., & Ayala, L. 2012. Quantification of Fracturing Fluid Migration due to Spontaneous Imbibition in Fractured Tight Formations. In SPE Americas Unconventional Resources Conference.

Gao, Y., Lv, Y., Wang, M., & Li, K. 2012. New Mathematical Models for Calculating the Proppant Embedment and Fracture Conductivity. In SPE Annual Technical Conference and Exhibition.

Gdanski, R., Weaver, J., Slabaugh, B., Walters, H., & Parker, M. 2005. Fracture face damage—it matters. paper SPE, 94649, 25-27.

Graham, J. W., & Richardson, J. G. 1959. Theory and application of imbibition phenomena in recovery of oil. Journal of Petroleum Technology, 11(2), 65-69.

Gray, F. F. and Kassube, J.R. 1963. Geology and stratigraphy of the Clarke Lake gas field, northeastern British Columbia. American Association of Petroleum Geologists, Bulletin 47: 467-483.

Hall, C. 2007, Anomalous diffusion in unsaturated flow: Fact or fiction?, Cem. Concr. Res., 37(3), 378–385.

- Haluszczak, L. O., Rose, A. W., & Kump, L. R. 2012. Geochemical evaluation of flowback brine from Marcellus gas wells in Pennsylvania, USA. *Applied Geochemistry*.
- Harper, J. 2008. The Marcellus Shale—An Old “New” Gas Reservoir in Pennsylvania. *Pennsylvania Geology*, 28(1), 2-13.
- Hayes, J. M., Takigiku, R., Ocampo, R., Callot, H. J., & Albrecht, P. 1987. Isotopic compositions and probable origins of organic molecules in the Eocene Messel shale.
- Heffernan, K., and Dawson, F. M. 2010. An Overview of Canada’s Natural Gas Resources. Canadian Society for Unconventional Gas (May 2010).
- Hlidek, B., Meyer, R., Yule, K., & Wittenberg, J. 2012. A Case for Oil-Based Fracturing Fluids in Canadian Montney Unconventional Gas Development. In SPE Annual Technical Conference and Exhibition.
- Horn River news. 2009. Encana estimates up to 500 trillion cubic feet in Horn River Basin, <http://hornrivernews.com/2009/09/10/encana-estimates-up-to-500-trillion-cubic-feet-in-horn-river-basin/> (accessed 17 July 2012).
- Hu, Q., Liu, X., Dultz, S., Robert P. E, and Harold D. R. 2010. Fracture-Matrix Interaction and Gas Recovery in the Barnett Shale-Department of Earth and Environmental Sciences, University of Texas at Arlington-Online.
- Iffly, R., Rousselet, D. C., & Vermeulen, J. L. 1972. Fundamental study of imbibition in fissured oil fields. In Fall Meeting of the Society of Petroleum Engineers of AIME.
- International Energy Agency. 2011. World Shale Gas Resources. Independent Statistics and analysis. www.iea.gov
- International Energy Agency. 2012. Special Report on Unconventional Gas? World Energy Outlook 2012. www.iea.gov
- Johnson, M., Walsh, W., Budgell, P., & Davidson, J. 2011. The Ultimate Potential for Unconventional Gas in the Horn River Basin: Integrating Geological Mapping With Monte Carlo Simulations. In Canadian Unconventional Resources Conference.

Jones, J., & Britt, L. K. 2009. Design and appraisal of hydraulic fractures. Richardson, TX: Society of Petroleum Engineers.

Kaufman, P., Penny, G., & Paktinat, J. 2008. Critical Evaluation of Additives Used in Shale Slickwater Fracs. In SPE Shale Gas Production Conference.

Kazemi, H., Gilman, J. R., & Elsharkawy, A. M. 1992. Analytical and Numerical Solution of Oil Recovery From Fractured Reservoirs With Empirical Transfer Functions (includes associated papers 25528 and 25818). SPE reservoir engineering, 7(2), 219-227.

Ketter, A., Daniels, J., Heinze, J., & Waters, G. 2006. A field study optimizing completion strategies for fracture initiation in Barnett shale horizontal wells. In SPE Annual Technical Conference and Exhibition.

King, G. 2010. Thirty years of gas shale fracturing: what have we learned?. In SPE Annual Technical Conference and Exhibition.

Kueper, B., Pitts M., Wyatt K., Simpkin T and Sale T. 1997. Technology practise manual for surfactants and cosolvents. Surfactant/Cosolvent Enhanced Recovery of NAPLs. <http://www.clu-in.org/products/aatdf/chap4.htm#E12E1> (accessed 29 January 2013).

LaFollette, R. 2010. Key Considerations for hydraulic fracturing of Gas Shales. In Online Webinar presented at the AAPG E-Seminar (Vol. 9).

Li, K., & Horne, R. 2001. Characterization of spontaneous water imbibition into gas-saturated rocks. SPE Journal, 6(4), 375-384.

Li, K., & Horne, R. 2004. An analytical scaling method for spontaneous imbibition in gas/water/rock systems. SPE Journal, 9(3), 322-329.

Li, K., & Horne, R. 2006. Generalized scaling approach for spontaneous imbibition: an analytical model. SPE Reservoir Evaluation & Engineering, 9(3), 251-258.

Li, Y. 2006. An empirical method for estimation of anisotropic parameters in elastic rocks. The Leading Edge, 25(6), 706-711.

- Li, Y., N. R. Morrow, and D. Ruth 2003, Similarity solution for linear counter-current spontaneous imbibition, *J. Petrol. Sci. Eng.*, 39(3–4), 309–326.
- Lucas, R. 1918, Ueber das Zeitgesetz des kapillaren Aufstiegs von Flüssigkeiten, *Colloid Polymer Sci.*, 23(1), 15–22.
- Makhanov, K., Dehghanpour, H., & Kuru, E. 2012. An Experimental Study of Spontaneous Imbibition in Horn River Shales. In SPE Canadian Unconventional Resources Conference.
- Mattax, C. C., & Kyte, J. R. 1962. Imbibition oil recovery from fractured, water-drive reservoir. *Old SPE Journal*, 2(2), 177-184.
- Mauger, S., & Bozbciciu, D. 2011. How Changing Gas Supply Cost Leads to Surging Production. Ziff Energy White Paper.
- McWhorter, D. B., and D. K. Sunada. 1990. Exact integral solutions for two-phase flow, *Water Resour. Res.*, 26(3), 399–413.
- Mody, F. K., & Hale, A. H. 1993. Borehole-stability model to couple the mechanics and chemistry of drilling-fluid/shale interactions. *Journal of Petroleum Technology*, 45(11), 1093-1101.
- Moore and Reynolds, 1997. D.M. Moore, R.C. Reynolds Jr. X-ray diffraction and the identification and analysis of clay minerals. Oxford University Press, New York (1997)
- Moseley, M. E., Cohen, Y., Kucharczyk, J., Mintorovitch, J., Asgari, H. S., Wendland, M. F., ... & Norman, D. 1990. Diffusion-weighted MR imaging of anisotropic water diffusion in cat central nervous system. *Radiology*, 176(2), 439-445.
- Muskat, M. 1949. *Physical Principles of Oil Production*, McGraw Hill, New York.
- Muherei, M. A., & Junin, R. 2009. Equilibrium adsorption isotherms of anionic, nonionic surfactants and their mixtures to shale and sandstone. *Modern Applied Science*, 3(2), P158.
- Nash, N. 2012. Hydraulic fracturing: focus on water, <https://www.bcwwa.org/resource-library/Hydraulic%20Fracturing%20Focus%20on%20Water.pdf> (accessed 19 October 2012).
- National Energy Board. 2006. Report: Northeast British Columbia's Ultimate Potential for Conventional Natural Gas. www.neb-one.gc.ca.

Novlesky, A., Kumar, A., & Merkle, S. 2011. Shale Gas Modeling Workflow: From Microseismic to Simulation--A Horn River Case Study. In Canadian Unconventional Resources Conference.

Oduşina, E., Sondergeld, C., & Rai, C. 2011. NMR Study of Shale Wettability. In Canadian Unconventional Resources Conference.

Paktinat, J., Pinkhouse, J., Williams, C., Clark, G., & Penny, G. 2006. Field Case Studies: Damage Prevention Through Leakoff Control of Fracturing Fluids in Marginal/Low-Pressure Gas Reservoirs. In SPE Gas Technology Symposium.

Palmer, I., Moschovidis, Z., and Schaefer, A. 2012. Microseismic Clouds: Modeling and Implications. In SPE Americas Unconventional Resources Conference.

Parmar, J., Dehghanpour, H., & Kuru, E. 2012. Unstable Displacement: A Missing Factor in Fracturing Fluid Recovery. In SPE Canadian Unconventional Resources Conference.

Passey, Q., Bohacs, K., Esch, W., Klimentidis, R., & Sinha, S. 2010. From Oil-prone source rock to gas-producing shale reservoir-geologic and petrophysical characterization of unconventional shale gas reservoirs. In International Oil and Gas Conference and Exhibition in China.

Penny, G., Zelenev, A., Lett, N., Paktinat, J., & O'Neil, B. 2012. Nano Surfactant System Improves Post Frac Oil and Gas Recovery in Hydrocarbon Rich Gas Reservoirs. In SPE Improved Oil Recovery Symposium.

Rajagopalan, K. 2012. 31. Minimising Industrial Wastes from the Fabricated Metal Products Industries.

Reed, R. M. 2007. Nanopores in the Mississippian Barnett Shale: Distribution, morphology, and possible genesis. In 2007 GSA Denver Annual Meeting.

Reeves, G. M., Sims, I., & Cripps, J. C. (Eds.). 2006. Clay materials used in construction (Vol. 21). Geological Society Publishing House.

Reis, J. C., and M. Cil. 1993. A model for oil expulsion by counter-current water imbibition in rocks: One-dimensional geometry, *J. Petrol. Sci. Eng.*, 10(2), 97–107.

- Reyes, L., & Osisanya, S. 2000. Empirical correlation of effective stress dependent shale rock properties. In Canadian International Petroleum Conference.
- Reynolds, M., & Munn, D. 2010. Development Update for an Emerging Shale Gas Giant Field- Horn River Basin, British Columbia, Canada. In SPE Unconventional Gas Conference.
- Rogers, S., Elmo, D., Dunphy, R., & Bearinger, D. 2010. Understanding hydraulic fracture geometry and interactions in the Horn River Basin through DFN and numerical modeling. In Canadian Unconventional Resources and International Petroleum Conference.
- Roychaudhuri, B., Tsotsis, T., & Jessen, K. 2011. An Experimental and Numerical Investigation of Spontaneous Imbibition in Gas Shales. In SPE Annual Technical Conference and Exhibition.
- Schembre, J. M., Akin, S., Castanier, L. M., & Kovscek, A. R. 1998. Spontaneous water imbibition into diatomite. In SPE Western Regional Meeting.
- Schmid, K. S., & Geiger, S. 2012. Universal scaling of spontaneous imbibition for water-wet systems. *Water Resources Research*, 48(3).
- Sharma, M., & Agrawal, S. 2013. Impact of Liquid Loading in Hydraulic Fractures on Well Productivity. In 2013 SPE Hydraulic Fracturing Technology Conference.
- Shouxiang, M., Morrow, N. R., & Zhang, X. 1997. Generalized scaling of spontaneous imbibition data for strongly water-wet systems. *Journal of Petroleum Science and Engineering*, 18(3), 165-178.
- Soeder J. D. 2011. Environmental impacts of shale-gas production. American Institute of Physics, page 8.
- Sondergeld, C. H., Newsham, K. E., Comisky, J. T., Rice, M. C., & Rai, C. S. 2010. Petrophysical Considerations in Evaluating and Producing Shale Gas Resources. Paper SPE 131768 presented at the SPE Unconventional Gas Conference, Pittsburgh, Pennsylvania, USA, 23–25 February.
- Song, K. W., Kim, Y. S., & Chang, G. S. 2006. Rheology of concentrated xanthan gum solutions: Steady shear flow behavior. *Fibers and Polymers*, 7(2), 129-138.

- Stoll, M., Hofman, J., Ligthelm, D., Faber, M., & van den Hoek, P. 2008. Toward Field-Scale Wettability Modification? The Limitations of Diffusive Transport. *SPE Reservoir Evaluation & Engineering*, 11(3), 633-640.
- Tan, C. P., Rahman, S. S., Richards, B. G., & Mody, F. K. 1998. Integrated approach to drilling fluid optimisation for efficient shale instability management. In *SPE International Oil and Gas Conference and Exhibition in China*.
- Takaya, H., Nii, S., Kawaizumi, F., & Takahashi, K. 2005. Enrichment of surfactant from its aqueous solution using ultrasonic atomization. *Ultrasonics sonochemistry*, 12(6), 483-487.
- The Canadian Association of Petroleum Producers. 2013. CAPP's Principles and Operating Practices for hydraulic fracturing. <http://www.capp.ca/canadaindustry/naturalGas/ShaleGas/Pages/defa-ult.aspx>
- U.S. Department of Energy. 2011. DOE's Early Investment in Shale Gas Technology Producing Results Today. http://www.netl.doe.gov/publications/press/2011/11008DOE_Shale_Gas_Research_Producing_R.html
- U.S. Energy Information Administration. April 1993. "Drilling Sideways: A Review of Horizontal Well Technology and Its Domestic Application", DOE/EIA-TR-0565.
- Wang, D., Butler, R., Liu, H., Liu, H., Ahmed, S., & Ahmed, S. 2011. Surfactant Formulation Study For Bakken Shale Imbibition. In *SPE Annual Technical Conference and Exhibition*.
- Wang, F. P., & Reed, R. M. 2009. Pore Networks and Fluid Flow in Gas Shales. Paper SPE 124253 presented at the SPE Annual Technical Conference and Exhibition, New Orleans, 4–7 October. [dx. doi. org/10.2118/124253-MS](https://doi.org/10.2118/124253-MS).
- Washburn, E. W. 1921. The dynamics of capillary flow, *Phys. Rev.*, 17(3), 273–283.
- Zhang, X., Morrow, N., & Ma, S. 1996. Experimental verification of a modified scaling group for spontaneous imbibition. *SPE Reservoir Engineering*, 11(4), 280-285.
- Zhou, D., Jia, L., Kamath, J., & Kovscek, A. R. 2002. Scaling of counter-current imbibition processes in low-permeability porous media. *Journal of Petroleum Science and Engineering*, 33(1), 61-74

